Volume 71C
Number 3
July–Sept. 1967

Engineering and Instrumentation

U.S. DEPARTMENT OF COMMERCE

SECTION C

JOURNAL OF RESEARCH

NATIONAL BUREAU OF STANDARDS

Journal of Research
of the
National Bureau of Standards

C. Engineering and Instrumentation

July–Sept. • 1967

VOLUME • 71C

NUMBER • 3

Editor: Martin Greenspan

Associate Editors: G. F. Montgomery, R. V. Smith, A. F. Schmidt

Publication dates:
Feb. 15, May 15, Aug. 15, Nov. 15, 1967

JOURNAL OF RESEARCH

The National Bureau of Standards Journal of Research reports research and development in the fields of activity shown at right. Also included from time to time are survey articles on topics closely related to the Bureau's scientific and technical program.

The Journal is published in three separate sections as follows:

A. Physics and Chemistry

Contains papers of interest primarily to scientists working in these fields. Issued six times a year. Annual subscription: domestic, $5.00; foreign, $6.00. Single copy, $1.00.

B. Mathematics and Mathematical Physics

Presents studies and compilations designed mainly for the mathematician and the theoretical physicist. Issued quarterly. Annual subscription: domestic, $2.25; foreign, $2.75. Single copy, 75¢.

C. Engineering and Instrumentation

Reports research and development results of interest chiefly to the engineer and the applied scientist. Issued quarterly. Annual subscription: domestic, $2.75; foreign, $3.50. Single copy, 75¢.

U.S. DEPARTMENT OF COMMERCE
Alexander B. Trowbridge, Secretary
NATIONAL BUREAU OF STANDARDS
A. V. Astin, Director

The National Bureau of Standards is a principal focal point in the Federal Government for assuring maximum application of the physical and engineering sciences to the advancement of technology in industry and commerce. Its responsibilities include development and maintenance of the national standards of measurement, and the provisions of means for making measurements consistent with those standards; determination of physical constants and properties of materials; development of methods for testing materials, mechanisms, and structures, and making such tests as may be necessary, particularly for government agencies; cooperation in the establishment of standard practices for incorporation in codes and specifications; advisory service to government agencies on scientific and technical problems; invention and development of devices to serve special needs of the Government; assistance to industry, business, and consumers in the development and acceptance of commercial standards and simplified trade practice recommendations; administration of programs in cooperation with United States business groups and standards organizations for the development of international standards of practice; and maintenance of a clearinghouse for the collection and dissemination of scientific, technical, and engineering information. The scope of the Bureau's activities is suggested in the following listing of its three Institutes and their organizational units.

Institute for Basic Standards. Applied Mathematics. Electricity. Metrology. Mechanics. Heat. Atomic Physics. Physical Chemistry. Laboratory Astrophysics.* Radiation Physics. Radio Standards Laboratory:* Radio Standards Physics; Radio Standards Engineering. Office of Standard Reference Data.

Institute for Materials Research. Analytical Chemistry. Polymers. Metallurgy. Inorganic Materials. Reactor Radiations. Cryogenics.* Materials Evaluation Laboratory. Office of Standard Reference Materials.

Institute for Applied Technology. Building Research. Information Technology. Performance Test Development. Electronic Instrumentation. Textile and Apparel Technology Center. Technical Analysis. Office of Weights and Measures. Office of Engineering Standards. Office of Invention and Innovation. Office of Technical Resources. Clearinghouse for Federal Scientific and Technical Information.**

*Located at Boulder, Colo. 80302.
**Located at 5285 Port Royal Road, Springfield, Va. 22151.

Order all publications from the Superintendent of Documents
U.S. Government Printing Office, Washington, D.C. 20402.

Use of funds for printing this publication approved by the Director of the Bureau of the Budget (June 22, 1966).

JOURNAL OF RESEARCH of the National Bureau of Standards—C. Engineering and Instrumentation
Vol. 71C, No. 3, July–August 1967

Procedure for High Precision Density Determinations by Hydrostatic Weighing

Horace A. Bowman and Randall M. Schoonover With Appendix by Mildred W. Jones

Institute for Basic Standards, National Bureau of Standards, Washington, D.C. 20234

(May 21, 1967)

There are several simplifications which can be made in the performance of the hydrostatic experiment which lead to more reproducible results. The operation of single-pan two-knife balances is discussed, and simple modifications suggested to adapt it to hydrostatic work. A data philosophy is presented which will be particularly applicable to a generation of now-developing force measuring instruments when used in hydrostatic work. A simplified formula for air density is presented and a formula for estimating day-to-day variability in the density of water. A simple balance calibration procedure is presented in an appendix, and simplified methods of fabricating suspension wires and degassing sample surfaces are described. The use of these techniques is illustrated by measurements on silicon crystals which indicate process reproducibility of a standard deviation to about one part per million.

Key Words: Air density, balance, balance calibration, balance equilibrium, balance sensitivity, density, double substitution weighing, hydrostatic balance, hydrostatic weighing, silicon density, substitution balance, volumetric measurement, water density, water weighing.

1. Introduction

1.1. Objectives and Accomplishments

The studies covered by this report were undertaken as a preliminary step to some volumetric and density standardization work being started at NBS [1][1] which will involve a great deal of hydrostatic weighing. Primary effort was directed toward a detailed study of the entire hydrostatic weighing process so that major sources of variability could be minimized, and experimental procedures simplified to the extent that nonspecialist workers could perform hydrostatic work approaching the state of the art. Secondary objectives were to evaluate the homogeneity (in density) in silicon boules.

We found, as have others, that major loss of precision occurs due to

(a) Imprecision inherent in the balance used in the hydrostatic work.

(b) Nonreproducibility of the surface tension forces associated with the meniscus formed around the point where the hydrostatic suspension penetrates the air-water interface.

(c) Variability in the buoyant forces exerted on the immersed sample by the gases adhering to its surfaces.

No existing balance was found to be ideal for hydrostatic work. The criteria upon which a balance should be selected are stated and the experiments and tests which should be put to any prospective balance are described. Additionally, simple modifications are suggested which will greatly improve balance performance in hydrostatic work without degrading its performance as an ordinary laboratory instrument.

Previous methods of minimizing surface tension errors have involved impractical hit-or-miss techniques, a great deal of luck, critical cleaning processes, detailed optical examination, and a rather small chance of a given suspension wire performing adequately. A simple heating technique was devised which eliminates the necessity for these operations and which gives the experimenter an excellent chance of meniscus stability to 2 or 3 tenths of a dyne per centimeter (a few micrograms in the case of an 0.001 in diam wire) on the "first try."

A simple boiling procedure gives minimization of surface bound gases on test samples at least as well as previous out-gassing methods ordinarily used in this work and with significantly less effort.

A formula is given for estimating air density directly from observations of temperature, pressure, and relative humidity which does not require using tables or graphs. Based upon previous observations of Chappuis and others a formula was constructed for estimating the day-to-day variability in water density.

Finally, we have written a section on "Operating Hints" which contains several items which, although not formally proved, we believe will improve and simplify the overall operation.

[1] Figures in brackets indicate the literature references on page 198.

Observations on three silicon crystals from the same boule grown in a vacuum indicated an average density of 2.328932 g/cm³ with individual crystals spread over a range of 0.000003 g/cm³. The average density of three crystals cut from a boule grown in argon was 2.329021 g/cm³ with individual values spread over a range of 0.000002 g/cm³. Repeat measurements made on all six crystals indicated a process standard deviation of about 1 ppm.

We believe that by use of the procedures described in this report, nonspecialist workers can duplicate these results.

1.2. Historical Background

There are two methods for determining the density of a solid object: first by independent measurements of its mass and geometry in terms of appropriate standards, from which its density may be calculated; and second, by comparison of its density with some reference density of known or assumed value. Direct measurement is a difficult and time-consuming task, and when great accuracy is called for, it is used only by the most advanced metrology laboratories. The vast majority of density determinations are made by hydrostatic weighing, in which the density of the unknown is obtained by comparison with the (assumed known) density of water.

During the very recent past, several branches of science have called for more precise density measurements. Such data is used in studies of stoichiometry, point defect concentrations in crystals, dimensional stability, atomic constants, and effects of various types of bombardment to name a few. It is well recognized that the larger the sample size, the better will be the precision; but unfortunately, the samples in which there is maximum technical interest are very small indeed. Frequently one needs small samples for verification of homogeneity. Bombarding beams often have limited diameters and penetrating powers, so recent effort has been directed to measurements on small samples.

Hydrostatic measurements on small samples present many problems not present in large sample work. There are three reasons for this:

(a) As balance capacity decreases below 1 kg, percentage precision decreases, although microgram precision increases (but at a lower rate). For example, a modern "convenience-type" balance can compare kilogram masses to 60 μg with ease. This is six parts in 100 million. On the other hand, the best 2-g balance can compare such loads to about 0.5 μg or 2.5 parts in 10 million.

(b) A major source of variability in hydrostatic work is meniscus instability. As loads increase, suspension wire size must increase. Tensile capacity increases as cross-section area, but meniscus forces increase only with circumference. Variability in such forces, for various reasons, may increase even more slowly.

(c) A tiny undetected air bubble will cause a much greater loss of precision on a small sample than on a large one.

Present effort to improve small sample work is indicated by two recent reports. In 1964 Henins [2] reported hydrostatic weighings on a group of objects averaging about 4.7 cm³ to a standard deviation of a single observation from the mean of about 4.5×10^{-6} cm³. In 1965 Bowman and Schoonover [3], using a cartesian diver technique on a group of 1.2 cm³ objects, reported 1.4×10^{-7} cm³. This is believed the best work to date. The diver is not a practical device for work on samples weighing much more than 10 g in water. The present studies are concerned with samples weighing from 10 to 20 g in water.

The foregoing comments have to do with precision and not accuracy. Precision refers to reproducibility of measured value—accuracy to correctness of measured value with respect to some standard. In this report, the measure of precision is the standard deviation of a single independent determination from the mean of several such determinations. In the density area (as in most fields of metrology), precision is better than accuracy which is limited by our imperfect knowledge of the true value of the various reference densities available to us. NBS is aware of its obligations in this area. The present study was undertaken as a preliminary step in the redetermination of several such densities and the development of a family of objects which will collectively become a density standard. However, aside from a few very fundamental studies, most work is aimed at determinations of density changes and density differences, and in work of this type, significant uncertainties in standards can usually be tolerated.

Many experimenters whose experience and training are far removed from metrology are attempting to achieve high quality hydrostatic data with inappropriate apparatus and obsolete techniques. We were particularly impressed by the simplicity of the setup used by Henins, and we used his approach as a starting point. Frequently, after much effort to improve upon it, we returned to it as a "best compromise." We acknowledge the great assistance we received from his work.

1.3. Hydrostatic Weighing Experiment

By classical definition, hydrostatic density measurement consists of weighing an object of *known mass*, M_X, while it is suspended from a balance in a liquid of some assumed value of density. The indicated loss of mass being equal to the mass of the displaced liquid, we are able to calculate the *true volume*, V_X, of the object and (by physical definition of density) calculate the unknown density. Thus

$$\rho_X = \frac{M_X}{V_X} .$$

The philosophy proposed here differs slightly from the classical concept. Our experiment consists of measuring the object's *apparent weight*, $\overline{W}$, in two media of different densities, where apparent weight is defined as the difference between the (downward) gravitational force exerted on the object, and the

(upward) buoyant force exerted on it by the medium. Thus

$$\overline{W}_A = g(M_X - \rho_A V_X) \qquad \text{(in air)}$$

$$\overline{W}_W = g(M_X - \rho_W V_X) \qquad \text{(in water)}$$

A simultaneous solution of the above pair provides values of M_X and V_X from which density may be calculated.

However, in our experiment, we demand of our balance only that it be linear in force, and the force units may be completely arbitrary—in which case the units for M_X and V_X will be unrecognizable. But their ratio (M_X/V_X) will be in the same units in which ρ_W and ρ_A are stated, since ρ_W and ρ_A are the true standards in the density measurement process. At the present state of the art the balance is the most linear force measuring instrument available, and balances (of the type we selected) are calibrated in classical mass units against classical mass standards. However, a new generation of elastic force instruments is growing up, and improving at a faster rate than ordinary balances. When these devices have achieved the precision presently obtainable on balances we believe they will supplant laboratory balances in this application. The verification of force linearity in such devices will be easier than calibration in terms of some particular standard.

As pointed out above, our efforts are primarily directed to improving precision, measured by the reproducibility of independent measurements. The definition of "independent" as used here means an observing process in which all random variables are permitted to operate. This specifically prohibits such procedures as:

(A) Stating a standard deviation in $\overline{W}_W$ based upon a series of "immersed pan empty"—"immersed pan loaded" differences, because in this instance the random properties of the meniscus and surface bound gas cannot operate.

(B) Stating a standard deviation in $\overline{W}_A$ based upon arresting and releasing the balance with the load stationary on the pan, because a major component of the arrestment error (namely the loading error [4]) cannot operate.

The above restrictions are stated because mistakes of both types have been made and reported in literature. A single independent density determination must consist of the following steps—*none of which may be used as a part of a different determination:*

(1) A thorough cleaning and degassing of the surfaces of the sample to be tested.

(2) A group of "immersed pan empty" and "immersed pan loaded" observations, with the differences averaged to provide a *single value* of $\overline{W}_W$.

(3) Removal of the sample from the bath, drying, and temperature soaking followed by a series of air weighings which are averaged to provide a *single value* of $\overline{W}_A$.

In the foregoing procedure, the parameters necessary for the calculation of ρ_W are measured in connection with step (2) and those for ρ_A in step (3). With measured values of $\overline{W}_A$ and $\overline{W}_W$, we may solve the simultaneous pair referred to above as follows

$$\rho_X = \frac{\overline{W}_A \rho_W - \overline{W}_W \rho_A}{\overline{W}_A - \overline{W}_W}.$$

At this point we still have little knowledge upon which to base a precise statement regarding our process reproducibility. To obtain such knowledge, it is necessary to repeat the entire experiment using a new sample of water.

2. Density of Water

About 1900 the thermal coefficient of expansion of normal (to be defined) water was measured [5, 6], and in 1937 Tilton and Taylor at NBS [7] published tables of the relative densities of water as a function of temperature from a formula they constructed to fit the early data. This table expresses density in grams per milliliter where the milliliter is defined as the volume occupied by 1 g of water at 3.98 °C. Around 1910 BIPM [8, 9, 10] undertook to measure the true volume (in cubic centimeters) of a milliliter by hydrostatically weighing objects of directly measured volume in normal water. These experiments were conducted prior to knowledge of isotopes, and we define "normal" water as that having a "normal" or "average" isotopic abundance ratio. Modern workers [11, 12] have shown that the isotopic abundance ratio in samples of water drawn from various locations on the earth may vary enough to result in density differences of as much as 5 or more parts per million. Without knowledge of the isotopic abundance ratio in the water used in measuring the milliliter we are left with an uncertainty of this amount in the accepted value of the volume of the milliliter. Additionally, there is an even larger source of uncertainty. The vapor pressures of the various isotopic forms of water are significantly different [13], so that distillation to remove impurities or boiling to eliminate dissolved gasses can further upset the isotopic abundance ratio from its "normal" value. Density differences as great as 20 ppm have been found [14] between the first and last fractions of a distillation.

Modern experiments on the thermal dilation of the pure isotope forms and of normal water [15] indicate no serious error in the Tilton and Taylor values; however, there is no modern equivalent of the milliliter evaluation experiment, and it is in this experiment in which significant differences are to be expected. The present work is performed in anticipation of such a repetition. Uncertainty exists in our work associated with the uncertainty in ρ_W which cannot be evaluated until this repeat experiment is performed.

Effect of dissolved air. There is very little data available on the effect of dissolved air on the density of water. Figure 1 is a plot of all such data which has come to our attention. The work of Marek is ordinarily used as a basis for making the required corrections, or for

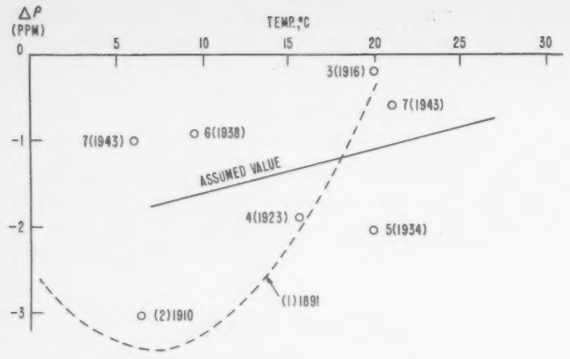

FIGURE 1. *(1) W. Marek, Ann. Physik, 3,* **4** *(1891). (2) P. Chappusi, Trav. & Mem. B.I.P.M.* **14** *(1910). (3) T. W. Richards and Harris, J. Amer. Chem. Soc,* **38** *(1916). (4) O. E. Frivold, Physik Z.* **21**, *p. 529–534 (1920);* **24**, *p. 86–87 (1923). (5) Emeleus, James, King, J. Chem. Soc, 1207 (1934). (6) Titani and Morita, Bull. Chem. Soc, Japan,* **13**, *409 (1938). (7) Voskuyl, Davis and Saxer, SAM Report A–727, June (1943).*

the justification of ignoring the effect. The plot of his data indicates that extrapolation into the temperature range of ordinary interest would yield extremely improbable values so we reject his data. Dorsey [16] gives other reasons for questioning his work. Our estimate of the probable effect is shown by the solid line whose point slope form is

$$\Delta\rho_W \text{ (in ppm)} = -2.11 + 0.053\ t_W$$

where t_W is water temperature.

Chappuis [17] reported that water reaerates after boiling at a rate such that at 13 °C and at a depth of 12 cm below the free surface, 50 percent saturation is achieved after 1 day and 75 percent after 4 days. No other information on the rate of reaeration was located. Our samples are usually held to within a few centimeters of a depth of 12 cm. The correction factor which we apply to the density of water is given by

$$1-(2.11-0.053\ t_W)\left(1-\frac{1}{1+t}\right)\times 10^{-6}$$

where t is the interval (in days) since deaeration.

Effect of pressure on water density. Water is not incompressible, therefore a correction must be applied to account for the effect of varying pressure. The pressure of the water displaced by the object of interest is a function of the barometric pressure at the free surface and the depth of immersion. The correction factor which we apply is given by

$$\frac{1}{1-c\left(\frac{B}{760}+\frac{I}{1033}-1\right)}$$

where c = compressibility = 47.7 ppm/atm
B = barometric pressure (in mm of hg)
I = depth of immersion (in cm).

The complete formula for ρ_W used in our experiments is as follows:

$$\rho_W=\left[1-\frac{(t_W-3.9863)^2}{508929.2}\times\frac{t_W+288.9414}{t_W+68.12963}\right]\left[0.999973\right]\left[\frac{1}{1-C\left(\frac{B}{760}+\frac{I}{1033}-1\right)}\right]\left[1-(2.11-.053t_W)\left(1-\frac{1}{1+t}\right)(10^{-6})\right]. \quad (1)$$

The first term is the Tilton-Taylor formula for ρ_W as a function of temperature in grams/milliliter. The second term reduces their values to grams/cubic centimeter. The third term is a correction for pressure and the fourth for dissolved air. The last two terms are ordinarily ignored, however they may alter the calculated value of ρ_W by as much as 1.5 ppm.

3. Density of Air

Major changes in ρ_A occur due to variation in the temperature, pressure, and relative humidity, and each of the parameters is carefully observed throughout the experiment. Changes also occur due to variation in the air analysis, however this was not investigated. The instrumentation used for monitoring these ambient parameters is not state-of-the-art-type apparatus, because it is necessary only to assure that the standard deviation in ρ_A is held to a few micrograms per cubic centimeter. Apparatus was chosen which is most convenient to use and maintain.

A. Temperature. It will be pointed out in the next section that air density is of interest in two spaces—the weighing chamber of the balance and also in the chamber housing the dial-operated weights. Each of these spaces is monitored by a mercury-in-glass thermometer, divided into 1/10 °C intervals over the range of 20 to 30 °C. The thermometer in the weighing chamber is calibrated for total immersion, and the one which monitors the weight chamber must be satisfied by partial immersion. Inasmuch as a platinum resistance thermometer is used to monitor the hydrostatic bath, these two mercury-in-glass thermometers should be calibrated periodically in this bath.

B. Relative humidity is measured on an electric hygrometer of the type discussed by Wexler [18] with its sensing element placed in the weighing chamber of the balance. This instrument usually contains a built-in thermistor type thermometer which is used to monitor the temperature in the immediate vicinity of the r.h. sensing element. *This should not* be used as a replacement for either of the mercury thermometers. Although it is quite adequate for the use intended by the manufacturer (and it should be used in connection with r.h. measurements) it will introduce serious uncertainties if used as a replacement for either of the mercury instruments.

Sling and aspiration psychrometers are unsatisfactory in this application. Their required air-flow

would cause unacceptable disturbances inside a balance, and they lack the required sensitivity and speed of response. Since there are free surfaces of water in the vicinity of the balance in the hydrostatic weighing experiment which exert a strong influence on r.h. the apparatus for monitoring this parameter should be selected with care. Wexler discusses electric hygrometers in detail and we believe that their convenience, speed of response and sensitivity are such that no other type instrument currently available should be considered. Wexler estimates their drift at about 2 percent per year, and feels that semiannual calibration is quite reasonable.

Calibration can be performed by the manufacturer, NBS, or the experimenter himself using various techniques leading to a calibration accuracy of about 1½ percent using the methods of Wexler and his associates [19].

C. Barometric pressure is most easily observed on an aneroid barometer. Such an instrument should be checked against a mercury barometer. Our barometer is, unfortunately, not equipped with an antiparallax mirror scale. We recommend specifying such a scale for instruments used in this work.

D. The basis for air density calculations. If we have a mass, m_G, of dry gas at pressure p and absolute temperature θ, whose molecular weight is M_G, then from the ideal gas law

$$pV = nR\theta = \left(\frac{m_G}{M_G}\right) R\theta$$

and

$$m_G = \frac{pVM_G}{R\theta}$$

and

$$\frac{M_G}{R\theta} = \frac{m_G}{V} \cdot \frac{1}{p} = \frac{\rho_G}{p} \tag{2}$$

where n is the number of moles involved and ρ_G the density of the dry gas.

If we have a mass, m_W, of water vapor at pressure e and temperature θ occupying volume V, then a similar argument gives

$$m_W = \frac{eVM_W}{R\theta}$$

If the above masses of gas and vapor are mixed in volume V, the barometric pressure, B, will be (by Dalton's Law of partial pressures) equal to $p+e$ and $p=B-e$. The density, ρ_A, of the mixture is

$$\rho_A = \frac{m_G + m_W}{V} = \frac{M_G}{R\theta}\left[B - e\left(1 - \frac{M_W}{M_G}\right)\right].$$

Using $M_G/R\theta$ from eq (2).

$$\rho_A = \frac{\rho_G}{P}\left[B - \left(e\ 1 - \frac{M_W}{M_G}\right)\right].$$

If the density of dry gas, ρ_G, is measured to be ρ_0 at some reference temperature θ_0, and reference pressure ρ_0, then its density at any temperature θ and pressure p is

$$\rho_G = \rho_0\left(\frac{\theta_0}{\theta}\right)\left(\frac{p}{p_0}\right)$$

and using this value of ρ_G in the above equation for ρ_A gives

$$\rho_A = \left(\frac{\rho_0\theta_0}{\theta p_0}\right)\left[B - e\left(1 - \frac{M_W}{M_G}\right)\right].$$

On the basis of the natural scale of atomic weights $M_W = 18.0160$ and $M_G = 28.966$ [20]. If $\rho_0 = 1.29304 \times 10^{-3}$ g/cm^3 when $\theta_0 = 273.16$ °K and $p_0 = 760$ mm Hg [21], then

$$\rho_A = 0.46475\left(\frac{B - (0.0037803)\ (e_s)\ (H)}{t_A + 273.16}\right)$$

where t_A is temperature in °C, e_s the tabulated saturation vapor pressure of water at t_A and H the relative humidity expressed as a percentage. This formula assumes moist air behaves in accordance with the ideal gas law, under which circumstances compressibility (defined as $\rho V/R\theta$) is unity. Goff and Gatch [22] have measured the compressibility of moist air and have found that over the range of temperature, pressure and relative humidity ordinarily existing in the laboratory it varies between 0.9995 and 0.9997, so the above formula provides values of ρ_A too high by this factor. We feel justified in multiplying its right member by an average value of 0.9996, so that

$$\rho_A = 0.46456\left[\frac{B - (0.0037803)\,(e_s)\,(H)}{t_A + 273.16}\right]. \tag{3}$$

Equation (3) may be used by the experimenter for calculation of air density based upon observed values of temperature, barometric pressure, relative humidity and tabulated values of e_s, the vapor pressure of water at saturation. In this equation ρ_A is a very weak function of e_s, changing by only 0.24×10^{-6}g/cm^3 for a 1 mm Hg change in e_s. Therefore it is possible to eliminate the inconvenience of using tables by making a *very crude* approximation for e_s in terms of the observed temperature without causing unacceptably large errors in ρ_A. Most weighings are conducted between 20 and 30 °C, and within this range we may assume

$$e_s = 1.435\ t_A - 11.72$$

under which circumstances

$$\rho_A = \frac{0.464554B - H(0.00252t_A - 0.020582)}{t_A + 273.16} \tag{4}$$

where ρ_A is in milligrams per cubic centimeter with adequately small error.

On the rare occasions when it is necessary to perform weighings outside of this temperature range some

adjustment in the approximation is called for. Over the temperature of 15 to 50 °C, air density may be approximated by

$$\rho_A = \frac{464.56B - H(0.085594t_A^2 - 1.8504t_A + 34.47)}{t_A + 273.16} \tag{4A}$$

where ρ_A is in micrograms per cubic centimeter. Although these two approximations result in very large errors in e_s, errors in ρ_A associated with their use do not exceed one microgram per cubic centimeter which is quite adequate for weighing work.

In order to test the ability of our system to report small changes in air density reproducibly, it was installed in a balance similar to the one used in the hydrostatic experiments. We made two series of tests (each test over an interval of several days) on the indicated difference in apparent weight of two stainless steel weights of nearly equal mass but of grossly different volume (one weight was hollow). Day-to-day changes in the indicated difference between the apparent weights were taken to be indicative of changes in air density, thus:

$$\rho_A = \frac{\Delta M - \Delta \overline{W}}{\Delta V} \tag{5}$$

where ΔM and ΔV are the mass and volumetric differences between the two weights (measured independently to be 35.466 mg and 42.769 cm³ respectively) and $\Delta \overline{W}$ the difference in apparent weights indicated by the balance. The data is summarized below. Ranges in temperature, barometric pressure and relative humidity, over which observations were made, are shown. $\Delta\rho_A$ is the value of ρ_A calculated from observations on ambient parameters minus the gravimetric determination of ρ_A based upon the above formula.

Test	Number of observations	Range in relative humidity	Range in baro.	Range in temp.	Average $\Delta\rho_A$	Std. dev. in $\Delta\rho_A$
		%	*mm* Hg	°C	$\mu g/cm^3$	$\mu g/cm^3$
First	29	17.3 40.9	742.3 756.3	24.0 27.0	−0.14	0.49
Second	42	7.3 36.3	746.0 769.4	21.5 26.7	+0.35	0.33

The above tests cannot be considered a "calibration" of our system because of possible errors in our values ΔM and ΔV, and some other features which assume importance when "absolute accuracy" is a requirement. The tests demonstrate that placement of the sensors in the balance case is adequate and that the sensors have adequate sensitivity, stability, and speed of response.

4. Apparatus

The two most important pieces of apparatus necessary in hydrostatic weighing are the hydrostatic balance and the hydrostatic suspension. This chapter contains a section on each of these two members. In order to obtain a hydrostatic balance of adequate precision, we found it necessary to select an ordinary laboratory balance and modify it to this use. The criteria upon which selection of a balance should be made will be stated, and additionally we have suggested how an "ideal" hydrostatic balance might work. The hydrostatic balance can weigh the immersed load only to an accuracy which is limited by the ability of the hydrostatic suspension to deliver this load (without error) from the immersed object, through the air-liquid interface, to the balance. An adequate solution to this problem is described in this section.

4.1. The Balance

Precision. The precision of a balance is defined as the standard deviation of a single observation from the mean of many observations made by it on the difference between two loads. In a skillfully conducted air weighing experiment of a given format of observations, the precision to which the difference between two loads is determined is almost entirely a function of the precision of the balance. In the air weighing cycle of the experiments reported here, precision is about 3 μg. In the water cycle, which includes almost all sources of variability occurring in the air cycle (plus many more) precision is believed to be about 4.5 μg, although this is difficult to prove experimentally. From this, it may be inferred that the variability introduced into the experiment by the balance is a major fraction of all variability. Therefore, the first criterion in the selection of a balance should be that it have an excellent precision as defined above.

Convenience. The second criterion in the selection of a balance is convenience of operation. In hydrostatic weighing the experimenter is a very busy individual indeed. He must monitor two extra temperatures not involved in air weighing (1 to about 0.001 °C), he must manipulate two extra arrestments, he must keep the water surface in the vicinity of the meniscus free of dust, he must observe the immersed structure to guard against rotation, and he must maintain the format of observations in accordance with a previously chosen time schedule.

Mechanical smoothness of operation is the third selection criterion, and it is equally as important as precision and operating convenience. Arrestment and release must be accomplished with no jolts or vibration and with near zero horizontal pan motion. Many otherwise fine balances must be rejected for hydrostatic work because of arrestment or weight changer design. While significant irregularities of pan motion will exert no effect on air weighing, they can completely destroy a water weighing measurement.

The importance of these three criteria cannot be overstated. Almer, Bowman, Jensen, Macurdy, Peiser, and Wasko [23] have pointed out how these criteria are best satisfied by a two-knife balance. We selected, as did Henins, a damped, single-pan, direct-reading balance almost entirely upon the basis of these three features. The balance we selected is designed to operate at a constant load of 20 g. This amount of dial-operated weights is built into the suspension and may be removed in increments of 0.01 g. When a load is placed on the pan, the built-in weights are removed from the suspension in a quantity sufficient to restore the balance to its design-load operating level. When the load removed from the suspension is within 0.01 g of the pan load, the beam swings to an angular position which indicates the residual unbalance.

Sensitivity is defined as the ratio between the angluar deflection of the beam and the magnitude of a load change on the pan.[2] High sensitivity is desirable for clear and unambiguous observation on the scale of the difference between pan load and the load dialed-off from the suspension. In the Introduction we defined the *apparent weight* of an unknown object, $\overline{W}_X$, as the gravitational force exerted on it minus the buoyant force exerted on it by the surrounding medium. Thus:

$$\overline{W}_X = (M_X - \rho_A V_X)g$$

where M_X and V_X are the mass and volume of the object, ρ_A the density of the medium and g the local acceleration of gravity. Also:

$$\overline{W}_X = M_X \left(1 - \frac{\rho_A}{\rho_X}\right) g$$

where ρ_X is the density of the object. In a vacuum $\rho_A = 0$, so

$$W_X = M_X g.$$

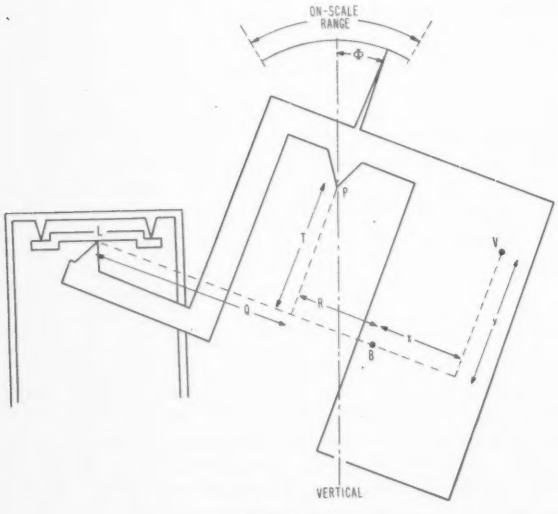

FIGURE 2

[2] This ratio is best defined when the load change tends to zero.

Referring to figure 2, point B is the center of mass of the beam alone, at which point its apparent weight, $\overline{W}_B$, acts. Point L, a distance of $Q+R$ from B, is the point on the load knife at which the compensating pivots concentrate $\overline{W}_H$, the apparent weight of the hanging load, which has two components:

(a) $\overline{W}_s$, the apparent weight of the suspension itself which includes whatever dial operated weights remain in place, and

(b) $\overline{W}_L$, the apparent weight of the load placed upon the pan. If the center knife is placed at point P with coordinates (Q, T) from the origin, L, along LB, the system will rotate (assuming vacuum operation) and decay toward an angular position Φ described by the following equilibrium equation:

$$(\overline{W}_S + \overline{W}_L)(Q + T \tan \phi)$$

$$= \overline{W}_B(R - T \tan \phi) \quad (6)$$

Differentiation of this equation gives us immediately an expression for system sensitivity, S, thus:

$$S = \frac{d\Phi}{d\overline{W}_L} = (-)\frac{\cos^2 \Phi(Q + T \tan \Phi)}{T(\overline{W}_B + \overline{W}_S + \overline{W}_L)}. \quad (7)$$

This expression for sensitivity appears in numerous forms, depending upon the trigonometric description of the beam used in writing the equilibrium equation. By suitable algebraic manipulation, they can be shown to be equivalent. Most expressions for S contain the *ratio* between the two moment arms or arm radii. These forms were originally written to apply to three-knife, symmetrical balances because, on such instruments, the *effective value* of the ratio can be determined gravimetrically (by transposition). Direct measurement of the individual arms sometimes leads to intolerable error in the ratio. When working values of the two arm lengths are required, the *sum* of the two arms (very nearly equal to the total distance between the two end knives) is obtained in *one length* measurement and this is solved simultaneously with the ratio. For high-sensitivity symmetrical two-pan, three-knife balances of conventional design, individual values of the two arms can be obtained in this manner with acceptably small error.

This technique is impractical on a nonsymetrical two-knife balance, so our system is described in terms of the ratio between Q and T, figure 2, thus:

$$Z = \frac{Q}{T}. \quad (8)$$

The effective value of Z may be approximated on a two-knife balance. It is noted that the measurable distance between the two knives is $\sqrt{Q^2 + T^2}$. When individual values of Q and T are demanded, they are available from a simultaneous solution of equations involving numerical values of $\frac{Q}{T}$ and $\sqrt{Q^2 + T^2}$. It is

noted that $Z = \cot$ PLB, however measurement of this angle is difficult.

If the total apparent weight of the system, $\overline{W}_T$, is the sum of the elements $\overline{W}_B + \overline{W}_S + \overline{W}_L$, then eq (7) becomes

$$S = \frac{d\phi}{d\overline{W}_L} = (-)\frac{\cos^2\phi}{\overline{W}_T}(Z + \tan\phi). \tag{9}$$

This shows that the system sensitivity is a function of the angular position of the beam with respect to gravity, and the dependence of S upon ϕ is

$$\frac{dS}{d\phi} = \frac{Z\sin(2\phi) - \cos(2\phi) - 1}{\overline{W}_T} \tag{10}$$

Maximum sensitivity and independence of S from ϕ exist when $\frac{dS}{d\phi} = 0$, under which circumstances $\cot\phi = Z$ and

$$Z = \overline{W}_T\,(S_{\max}). \tag{11}$$

Linearity and *on-scale range* are the fifth and sixth criteria in hydrostatic balance selection. It was pointed out in the introduction that the balance is used as a linear force indicator, and that the units of force indicated could be perfectly arbitrary, provided that they were consistent in the water-weighing and air-weighing cycles of the experiment. A large *on-scale range* is desirable so that a large difference can exist between the pan load and the removed dial-operated load. In addition to simplifying the operation (it is easier to read a difference than to dial it out) fewer dial operated weights become involved so calibration uncertainties are minimized. The requirements for large sensitivity and large on-scale range taken together demand that the balance swing over a very large range in Φ. But eq (10) shows that S is dependent upon Φ, except at the single point defined in eq (11), so that linearity is sacrificed to achieve sensitivity and range.

There are techniques for providing uniform apparent sensitivity over the entire on-scale range (such as an observing system with compensating nonlinearity) and it does not matter to the experimeter what, if any, technique is used. He must, in any event, verify uniformity of sensitivity or evaluate nonuniformity by experiment. Figure 3 is a plot of the data taken on our balance, which shows the dependence of S upon Φ shown in eq (10) as well as nonuniformity due to other causes. The on-scale range of our balance is 20 mg for beam motion of 0.044 rad. The experiment consisted of plotting observed changes in Φ (expressed in milligrams) for the application of the same 5 mg weight at various points in the on-scale range. Figure 3 shows our lack of linearity to be quite trivial, nevertheless, we constructed an empirical formula to eliminate this source of nonlinearity,

$$s_t = s_0 + (10 - s_0)^2\,(0.00007)\text{ milligram} \tag{12}$$

where s_t is taken to be the corrected screen reading

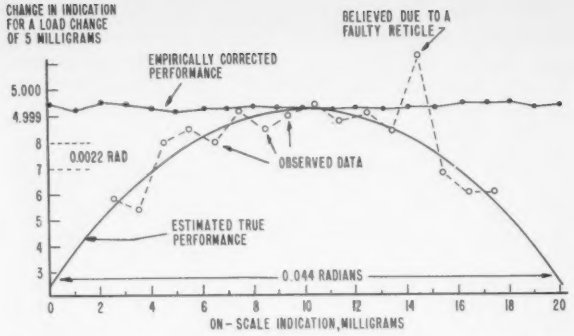

FIGURE 3. *This is the average of four sets of measurements on the sensitivity of our balance at various points over the on-scale range.*

The open circles are observed data. For various reasons it is difficult to obtain reliable data at the end-points of the range. The solid line is our estimate of true performance, and the approximately horizontal line is the performance when observations are corrected by an empirical formula as explained in the text.

and s_0 the reading actually observed. It should be noted that if the balance is moved from one location to another, or if the leveling screws are changed, the characteristics of linearity will be altered, which would require a change in the empirical formula.

Another source of nonlinearity lies in the maladjustment of the built-in weights, for example, failure of a 10-g weight to be precisely twice that of a 5. This effect may be minimized by a simple calibration procedure in which a set of standard weights is "weighed" on the balance in various combinations utilizing all settings of each dial. This procedure, worked out by M. Jones, NBS, and described in detail in the appendix, leads to a table of corrections which are applied to the dial settings on the balance. The corrected dial reading, D_t, is obtained by

$$D_t = D_0 + C \tag{13}$$

where C is the appropriate correction selected from the table, and D_0, the observed dial reading.

Load pan fall, F, is the vertical distance through which the suspended load moves as the balance swings through its on-scale range. For balances of conventional design

$$F \cong Q\Phi_T$$

where Φ_T is the total angle (in radians) through which the beam swings. The greater the value of load pan fall the longer must be the length of suspension wire which must be adequately coated. This is discussed later in detail, but it can be stated here that F should be held to a minimum. Minimizing either Q or Φ_T to reduce F, will, unfortunately, degrade either sensitivity or on-scale range.

Buoyant Equilibrium. Equations (6) through (11) hold for operation in a vacuum. They also hold for operation in a medium of density ρ_A if the balance is in buoyant equilibrium, by which we mean two requirements are met:

(1) The beam is homogeneous or effectively so. Effective homogeneity exists when the center of mass of the beam coincides with its center of volume.

(2) The net density of the suspension (the sum of all hanging masses divided by the sum of their volumes) equals the net density of the beam.

In the case of the suspension, effective homogeneity is not demanded, because both downward mass forces and upward buoyant forces are concentrated at point L in the diagram. Violation of the requirements for buoyant equilibrium results in changes in sensitivity and equilibrium values of ϕ with ρ_A (zero drift) as explained below.

When requirement 1 is violated the center of volume of the beam, V, lies at coordinates (x, y) from the center of mass at point B, and the equilibrium equation is

$$(\overline{W}_L+\overline{W}_S)(Q+T\tan\phi)=(M_Bg)(R-T\tan\phi) - g\rho_AV_B(R-T\tan\phi+x+y\tan\phi). \quad (14)$$

Differentiation of eq (14) to obtain an expression for balance sensitivity under these conditions gives:

$$S=\frac{d\phi}{d\overline{W}_L}=(-)\frac{\cos^2\phi(Z+\tan\phi)}{\overline{W}_T+\dfrac{\rho_AV_Bgy}{T}}. \quad (15)$$

This expression is seen to be identical to the previously developed sensitivity formula (eq (9)) except for the addition of the second term in the denominator which shows the various extraneous factors which exert an effect on sensitivity when the balance is in violation of requirement 1 for buoyant equilibrium. It is seen that x has dropped out, a fact which tends to simplify adjustment.

Violation of requirement 2. When the density of the hanging load, ρ_H, differs from that of the beam, ρ_B, air density, ρ_A, exerts an effect on ϕ, thus:

$$\frac{d\phi}{d\rho_A}=\frac{\cos^2\phi\left[\dfrac{\overline{W}_H(Q+T\tan\phi)}{\rho_H-\rho_A}-\dfrac{\overline{W}_B(R-T\tan\phi)}{\rho_B-\rho_A}\right]}{T\overline{W}_T} \quad (16)$$

When $\rho_H=\rho_B$ this function becomes zero, however, this is rarely the case, because the density of the load on the pan (which cannot be anticipated by the manufacturer) exerts an influence on the net suspension density, ρ_H. What the balance maker can do is adjust the density of his beam and of his suspension (with all built-in weights in place) to *midrange* between the maximum and minimum values of ρ_H which is likely to be encountered in laboratory work. Our (loaded) suspension weighs about 50 g, 20 of which are made up of built-in weights of density 7.75 g/cm³. The densities of the suspension and beam are each about 4 g/cm³. When the built-in weights are removed and replaced alternatively by a 20-g pan load of aluminum and then platinum, ρ_H changes only from about 3 g/cm² to 5 g/cm³.

The effects of buoyant inequilibrium are not always insignificant, and it is difficult to separate the effects of beam shortcomings and suspension shortcomings. What one can demand, however, is that the "observed zero" on the calibrated scale and sensitivity be independent of ρ_A. We observed our system on days of high values of ρ_A and low. We could not detect a systematic relationship between Φ and ρ_A over the limited range of ρ_A available to us because of other sources of zero drift. Out of curiosity we placed our balance in a closed system and reduced ρ_A from about 0.0012 g/cm³ to near zero by evacuating it. The beam rotated to indicate an increase in $\overline{W}_L$ of about 1700 μg which was taken to indicate adequate buoyant equilibrium. This test is unnecessary and is not recommended.

Damping. A direct-reading balance used in air-weighing should be damped so that the beam swings quickly to its equilibrium position and thereafter remains motionless. Viscous (i.e., air) damping is used on most direct reading balances. A person not familiar with balances is usually shocked at the apparently gigantic size of the damper, considering the vanishingly small forces to be damped. The answer lies in the clearance which must be left between the damping vane and dash pot. The clearance must be large, because a particle of dust caught between these members could completely destroy the precision of the system. However the damping vane cannot be made indefinitely larger because zero drift (resulting from sail effect) would become intolerable. Damper requirements are minimized when the moment of inertia of the system is minimized, and also (for any given beam frequency) sensitivity is maximum. Moment of inertia is minimized when both the load arm and counter-weight arm are minimum. In our system, both arms are held to within a few millimeters of 5 cm. The damping vane is about 1 in in diameter, and zero drift is rarely more than a few micrograms per minute. In hydrostatic operation, the damping associated with the immersed load is far greater than that obtained during an air weighing, so air damping is not an essential feature of a direct reading balance used only in hydrostatic work.

The ideal hydrostatic balance. From the foregoing comments it is obvious that the criteria upon which a direct-reading hydrostatic balance is judged differ significantly from criteria applied to air-weighing systems. Equation (7) shows that the principal masses in the system (the beam, the suspension, and the load) are equally important in the static situation; but in the distribution of total mass, the designer must operate under dynamic and engineering-type restrictions. For maximum sensitivity and beam frequency, minimization of moment of inertia is called for. He obviously wants the useful load to be a large fraction of

the total, which demands a suspension sufficiently massive to support the load and a beam sufficiently massive to support the loaded suspension and maintain the integrity of triangle LPB. As total mass increases, sensitivity is lost. Increasing the Z ratio to regain S results eventually in loss of adequacy of rigidity. Decreasing total size to improve S results in knife imperfections assuming importance. Attempts to decrease F result in degradation of sensitivity and range.

It occurs to us that many of these restrictions would disappear in a system in which the beam is driven to a null position (probably cot $\Phi = Z$) by a servo-controlled force. Almer and Bowman [4] have pointed out how such an arrangement will minimize arrestment and knife-edge problems. Various corrections as well as damping could be inherent in the feed-back loop so zero drift could be reduced.

This would give the designer great latitude in non-symmetrical configuration. Torsion fiber balances may have on-scale ranges much larger than that of our balance. If the major load were supported by knife edges and the servo-controlled torque applied by means of a torsion fiber, there would be an enormous increase in sensitivity, linearity, and on-scale range. It would be quite practical to restrict mechanically the beam to a very small Φ_T, so that F would be very nearly zero, thereby minimizing many suspension wire problems. With greater on-scale range, an entire decade of built-in suspension weights could be eliminated (along with their calibration uncertainties). Elimination of the smallest decade (0.01 g to 0.1 g) would make it possible to use ring weights centered on the suspension for dial operation. This would minimize the horizontal suspension forces associated with off-center dial-operated weights.

Many years ago, H. S. Peiser, NBS, proposed by private communication total immersion of a torsion fiber balance in the hydrostatic fluid as a means of eliminating meniscus uncertainties and minimizing the thermal drift in the balance. Certain practical problems prevented pursuit of this approach; however, the same basic idea could be applied to a force measuring system built around a load cell. If the cell itself were immersed in the hydrostatic fluid, there would be no air-water interface, and the entire meniscus uncertainty would be eliminated from the measurement. Semiconductor strain gauges of adequate sensitivity are currently on the market. Their principal drawback is temperature dependence. Immersion of the cell in the (very well thermostated) fluid would minimize uncertainties from this cause.

These comments are largely speculative but not entirely so. We experimented with an electronically controlled equal-arm balance. Although it was not a null-balance type servo-control (it was an electronic spring type) we were delighted at the speed of response, stability, damping and small load pan fall. For various reasons, not pertinent here, the precision was inadequate. NBS staff members have experimented with large size load cells (1000 kg) in certain high precision weighing situations, and found that when properly used, they can be made to rival the performance of high quality balances.

Balance modifications. Whereas Henins used his balance in the "as delivered" condition, we made a few minor modifications to ours to adapt it to the hydrostatic situation.

(a) Performance is degraded when the balance door is opened. In the water-cycle of our experiment the door must be opened twice during each observation—first to place a sensitivity weight on the pan, and second to remove it. In the air cycle two of the four door openings in each observation are for manipulation of this weight. We drilled a small hole in the door of the balance to permit placing this weight on the pan and removing it by a rotating rod—thereby eliminating four of the six necessary door-openings.

(b) When the relative humidity in the laboratory was quite low (in the winter) we had problems associated with surface evaporation in the vicinity of the meniscus. To minimize this, a small dish of water was placed below the balance and near the hole in the bench through which the suspension to the hydrostatic fluid led. This required raising the legs of the balance by about 2 in to accommodate the dish. At the same time the open space between the bottom of the balance and the bench top was sealed by aluminum foil held in place by masking tape to protect the exposed hydrostatic suspension from drafts.

(c) Measurements made on balances of this type are based upon the assumption that the apparent weight removed from the suspension by dialing is equal to the apparent weight of the pan load (except for the indicated difference on the scale). Apparent weight by definition is a function of air density, so we drilled holes in the top of the balance to receive temperature and humidity sensors for the upper balance compartment where the dial operated weights were stored. Sensors for the pan compartment were already in place. We found that the air density in the upper compartment was usually within a microgram per cubic centimeter of that in the pan compartment. Inasmuch as the built-in weights displaced about 2 cm^3, the systematic error involved was only marginally significant. Great effort was expended to assure that the upper and lower temperature and humidity sensors did not carry a residual bias.

4.2. Hydrostatic Suspension

This assembly delivers to the balance alternately the "pan-loaded" information and the "pan-empty" information, the difference being the apparent weight in water of the unknown object, $g(M_x - \rho_w V_x)$, which is used in our simultaneous solution for ρ_x. It hangs below the balance pan, passing through a hole in the floor of the balance case, penetrating the water surface, and extends to a depth of a few inches below the water surface. The portion of the assembly which is actually supported by the balance pan must be considered as part of the load capacity of the balance, so the heavier the load portion of the suspension assem-

bly, the smaller the maximum allowable load which we may test. This assembly has several components which will be discussed separately, commencing at the bottom.

The sample unloading device, as the name implies, is the mechanism which removes the unknown object from the immersed pan when it is desired that the balance report on the loading under the "pan-empty" condition. This assembly is made of stainless steel in hopes that no water contamination will result from its surfaces. Figure 4 shows it to be a pair of linear

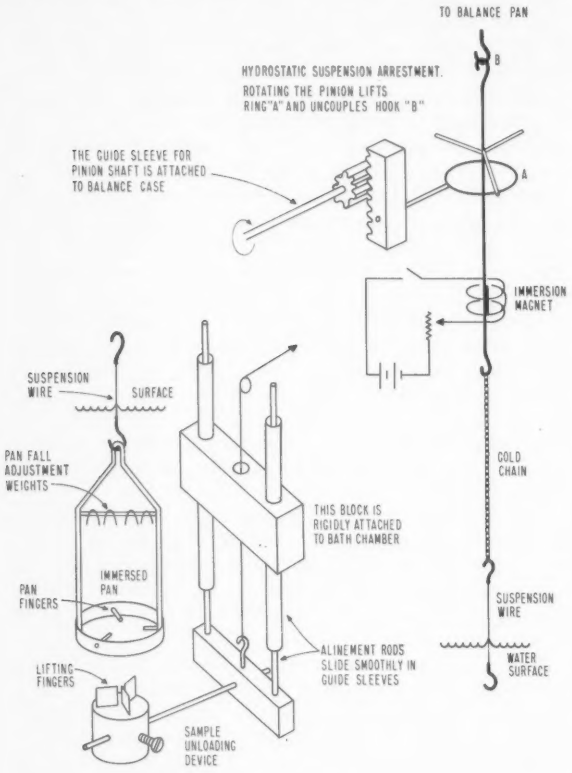

FIGURE 4

motion guides alined parallel so that the fingers which lift the unknown object from the pan will move approximately vertically. It is rigidly attached to the hydrostatic bath which has all degrees of freedom of position adjustment. The fingers which carry the unknown load when it is off of the pan form a plane, and this plane must be adjusted (by chamber adjustment) so that it is parallel to the plane formed by the pan fingers which carry the unknown load when the load is on the pan. In this way the unknown load is lifted smoothly off of the pan without tilting, and redeposited on the pan as required by the experiment.

The immersed pan hangs at the bottom of the suspension. It is made of brass to which are soft soldered the copper wire fingers which carry the unknown load during the "pan-loaded" cycle. The entire assembly is chrome-plated to avoid the contamination of the water by any oxides which may form on its surfaces. The plane formed by the pan fingers is adjusted to the horizontal by tiny wire weights and bending of the fingers, when the pan is empty and suspended by the top hook. This adjustment is important, and when once made need not be repeated. The intent of this adjustment is to achieve a horizontal pan finger plane, and when the lifting finger plane is made parallel to it, both planes are horizontal. Under these conditions, raising and lowering the lifting finger plane, by manipulating the sample unloading device, transfers the load of the unknown object alternately from the pan to the sample unloading device. If this load exchange is performed several times before the start of the experiment, the unknown load will move horizontally until its effective center of mass lies vertically below the suspension, at which time horizontal motion ceases. Thereafter the load may be lifted from the pan completely free from shock due to malalinement or tilting of the sample, both of which cause horizontal motion of the suspension which results in serious variability in data.

The suspension wire. Variability in the (downward) surface tension force associated with the meniscus surrounding the point of penetration of the water surface by the suspension wire has always been a major limitation in high reproducibility hydrostatic work. The problems become much greater as the size of the sample is reduced as the following argument shows:

(a) The actual magnitude of the force for a water meniscus is about 72 dyn per centimeter length of the meniscus, which is approximately equal to the circumference of the wire; therefore the wire is properly made no larger than is actually required to support the tensile load.

(b) If the load is reduced by a factor of four, the minimum acceptable cross-section area is also reduced by this factor, but under these circumstances the circumference is reduced by only a factor of two. Thus, if the percentage reproducibility of the surface tension force remains constant, the actual variability (in terms of total load) is doubled.

The above remarks are probably too optimistic, because the effective length of the meniscus is greater than the circumference of the wire, therefore the meniscus length actually decreases at a rate slower than the circumference. Additionally, since the total surface tension force is not distributed evenly around the meniscus (microscopic examination shows it may climb higher in some spot than others), an averaging process operates more efficiently on a long meniscus than on a short one.

The magnitude of this force for a wire 0.001 in in diameter is about 0.6 dyn. Inasmuch as we are attempting to measure total force to 0.003 or 0.004 dyn, severe requirements are placed upon meniscus stability, especially when it is considered that convective and turbulent water motion can account for a large part of this allowed variability. For years, experimenters have depended upon rough coatings

of gold, platinum, and other materials electrically deposited on the wire surface, so that water would flow up the sides of the wire by capillary attraction, thereby forming a zero (and hence reproducible) contact angle. These devices work, but not reliably.

We experimented with numerous suspension wires of various materials with coatings formed by several electrochemical techniques. About 25 percent of these wires were found to contain a section which provided meniscus stability to about 0.01 dyn. The usable sections of these wires were photographed, and it was noted that in each case the coating had a fairly fine granular structure uniformly covering the wire.

Figures 5A and 5B are photomicrographs of different sections of the same piece of wire treated by classical techniques to achieve the desired granular rough surface illustrated. When the meniscus was formed around the section shown in figure 5A, the hydrostatic performance was inadequate. After lowering the level of the water in the weighing chamber several times to permit the meniscus to form around different sections of the wire, a spot was finally located where performance was satisfactory. This section is shown in figure 5B. The difference between good and bad performance is ascribed to the presence of spots on the wire where the rough coating either did not form or where, after formation, it flaked off. Formation is inhibited when one of the tiny gas bubbles, which form on the wire surface during electrodeposition, clings to the wire rather than breaking away and rising to the surface of the electroplating bath. To prevent these bubbles from remaining on the wire surface it is customary to agitate mechanically the wire during the plating process; however the agitation itself will frequently cause the fragile coating already formed to flake away, leaving a bare (and hence unsatisfactory) surface. Unsatisfactory plating also results from inadequate control of electric current density at the plated surface and from improper solution strength or process temperature. After plating, the wire must be thoroughly cleaned to eliminate traces of the electroplating solution, otherwise contamination of the hydrostatic weighing water results. Henins followed the plating and cleaning processes with a careful optical examination of the wire surface at 200X. The fabrication of a wire by classical techniques to these performance tolerances is a task requiring much patience, skill and luck.

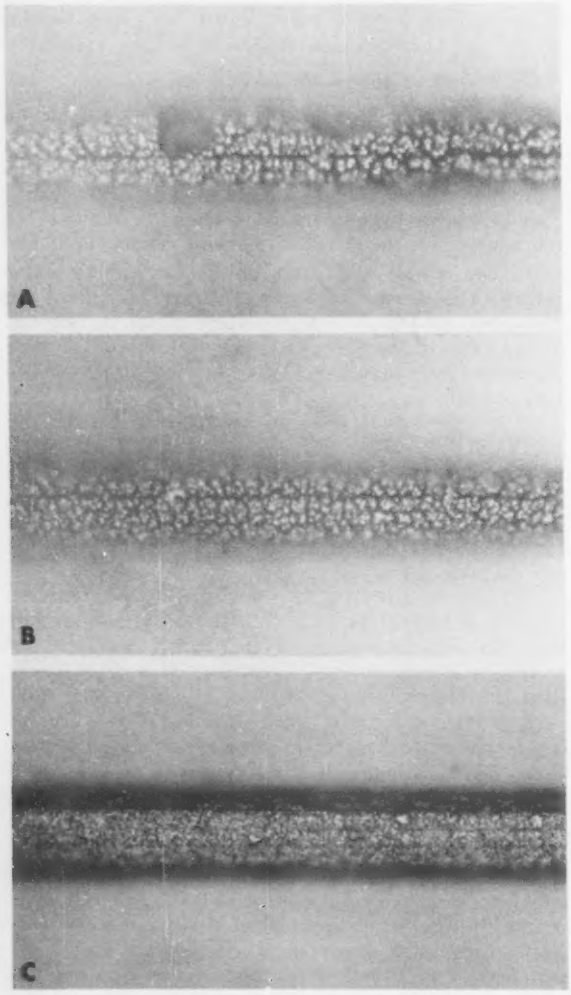

FIGURE 5

We experimented with several alternative methods of wire fabrication and found that the most simple technique was the most reliable. A coating of chromium oxide was formed on the surface of nichrome wire by electrically heating it to a medium red heat in a 1 to 10 μ vacuum for about an hour.

While hot, the oxide coating is smooth, but when the electricity is turned off the parent metal cools and contracts, resulting in the brittle oxide coating breaking up into the desired surface structure. Such a wire is shown in figure 5C. It is evident that the surface is much more uniformly granular than in figures 5A or 5B, and that the grain size is significantly smaller.

During the past year several dozen wires have been made by this technique and every wire performed adequately. In about one-half of the tests the first section of wire tried out gave satisfactory performance. In the other half it was necessary to drop the water level a few millimeters (so that the meniscus formed on a different section of the wire) to find a section of adequate performance. We have rarely been required to try out a third section. This is in sharp contrast to performance of electrically coated wires which frequently (after trying out many sections) turn out to have *no* adequate section whatsoever.

This process has an important by-product. During the heating cycle, all traces of dirt and grease are burned away, and it is possible to place the wire in service immediately upon completion of fabrication

without an intermediate cleaning process or optical examination.

Our procedure for making hydrostatic suspension wires is as follows:

(a) Two hooks are bent from #18 copper wire, figure 6, and a piece of 0.001″ nichrome wire tied between them. After tying, the nichrome length should be 6 cm.

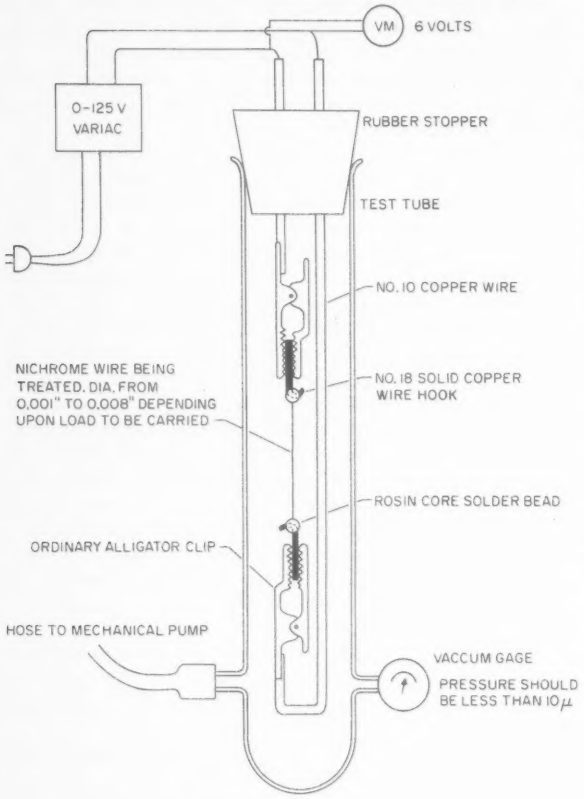

FIGURE 6

(b) Using rosin core solder, a bead is made at each hook. Although this solder does not wet the nichrome, it holds it firmly in place mechanically. The unit is soaked in benzene to remove the rosin.

(c) It is then placed in a holder built into a rubber stopper which may be inserted into a vacuum system and electrical leads are attached (see fig. 6).

(d) The vacuum pump is turned on and when the pressure is down to 1 to 10 μ the electricity (set to 6V ac) is turned on.

(e) After 1 hr the pump and current are turned off and the wire is put into service.

We have recently found that if the wire is initially wet with a stream of steam just before placing it in water the performance is improved. Although this is a tempting path of further investigation, other errors of greater magnitude demand attention.

The immersion magnet. This is a very useful contribution to the art from Henins. It is a tiny wire magnet weighing perhaps 0.2 g which is cemented to the suspension link between the upper hook of the suspension wire and the hydrostatic suspension arrestment. Surrounding the suspension in the vicinity of this magnetic wire is a 30-turn electric coil which when energized causes the suspension to dip a few millimeters. Henins used this device as a test of proper functioning of the suspension wire. In such service it is excellent however, as will be explained later, this is only one-half of the test. That is, a wire which fails this test will not function at the position tested; however wires which do pass this test may fail on even more critical tests later. The tests are quite simple (10 min maximum to find a satisfactory spot) if the proposed method of wire treatment is used. Before attaching a magnet to the suspension system of a balance, one should verify that ambient field changes will not cause significant balance drift. In one of our experiments, nonreproducibility was traced to field changes caused by work in a nearby laboratory.

The hydrostatic suspension arrestment is the device which uncouples the hydrostatic suspension from the balance for air-weighing operation. Its design is not critical, the only requirements being that:

(a) It operate without mechanically shocking the system, and

(b) arresting and releasing the hydrostatic suspension results in reproducible coupling of the suspension to the balance pan. Our design is shown in figure 4.

5. Sample Handling and Degassing

It is generally recognized that air adhering to the surfaces of the test sample is a major source of nonreproducibility in independent density measurements. If this surface-trapped air were a random phenomenon, the only effect would be to degrade the standard deviation of a single observation, and exert little effect on the mean value of several observations. However, surface air causes a *systematic* effect in that it always acts to make the measured value of $\overline{W}_w$ (and hence the calculated density) appear lower.

A bubble of air large enough to displace 1 μg of water can be removed after detection by a suitable optical arrangement. On the other hand, the same amount of air dispersed among a large number of very tiny bubbles would go completely undetected except for its derogatory effect on precision.

The method initially used for comparison of degassing techniques was to measure the density of samples after being degassed by various methods. The difficulty in this method was that as degassing methods improved, the indicated density changes became smaller and finally, when they became of the order of the experimental variability, they were

impossible to detect without an impractically large number of observations.

We were fortunate to have a Cartesian diver whose standard deviation was significantly lower than that of classical hydrostatic systems, which we could use for comparison of degassing techniques. Actually, the problem was first attacked because surface gas was seriously degrading Cartesian diver data.

Our Cartesian diver system [3] provides values of $\overline{W}_w$ to a much higher precision than the system described here but with inordinately greater effort. Additionally, values of $\overline{W}_W$ are not degraded by meniscus uncertainties inasmuch as it is a completely immersed system. Since it operates at 3.98 °C slight errors in thermostating do not cause significant variability in ρ_W. Variability in values of density calculated from diver data is caused almost entirely by variability in surface-bound gas on the sample.

In these experiments we used two thin disks of single crystal silicon. This geometric form is ordinarily avoided in hydrostatic work because of the relatively large surface area upon which gas may adhere, but in this experiment we particularly wanted a large area to magnify the effect.

Three series of experiments were performed: The first, in which the crystals were cleaned by the technique used by Henins, that is, by immersion of the crystal in water below a vacuum; the second by ordinary outgassing for 24 hr under a 1 μ vacuum and a temperature estimated to be about 75 to 100 °C from an infrared heat lamp; the third series of experiments utilized a boiling technique to be described.

Between each measurement in a given series, both crystals were removed from the hydrostatic system, exposed to air, dried, and recleaned and degassed. Ordinarily they would have been air weighed between each measurement, but we wanted to eliminate any variability in the calculated value of ρ_X from variability due to this source, so they were air weighed only once for each series, immediately prior to the first hydrostatic experiment in the series, The data is shown below.

	Henins method		Heat and vacuum		Boiling	
	Sample 1	Sample 2	Sample 1	Sample 2	Sample 1	Sample 2
Test 1	2.3289957	2.3289972	2.3289937	2.3289991	2.3289950	2.3290012
Test 2	2.3289970	2.3289986	2.3289975	2.3289997	2.3289958	2.3290018
Test 3	2.3289930	2.3289972	2.3289964	2.3290013	2.3289944	2.3290017
Test 4	2.3289965	2.3289980	2.3289959	2.3290013	2.3289950	2.3290015
Test 5	2.3289946	2.3289964				
Std. dev.....16		08	16	10	06	03

The above data show that the boiling technique results in a standard deviation in density significantly lower than either of the other two techniques which was most gratifying because the boiling procedure is far simpler than either of the other two methods. It is also noted that the standard deviation of measured values of density of sample #1 is always about twice as great as that for sample #2, regardless of the degassing technique used. We frequently observe this phenomenon, and whenever it has occurred previously, a careful microscopic examination has always disclosed a crack or crevice in the sample. A most methodical examination failed to disclose such a shortcoming on the surface of sample #1 in these experiments and we can offer no explanation for this observed effect.

The boiling technique, which is shown by the above data to provide the best degassing of the three methods being compared, is performed as follows:

(1) The sample is immersed in a small vessel containing room-temperature (but previously boiled) water.

(2) Using a hot plate or very low flame, it is brought slowly to a boil and allowed to boil for several minutes. At the end of this boiling interval, the boiling should be quite vigorous.

(3) The water is cooled to a fairly low temperature with the vessel covered. The lower the temperature, the better as long as there is no freezing.

We have the impression that there are two mechanisms involved in this boiling process. First is that steam will form on particles of surface-trapped air as though the air were acting as a seed. When boiling is "just" commencing, many tiny trains of steam bubbles can be seen originating from stationary discreet points on the sample surface. These points do not wander around on the surface; however, without warning, a train of bubbles will stop forming. We take this to indicate that the train of steam bubbles has either removed the air gradually or that the mechanical agitation associated with the boiling has broken it loose from the sample surface and permitted it to rise to the water surface. The second mechanism believed operating is that in the cooling of the water it becomes a better solvent for any residual surface-trapped air.

We are unable to explain why the boiling associated with the vacuum in the other two processes fails to act as efficiently as the boiling associated with heating. It is possible that the cleaning procedures used to clean samples prior to density measurements leave a grease coating on the sample which holds air between the coating and the sample, and that heating melts the grease and permits the air to escape.

This degassing technique has been used in connection with density measurements on rutile, fused silica, nichrome, gold, platinum, and titanium in addition to single crystal silicon. No systematic effect on the efficiency of this method as a function of material was noted and we believe, without proof, that it will perform adequately on many materials for which density measurements by water weighing are appropriate.

6. Weighing Procedure

In this section we are concerned with obtaining values of 0_A and 0_W, the balance observations when

the object of interest is immersed in air and water respectively, from which the values of $\overline{W}_A$ and $\overline{W}_W$ are calculated. For various reasons to be explained, the air weighing should be performed first.

6.1. Air Weighing Cycle

After cleaning, the object of interest should be kept in the balance case several hours to come in to thermal equilibrium with the surrounding air. The air weighing cycle of the experiment consists of observing the balance under five conditions.

(a) The balance pan empty.

(b) The pan loaded by the object of interest.

(c) The pan loaded by the object of interest and also by the remotely controlled sensitivity weight discussed in section 4.

(d) The object of interest removed from the pan, but with the sensitivity weight remaining in place.

(e) The sensitivity weight removed, that is, a repeat of the first condition.

Under each of the above five conditions we obtain an observation of the dial indication, D_0, and an accompanying screen observation, s_0. Each value of D_0 is corrected into a value of D_t by eq 13. If the screen is assumed to be adequately linear the five values of s_0 may be used as recorded, in which case they are named s_t rather than s_0. If tests have shown the screen to be nonlinear, then an appropriate correction must be applied to each s_0 to convert it into s_t, in a manner comparable to eq (12) (which applies *only to our balance*).

The first, fourth, and fifth values of D_t are equal as are the second and third, thus:

$$D_{t1} = D_{t4} = D_{t5}$$
$$D_{t2} = D_{t3}.$$

This reduces to two (D_{t1} and D_{t2}) the number of dial readings which must be operated upon. These two values of D_t and the five values of s_t are combined in the following formula to provide a value of 0_A, the balance observation in the air cycle:

$$0_A = D_{t2} - D_{t1} + \frac{G(S_{t2} - s_{t1} + s_{t3} - s_{t4})}{s_{t3} - s_{t2} + s_{t4} - s_{t5}} \qquad (17)$$

where G is the mass of the sensitivity weight (in our experiment $G = 0.0049992$ g). Use of this five-observation format, reduced as shown in eq (17), tends to minimize the effects of balance drift on the value of 0_A. In our work we always carried out this entire procedure four times, thereby obtaining four values of the balance observation and averaged them to obtain a single value of 0_A. In conjunction with these air weighings, temperature, barometric pressure and relative humidity were observed and recorded for later calculation of air density.

6.2. Water Weighing Cycle

When the various parts of the immersed structure are thoroughly cleaned, they should be assembled as described in section 4. Following this, the water weighing chamber should be filled with distilled water. In the filling process air bubbles will be trapped on most of the immersed surfaces. After filling, we have found it convenient to boil the entire system for a few minutes with immersion heaters to remove this air. After boiling, the system requires several hours (usually overnight) to attain thermal stability. The water weighing procedure is divided into four distinct groups of tasks, the first three of which may be performed during the latter part of the stabilizing period: (a) degassing the sample, (b) adjusting the system, (c) testing the system, (d) making the observations.

(*a*) *Degassing the sample* should be performed as described in the immediately preceding section. Then the sample should be transferred, while completely immersed in a dipper, into the hydrostatic bath. During this procedure, the balance should be arrested and the hydrostatic suspension arrestment should be in the "release" position. The immersed pan unloading device should be in the "unload" position and the sample should be placed on the lifting fingers of this device—*not* on the immersed pan fingers. During this loading process, a small amount of off-temperature water will be added to the system (from the dipper) which will change the bath temperature. Inasmuch as the bath has presumably not yet come into equilibrium, this additional upset causes no extra waiting; however, this loading procedure should be performed early in the experiment.

(*b*) *Adjusting the system* should be performed late in the waiting period because, although there are several tasks involved, individually they require only a few minutes each. There should be a smooth transition between these preliminary tasks and the primary task of making the observations. These comments hold only for a freshly filled system. We find that we are able to operate a system for four or five days before it becomes so corrupted by dust and dirt that recleaning is necessary. For a previously filled system, steps (b) and (c) may be performed as soon as the P.R.T. (platinum resistance thermometer) indicates that the thermal shock associated with loading has dissipated. The objective of the tasks in group (b) is to achieve a system adjustment such that the sample may be loaded and unloaded from the immersed pan and the dial-operated weights in the balance may be changed without mechanically shocking the system. These tasks are performed as follows:

(1) The sample should be loaded and unloaded from the immersed pan several times until its center of gravity is located directly below the vertical axis of the hydrostatic suspension. This is easily accomplished by external manipulation of the immersed pan unloading device as discussed in section 4. This process is performed with the balance arrested and the hydrostatic suspension arresting device in the "release" position.

(2) The operator should next release the balance in accordance with the manufacturer's instructions and determine by experiment the *dial positions* which

place the system in on-scale equilibrium for both the immersed pan-empty and the immersed pan-loaded conditions. Even the best direct-reading balances have residual malalinement of the built-in dial-operated weights, and the operator will find that certain combinations (dial positions) will result in violent kicking of the suspension when released. We have gained some experience in overcoming this difficulty and possible remedies are discussed in the section on Operating Hints. Manufacturers give scant attention to this problem because it is bothersome only to experimenters doing water weighing. The effect of this weight misalinement appears to be negligible in ordinary air weighing.

(3) The final step in group (b) is to clean the water surface in the vicinity of the meniscus. This is accomplished by opening a port in a glass tube surrounding the suspension (to protect it from air currents) and vacuum cleaning the surface with a drawn-out glass tube. This is critical inasmuch as a particle of dust at the meniscus will destroy its reproducibility. We have found that back-lighting this surface makes specks of dust floating on the surface stand out clearly in the specular light.

This concludes the system adjustment. When properly performed, it should be possible to load the immersed pan and set the dials, so that when the balance is released it moves smoothly to an indication on the screen. Then after arrestment and immersed pan unloading, the dials should be set to predetermined positions and upon balance release there should be no mechanical shock to the hydrostatic suspension and the balance should move smoothly to a screen reading within about a few milligrams of the previous reading.

(*c*) *Testing the system* is the last of the preliminary steps prior to observations. As previously mentioned, there should be a smooth transition from this step to the final step of making the observations. In other words, as soon as these tests indicate adequate performance, testing (as such) is terminated and observations begin. The test procedure is very similar to the observing procedure, but the operator *must not* use the "last few" test runs as observing runs since this is comparable to data selection in which case the statistical analysis of the results would be put in jeopardy. In the system test procedure, we are basically testing the operation of our suspension wire. We have stated that 100 percent of the wires made by the procedure described have contained a section of adequate surface roughness and uniformity to provide high quality water weighing data. On the other hand, we have found that in about 50 percent of the cases the first section of the wire we attempt to use is inadequate and we must lower the water level a bit to expose a different section. We have occasionally had to try out a third section, but, to date, we have not had to make a fourth try. The system test to be described is basically a quick method of determining whether the section of wire being tried out is adequate for the task. It is performed in two steps, the first is a rough test only, using the suspension magnet (fig. 4) to deflect the balance, but in the second step the built-in sensitivity weight is actually used as in the final measurements.

When we are ready to start the system test procedure, we release the balance with no load on the immersed pan and we adjust the magnet current to dip the hydrostatic suspension deeply enough to cause the balance screen reading to increase by about 10 to 12 mg. The magnet is energized a few times to insure that the section of wire immediately above the section to be tested is thoroughly wetted by the hydrostatic water. The test is then performed as follows:

(1) The balance is released and the screen reading is observed and recorded.

(2) Without arresting the balance, the magnet is energized until the "deep" position is attained, after which it is de-energized and the balance permitted to return to its normal position. The screen is again read and recorded.

(3) Steps 1 and 2 are repeated several times, arresting and releasing the balance each time after making the observation called for in step 2. If the differences between the observations recorded in steps 1 and 2 are constant to within a few micrograms, we may proceed to step 4. If they are not constant, we may assume that the active section of the wire surface is inadequate and the water level is lowered a few millimeters to expose a new surface, and the above test procedure is repeated. When an adequate section of wire is located, we proceed with step 4.

(4) In step 4 the balance is observed under each of 5 conditions, and in each condition a value of D_0 and an accompanying value of s_0 is taken.

(a) The balance is released and observed in the "immersed pan empty" condition, after which it is arrested.

(b) Using the immersed pan unloading device described in section 4, the sample is placed on the immersed pan. The balance is then released and observed, after which it is arrested.

(c) The sensitivity weight is then loaded by the remote linkage. The balance is then released and observed, after which it is arrested.

(d) Using the immersed pan unloading device, the sample is removed from the immersed pan. The balance is then released and observed, after which it is arrested.

(e) The remote control sensitivity weight is removed from the pan. The balance is then released and observed, after which it is arrested. This is a repeat of the first condition.

(5) Values of D_0 and s_0 recorded during the water weighing cycle are corrected into values of D_t and s_t in the same manner as described above in "Air Weighing Procedure." Again $D_{t1}=D_{t4}=D_{t5}$ and $D_{t2}=D_{t3}$, so we confine operations to only two D's and five s's. These are combined into a value of 0_W, the balance observation in the water cycle, as follows:

$$0_W = D_{t2} - D_{t1} + \frac{(G)\ (s_{t2} + s_{t3} - s_{t1} - s_{t4})}{(s_{t3} + s_{t4} - s_{t2} - s_{t5})}. \qquad (18)$$

The system is judged to be performing adequately when successive values of 0_W repeat to within about 5 μg.

(*d*) *The observations* are made in the exact same manner as described immediately above. We repeat the process four times to obtain four values of 0_W which are averaged to a single value.

(*e*) *While making the observations* leading to 0_W, the parameters necessary for the calculation of air and water densities are recorded.

As stated in the introduction we are interested in obtaining the apparent weight of the sample in media of two different, but known, densities. The apparent weights of the object in air and water, $\overline{W}_A$ and $\overline{W}_W$, respectively, are given by

$$\overline{W}_A = 0_A\,(1-\rho_{AU}/\rho_s) \tag{19}$$

$$\overline{W}_W = 0_W\,(1-\rho_{WU}/\rho_s) \tag{20}$$

where ρ_s is the density of the built-in weights (7.75 g/cm^3 in our balance) and ρ_{AU} and ρ_{WU} the air density in the upper balance chamber housing the built-in weights during measurements of 0_A and 0_W respectively. As previously pointed out, there is usually no significant difference between the air density in the upper and lower balance chambers, so, except for the most critical work separate sensors in both of these two chambers are unnecessary. ρ_{AU} and ρ_{WU} are calculated by eq (4) from observations of temperature, barometric pressure and relative humidity recorded during observations for 0_A and 0_W respectively.

7. Data Reduction and Measurements on Silicon

7.1. Calculations of Density

In the Introduction it was stated that the unknown density was obtained from a simultaneous solution of

$$\overline{W}_A = g(M_X - \rho_A V_X)$$

$$\overline{W}_W = g(M_X - \rho_W V_X)$$

This presupposes that V_X has the same value in both the air and water cycles of the experiment, which occurs only when the sample has the same temperature in both cycles. We are ordinarily interested in sample density at some temperature, T_N, which is not perfectly achieved in either cycle. The simultaneous pair for these general conditions is properly written

$$\overline{W}_A = gM_X - g\rho_A V_{T_N}\,[1-K(T_N-t_A)]$$

$$\overline{W}_W = gM_X - g\rho_W V_{T_N}\,[1-K(T_N-t_W)]$$

where V_{T_N} is the volume of the object at the temperature of interest, K the volumetric coefficient of thermal expansion of the object, T_A the air temperature in the pan compartment of the balance during observations for 0_A and t_W the temperature of the water during observations for 0_W. We are justified in assuming that the object of interest lies at temperatures t_A and t_W during the air and water cycles respectively, under which circumstances the solution of the foregoing pair for sample density at temperature T_N is given by

$$\rho_{T_N} = \frac{\overline{W}_A\rho_W Y - \overline{W}_W\rho_A X}{\overline{W}_A - \overline{W}_W} \tag{21}$$

where

$$X = 1-K(T_N-t_A) \tag{21A}$$

$$Y = 1-K(T_N-t_W). \tag{21B}$$

During the two cycles of the experiment, numerical values of the parameters tabulated below are recorded. Where instrumental corrections are appropriate they are assumed made.

Air Weighing Cycle

0_A = the balance observation in whatever units it is calibrated as explained in Air Weighing Procedure, (eq (17)).

t_A = the temperature in °C in the pan compartment of the balance.

t_{AU} = the temperature in °C of the air in the upper balance compartment.

H_A = the relative humidity (in %) in the pan compartment of the balance.

H_{AU} = the relative humidity (in %) in the upper chamber of the balance.

B_A = the barometric pressure in mm Hg in the laboratory.

ρ_S = the density of the built-in weights in g/cm^3.

K = the assumed value of the volumetric coefficient of expansion of the object of interest in parts per part per degree C.

NOTE: As previously pointed out, it is usually unnecessary to install separate temperature and humidity sensors in the two balance chambers; thus t_{AU} may be assumed equal to T_A and H_{AU} to H_A.

Water Weighing Cycle

0_W = the balance observation in units consistent with those in which 0_A are measured as explained in the Water Weighing Procedure (eq (18)).

t_W = the water temperature in °C.

t = the interval, in days, since boiling water for degassing.

B_W = the barometric pressure in mm Hg in the laboratory.

I = the depth of sample immersion in centimeters.

C = compressibility of water (47.7×10^{-6}/atm).

t_{WU} = upper balance chamber air temperature in °C. May be observed on thermometer in pan compartment as previously explained.

H_{WU} = upper balance chamber humidity (in %). May be observed on sensor in lower chamber as previously explained.

T_N = the temperature (in °C) at which the sample density is to be determined.

One method of reducing this data to a value of ρ_{T_N} is shown in the scheme graphically presented in figure 7.

In this calculation format it is assumed that the temperature of the unknown object is T_A during the air weighing cycle of the experiment and t_W during the water cycle. These assumptions are valid, however the use of an assumed value of K may introduce significant error because the actual value of K, for a particular object, may differ greatly from its tabulated value. Errors in calculated values of ρ_{T_N} associated with erroneous assumptions as to the value of K may be minimixed by holding the factors $(T_N - t_A)$ and $(T_N - t_W)$ near zero by careful adjustment of both the room temperature (and hence t_A) and the water temperature, t_W, to the desired temperature. T_N.

This may be impractical since room temperature adjustment is rarely very precise. An alternative approach is to perform the air weighing cycle first at any temperature, t_A, at the conclusion of which the water cycle is performed with the (relatively easily adjusted) water temperature, t_W, adjusted to within close tolerance of the previously used t_A. The value of T_N used in the calculation would then be arbitrarily assigned a value of T_1, midway between t_A and t_W, in which case the density at T_1 is determined. If T_1 is too far removed from T_N, this procedure may be repeated at T_2 (on the opposite side of T_N from T_1) and ρ_{TN} obtained by interpolation between ρ_{T1} and ρ_{T2}.

A third approach is to make several weighings both in air and water at various temperatures and form a least squares solution for M_X, V_{T_N}, and K, from which $\rho_{T_N} = \left(\frac{M_X}{V_{T_N}}\right)$ may be calculated, and by virtue of knowledge of K the density at any other temperature may be inferred.

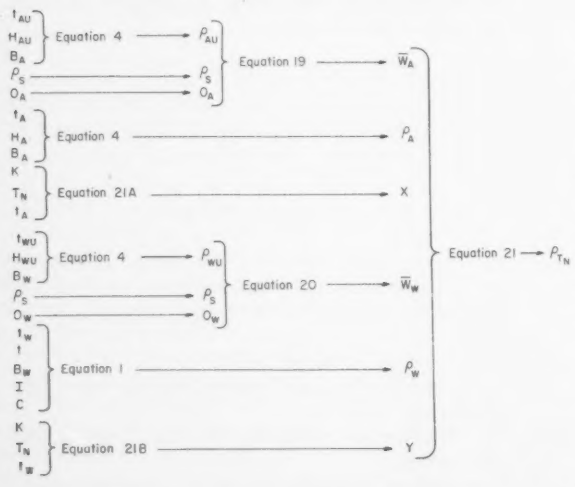

FIGURE 7. *Outline of calculations for density.*

7.2. Observations on Silicon

As stated in the introduction, one of the objectives of these studies was to determine how much variability in density was to be expected in crystals of silicon weighing 15 to 20 g cut from the same boule. Experiments (unreported) performed several years age indicated that differences of 20 to 30 parts per million could occur. Recently, two manufacturers submitted samples to NBS for evaluation, which, they felt would prove to be far more homogeneous than the samples previously examined. One boule was grown in a vacuum and one in argon. Three crystals were cut from widely dispersed positions in each boule and each of the six samples were hydrostatically weighed four times using the procedures described in the foregoing sections.

The raw data were reduced as shown in figure 7 to density values presented in table 1 and figure 8. The average value of the crystals cut from the vacuum grown boule was 2.3289824 g per cubic centimeter with the three crystals spread (in density) over a range of about 2 ppm. For the argon-grown boule the average was 2.3290221 g per cubic centimeter and about the same range in values.

TABLE 1

Vacuum grown boule		Argon grown boule	
	G/cm^3		G/cm^3
	2.3289824		2.3290218
	815		222
	806		167
	822		235
Avg.	2.3289817	Avg.	2.3290210
Est σ	0.0000009	Est σ	0.0000034
	2.3289821		2.3290247
	854		198
	844		238
	861		217
Avg.	2.3289845	Avg.	2.3290225
Est σ	0.0000020	Est σ	0.0000012
	2.3289793		2.3290225
	799		219
	849		230
	834		243
Avg.	2.3289819	Avg.	2.3290229
Est σ	0.0000028	Est σ	0.0000012

8. Operating Hints

During these experiments we have found several techniques which will make the hydrostatic operation much more convenient. The water temperature must be measured with great care inasmuch as this is the parameter responsible for major changes in water

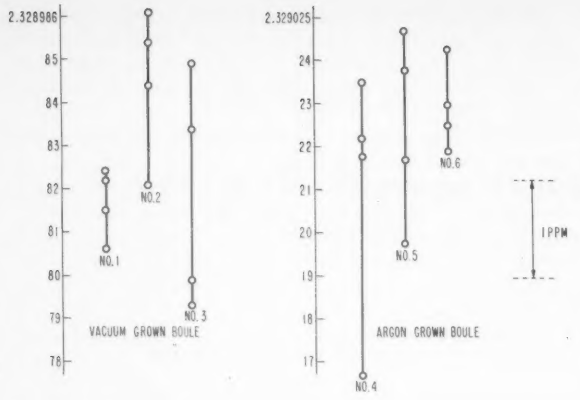

FIGURE 8. *This is a plot of all data taken on all six crystals, from which we may conclude that it is unlikely that the crystals cut from the same boule differ in density by much more than a very few parts per million.*

density. We use a platinum resistance thermometer, capsule type, placed at the same horizontal level and close by the sample being measured. This thermometer works into a Mueller Bridge with a wall galvanometer to indicate bridge unbalance. Good practice calls for a reversing switch in the battery line which we habitually use in the measurement. This is not a convenient measurement. In addition to the P.R.T. we also have a high sensitivity electronic thermometer which lacks the accuracy and stability of the P.R.T. but has the virtue of being direct reading to about 0.001 °C. This thermometer is primarily used to indicate when measurements should commence after a load change.

We have a thermal and (therefore) density gradient in the water in our hydrostatic chamber. When samples are removed from the pan and replaced by other samples, turbulent water motion exists thereafter for several minutes (sometimes 20 to 25 min when the process is carelessly performed). The electric thermometer shows rapid temperature changes of as much as 0.01 °C, up and down, while turbulence exists. When turbulence has subsided, as indicated by a stable temperature, the measurements are commenced.

We habitually keep the ends of the tongs and tweezers used to change the immersed pan loads submerged in the hydrostatic fluid. Although this undoubtedly provides a path for ingress or egress of heat, it has the overriding virtue of guarding against bubbles of air being transferred from the tools to the samples under observation.

Our hydrostatic weighing water is always maintained at a temperature slightly below room temperature. The room temperature may vary as much as ½ to 1 °C during a series of measurements. Water temperature is adjusted to about a degree below the lowest expected room temperature, although we have found that satisfactory measurements can be made with the water as low as 7 or 8 deg below room. If the water temperature is allowed to climb much more than 1 deg above ambient, measurements frequently become erratic. This is usually accompanied by a slight fogging of the glass tube penetrating the water surface, so we assume the upset in measurements is caused by condensation of moisture on the suspension chain within the tube.

When hydrostatic tests are called for upon samples which are too small to fit upon the immersed pan loading device we have found it convenient to use an auxiliary pan (for example, a thin disk of fused silica) which will fit on the unloading device. We then hydrostatically weigh this disk and calculate a value of $\overline{W}_W$ for it and then place the sample on the disk and determine a value of $\overline{W}_W$ applying to both, followed by a second value of W_W applying only to the disk. From these measurements it is possible to calculate a value of $\overline{W}_W$ applying only to the sample. The reproducibility in a measurement of this type is usually not very good, so such processes must frequently be repeated.

Knife edge balances perform surprisingly well while resting on surfaces which are not perfectly stable (such as a laboratory table with wooden legs). When such balances are used in hydrostatic weighing, vibrations become critical because the surface of the water in the vicinity of the meniscus must be quiet. We have found that looking at the reflection of a brightly lighted object from the underside of the water surface (that is, looking upward through the water at the surface) is a very simple and sensitive test of adequacy of stability. If the reflection of the object is motionless to the unaided eye the vibration level is sufficiently low. If the reflection is unstable, experimental reproducibility will be degraded. This test indicates which doors may not be opened or closed during an experiment or where people may not walk. We believe, without proof, that stability of the hydrostatic weighing chamber is most important, and that vibrations transmitted down the hydrostatic suspension from the balance to the water are somewhat less significant. A slight tap on the hydrostatic weighing chamber will set the water surface in motion, while a similar tap on the balance will hardly be detected.

We have received generous assistance from several people, both inside and outside NBS. Daniel P. Johnson provided guidance on theoretical problems. Richard Deslattes has consulted on a continuing basis and made careful x-ray measurements to insure that we experimented on truly state-of-the-art silicon. These remarkably fine crystals were provided by the Dow Corning Corporation and the Texas Instrument Corporation. M. R. Meyerson and J. Kruger consulted on metallurgical problems associated with the suspension wire experiments and Mrs. Theodora S. Welsko made many many fine metallurgical micrographs. Dr. Brenner of the Sigmund Cohn Corporation furnished ideas and experimental samples to aid in the wire experiments. The section on Air Density was prepared with detailed

guidance from Arnold Wexler, and that on Water Density from John Taylor. Geraldine Hailes and David Wooten assisted in automation of the data reduction and Robert Raybold and Hsien Ku gave guidance in experimental design and statistical analysis. The frequency of our references to Ivars Henins indicates the extent to which we borrowed from his work. H. S. Peiser assisted with manuscript preparation. His interest in density measurements as a tool for his own field (crystallography) has been a driving force in this and related work for many years. The authors are particularly indebted to Paul Pontius and A. G. McNish for many ideas and continuing encouragement and support.

9. References

[1] H. A. Bowman, R. M. Schoonover, W. H. Gallagher, 14.8–4–65, Proc. ISA–Los Angeles (1966).
[2] I. Henins, J. Res. NBS 68A (Phys. and Chem.), No. 5, 529–533 (1964).
[3] H. A. Bowman, R. M. Schoonover, J. Res. NBS **69C** (Engr. and Instr.) No. 3, 217–223 (1965).
[4] H. A. Bowman, H. E. Almer, J. Res. NBS **67C** (Engr. and Instr.) No. 3, 227–235 (1963).
[5] M. Thiessen, K. Schell, H. Disselhorst, Wiss. Abh. Phys.-techn. Reichsanst **3**, 1–70 (1900).
[6] P. Chappuis, Trav. mem. BIPM **13**, D1–D40 (1907).
[7] L. W. Tilton, J. K. Taylor, J. Res. NBS **18**, 205 (1937) R.P. 971.
[8] C. E. Guillaume, Trav. mem. BIPM **14**, A1–A276 (1910).
[9] P. Chappuis, Trav. mem. BIPM **14**, B1–B163 (1910).
[10] J. M. deLepinay, H. Buisson, J. R. Benoit, Trav. mem. BIPM **14**, C1–C127 (1910).
[11] I. Friedman, A. C. Redfield, B. Schoen, J. Harris, Rev. Geo. **2**, 177–224 (1964).
[12] A. C. Redfield, private communication.
[13] M. Woh and H. C. Urey, J. Chem. Phys. **3**, 411–414 (1935).
[14] Christiansen, Crabtree, Loby, Nature **135**, 870 (1935).
[15] F. Steckel, S. Szapirs, Trans. Faraday Soc. **59**, p. 333 (1963).
[16] Dorsey, Properties of Ordinary Water Substance (Reinhold, New York, 1940).
[17] P. Chappuis, Trav. mem. BIPM **14**, D1–D163 (1910).
[18] A. Wexler, NBS Circ. 586 (1957).
[19] A. Wexler, W. G. Brombacher, NBS Circ. 512 (1951).
[20] Harrison, L. P1, pp. 15–16, Humidity and Moisture, **3**, edited by Wexler, A. and Wildhack, W. (Reinhold, New York, 1965).
[21] NBS Circular 564, table 2A, p. 25 (1955).
[22] Goff, J. A. and Gratch, S., Smithsonian Meteorological Tables, 6th edition, Smithsonian Institution, Washington, D.C. (1958).
[23] Almer, H. E., Bowman, H. A., Jensen, M. W., Macurdy, L. B., Peiser, H. S. Wasko, B., J. Res. NBS **68C** (Engr. and Instr.), No. 3, 141–154 (1964).

10. Appendix. The Calibration of Built-in Weights of Direct Reading Balances

M. W. Jones

A convenient procedure for obtaining an estimate of the adjustment errors of built-in weights in direct-reading balances is to load the pan with standard weights, and to ascribe failure of the balance to indicate this known load correctly to adjustment error. This procedure may be carried out for each dial position, except zero, for each of the dials controlling the built-in weights. Thus, nine loads from 1 to 9 g in 1 g steps serve to calibrate the 1 g dial, or 0.1 to 0.9 in 0.1 g steps for the 0.1 g dial.

Good practice demands that each comparison of a "known" pan load to an "unknown" built-in load be carried out by the double substitution weighing procedure. With one exception, the double substitution format described in the paragraph "Air Weighing Procedure" of section 6 of the paper is quite adequate for the calibration experiment. In the density measurement procedure described in the basic paper the equation for 0_A, requires *corrected* values of the dial readings. Inasmuch as this experiment is directed toward the determination of the dial corrections we must alter the meaning of D_{t1} and D_{t2} from corrected dial readings to their raw values.

In the calibration mode the value of 0_A is properly written

$$0_A = D_2 - D_1 + \frac{G(s_2 - s_1 + s_3 - s_4)}{(s_3 - s_2 + s_4 - s_5)}$$

and since in an air weighing experiment of this type, D_1 is always zero, the expression becomes

$$0_A = D_2 + \frac{G(s_2 - s_1 + s_3 - s_4)}{(s_3 - s_2 + s_4 - s_5)}$$

where D_2 is the dial position under calibration, G, the values of the sensitivity weight and s_1 to s_5 the screen readings observed during each of the five steps of the double substitution experiment. With a value of 0_A, we may calculate C, the correction to D_2, thus:

$$C = \frac{(M_S + C_S)\left(1 - \frac{\rho_S}{\rho_A}\right)}{1 - \frac{\rho_{BW}}{\rho_A}} - 0_A$$

where M_S, C_S and ρ_S are the mass, correction and density, respectively, of the standard weight on the pan, ρ_{BW} the density of the built-in weights and ρ_A the air density in the balance case at the time of the experiment.

Statements concerning the accuracy of measured values of loads obtained on direct reading balances calibrated by the foregoing procedure should be made with extreme caution. If the standard deviation of a single measurement on such a balance in the double substitution mode is σ, then our knowledge of the corrections to the built-in weights is limited to about σ if the calibration operation was performed once. When a single measurement on an unknown load is made on this balance the variability of the balance comes into play a second time, so our knowledge of the unknown load is limited to a bit less than 2σ, and for a 99 percent confidence interval this figure should be multiplied by 3. Additionally, it is necessary to add 1 or 2 μg as our estimate of the uncertainty of the corrections to the standard weights used in the calibration.

(Paper 71C3–254)

JOURNAL OF RESEARCH of the National Bureau of Standards—C. Engineering and Instrumentation
Vol. 71C, No. 3, July–September 1967

Study of the Storage Stability of the Barium Fluoride Film Electric Hygrometer Element

Frank E. Jones

Institute for Basic Standards, National Bureau of Standards, Washington, D.C. 20234

(May 25, 1967)

A study of the aging properties of the barium fluoride film electric hygrometer element and of possible causes of the drift of calibration with time in storage has been made. It was found that exposure of aged elements to glow discharge bombardment resulted in near recovery of the prestorage calibration, indicating that the calibration drift was not irreversible and providing insight into the mechanism of aging. Based on the likelihood that aging was due, at least in part, to contamination of the barium fluoride film, production procedures were formulated which resulted in elements with significantly reduced drift. If an adjustment is made similar to the "lock-in" procedure in the operational use of radiosonde humidity elements, then the poststorage resistance values can be adjusted to correspond closely to the prestorage calibration curves. Experimental evidence supports the hypothesis that contamination of the elements by diffusion pumping fluid in the production process was a source of the calibration drift. Applications of the element as a research tool in cloud physics, atmospheric turbulence and radio refractive index structure studies, evaporation and evaporation reduction studies, water vapor flux determinations, and tropospheric humidity distribution studies are mentioned.

Key Words: Adsorption, barium fluoride, electric hygrometer, humidity, thin films, vacuum.

1. Introduction

Possible use of the barium fluoride film electric hygrometer element [Jones, 1963; Jones, 1962a; Jones, 1962b; Jones and Wexler, 1960] on a routine operational basis has been limited by the increase in electrical resistance of the element with time in storage which results in a drift of the calibration (also referred to as "aging" of the element). It is the purpose of this paper to present results of a study of the drift problem.

The barium fluoride element, illustrated in figure 1, consists of a glass substrate on which a film of barium fluoride, 0.3 μ thick, has been deposited by vapor deposition over closely spaced metallic film electrodes between which the electrical resistance can be measured or otherwise utilized in an electrical circuit. The measured resistance varies with relative humidity, RH. Laboratory determinations indicated the response time of the element to be approximately 1 sec at an ambient temperature of -20 °C and 3 sec at -40 °C. However, the results of field experiments, as yet unpublished, tended to show that the element was capable of more rapid response than laboratory tests have indicated. A series of radiosonde flights, previously reported [Jones, 1963], provided information on the performance of the element under conditions encountered in radoisonde flights and provided information to be used in assessing the capability of the element as an experimental tool for use in tropospheric humidity studies. The results for the flights corroborated laboratory test data in several areas. For example, exposure to high humidity and apparent passage through precipitation did not seem to adversely affect the functioning of the element. There was a correlation of indications of saturation or near-saturation with the presence of clouds and precipitation.

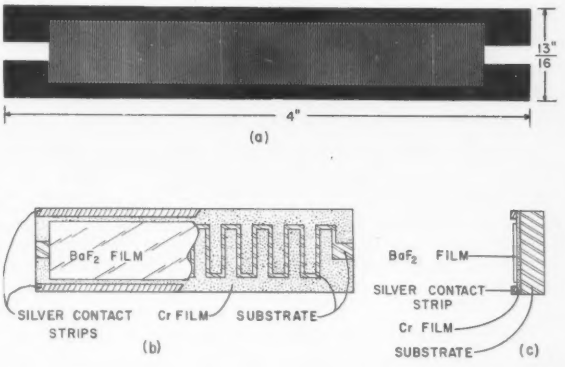

FIGURE 1. *Barium fluoride film electric hygrometer element construction and electrode configuration.*

2. Glow Discharge Bombardment of Aged Elements

Elements which had been stored for approximately 6 years were recalibrated at room temperature, 23 °C. The effects of the prolonged storage on element calibration are illustrated in figure 2. It can be seen that the measured resistance had become insensitive to changes in relative humidity below about 40 percent RH and that at the higher humidities the resistance had increased by 1 to 3 orders of magnitude. The aged elements were then exposed to glow discharge in a vacuum chamber. The elements were recalibrated and the results, plotted on figure 2, indicate the effectiveness of the glow discharge procedure in accomplishing near recovery of the prestorage calibration.

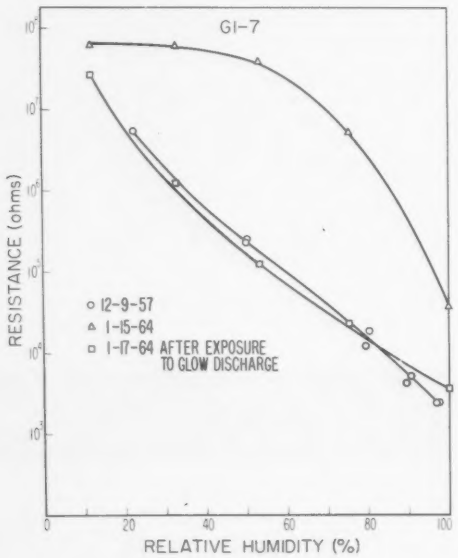

FIGURE 2. *Example of the effect of long-term storage on the calibration curve and the effectiveness of the glow discharge bombardment procedure in accomplishing near recovery of the original calibration.*

The apparatus, illustrated in figure 3, in which the glow discharge procedure was performed consisted of a glass bell jar evacuated by a mechanical pump and an oil diffusion pump. The pumps were fitted with liquid-nitrogen-cooled traps intended to prevent flow of oil vapors from the pumps into the bell jar. The elements were placed, with barium fluoride film side up, on a plate electrically insulated from the system. The pressure in the bell jar was reduced to, and maintained at, 80 μ of mercury by the mechanical pump. Liquid nitrogen was maintained in the mechanical pump trap. A potential difference of approximately 1,000 V dc applied between the aluminum rings produced a glow discharge which was maintained for 35 min. The current maintained by a high

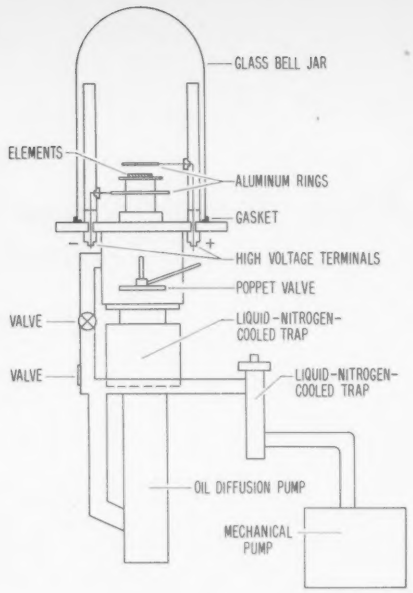

FIGURE 3. *Vacuum evaporator apparatus in which the glow discharge bombardment procedure was performed.*

voltage power supply was approximately 375 mA. The polarity of the aluminum ring electrodes and the location of the elements were chosen such that the elements were at least partially shielded from electron bombardment. It was assumed, therefore, that in the glow discharge the elements were bombarded by species which were predominantly positive ions.

In all cases, the glow discharge procedure was effective in reducing the resistance of the aged elements, in most cases to values near those for the original calibrations.

The outcome of the glow discharge experiment was a development of primary significance for two reasons. First, it indicated that the aging of the elements was not irreversible, at least in regard to the effects on calibration; and, second, it provided a basis for gaining insight into the mechanism of the aging process or processes. Before there points are discussed, it will be helpful to state the following ***working hypotheses*** concerning the functioning of the element: (1) The dominant process in the functioning of the barium fluoride film electric hygrometer element is physical adsorption of water vapor on the surface of the vacuum deposited film, of whatever composition, structure, and state of contamination. (The term "barium fluoride film" is used as a convenience and should not be construed to imply the true nature of the film.) (2) The electrical conduction process of primary interest is ionic transport in an adsorbed water film.

One can, on the basis of these hypotheses and on the basis of the glow discharge procedure results, conjecture that the aging of the elements is due, at least in part, to *contamination* of the adsorbent film by species other than water vapor. The effect of the

contaminant would be to diminish the active surface free to adsorb water vapor, therefore reducing the enhancement of conductivity attributable to the adsorbed water film. The effect of the ion bombardment of aged elements in the glow discharge could then be to provide active surface free (or relatively so) of contaminants (or of a specific contaminant).

A possible source of contamination of the elements is backstreaming oil vapors from the mechanical pump and the oil diffusion pump into the vacuum chamber in which the barium fluoride films were deposited. Holland and others [Holland, 1963; Holland and Bateman, 1961; Holland, 1960; Holland and Bateman, 1960; Holland, 1958; Bateson, 1952] have investigated the sources of surface contamination in vacuum evaporation systems. The following points summarized from the published accounts of their investigations are considered to be pertinent to the present discussion. (1) A chemically clean surface exposed in a vacuum system evacuated by oil diffusion pumps and/or sealed by Neoprene gaskets becomes partially covered by a physically adsorbed layer in equilibrium with organic vapors. (2) A highly reactive surface, created "in vacuo" by fracturing glass or depositing a silica film from the vapor phase, rapidly chemisorbs contaminants. (3) If a freshly deposited silica film is held at a temperature of about 200 °C in the presence of vapor from a silicone pumping fluid, a silicone film is chemisorbed at a greatly reduced rate. (4) *Electron* bombardment in hydrocarbon vapors produces hydrophobic films; electron bombardment in silicone vapors forms hydrophilic polymerized films. (5) A fluorinated hydrocarbon, Viton, and a silicone diffusion pumping fluid with an exceptionally low vapor pressure, DC705, help to decrease the partial pressure of organic contaminants in a vacuum atmosphere but do not completely eliminate possible surface contamination. (6) Holland has devised a glow discharge cleaning apparatus in which the cathode electrode is shielded and in the application of which it is claimed that the glass surface is exposed to the plasma or positive column only of the discharge. (7) A clean surface attained in glow discharge can become contaminated if organic molecules are present in the vacuum atmosphere. Therefore, the time interval between glow discharge cleaning and reducing of pressure to that for evaporation must be kept to a minimum to avoid substrate contamination.

The vacuum evaporator in which the barium fluoride films have been deposited is evacuated by a mechanical pump and an oil diffusion pump. Initially, the fluid in the diffusion pump was Octoil (di-2-ethyl hexyl phthalate). Subsequently, Octoil S (di-2-ethyl hexyl sebacate) was used, which, in turn, was replaced by DC704 silicone and then by DC705 silicone. The original bell jar gasket material was Neoprene. Subsequently, this was replaced by Viton. The cathode in the glow discharge apparatus originally was not shielded effectively and, therefore, bombardment of substrates by electrons probably occurred. In the early work on the barium fluoride element, the pumps had not been fitted with liquid-nitrogen-cooled traps. The efficiencies of the traps, installed for later work, in preventing the backstreaming of oil vapors into the vacuum chamber are not known. It is evident, therefore, that sources of contamination in the vacuum evaporation system of the sorts investigated by Holland and others can be considered to have been present in some degree throughout the previous barium fluoride film work.

3. Production of Elements of Reduced Calibration Drift

In consideration of the arguments in the preceding section, the procedures for the production of barium fluoride elements were modified in the following respects:

(1) In the final cleaning in the vacuum chamber, the glass substrates were shielded from direct electron bombardment from the negative glow discharge electrode.

(2) After the barium fluoride film was deposited, the elements were subjected to glow discharge before they were exposed to the ambient atmosphere. For the post-deposition bombardment, liquid nitrogen was maintained in the mechanical pump trap.

Using the modified procedures, elements were produced and stored in sealed containers over a desiccant, barium oxide (BaO), from which they were occasionally removed for room temperature calibration.

The data for repeated calibrations of a typical element produced by the modified procedures are plotted in figure 4. It can be seen that, in general, the resist-

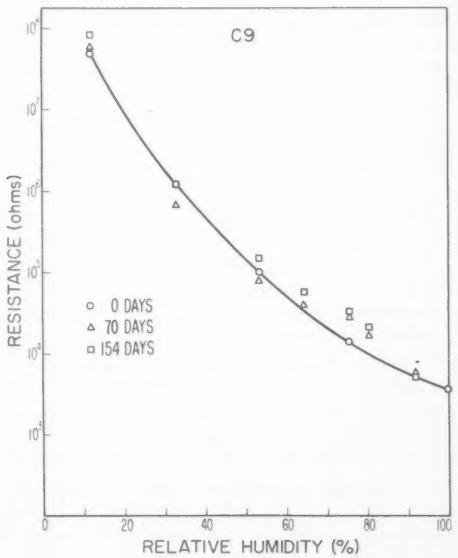

FIGURE 4. *Example of the effect of storage on the calibration of elements produced by procedures in which the substrate and the finished element were subjected to glow discharge bombardment.*

ance of the element had increased in storage over BaO. However, the increase in resistance is significantly smaller than that for elements produced by the conventional procedures.

As an indicator of the effect of storage on the calibration of the elements, the ratio of the resistance after storage, R, to that before storage, R_0, is tabulated in table 1. Maximum, minimum, and arithmetic mean values of R/R_0 throughout the room temperature humidity range, 12 percent to 92 percent RH, have been tabulated for storage periods of various lengths.

TABLE 1. *Resistance ratios,* R/R_0, *after storage over barium oxide*

Element	Max [1]	Min [2]	Mean	Max [1]	Min [2]	Mean	Max [1]	Min [2]	Mean
	27 Days			70–75 Days			154–157 Days		
C1	5.1	1.4	3.0	4.3	1.7	2.6	3.9	1.7	2.9
C2	1.9	1.3	1.6	3.1	1.2	1.3	2.2	1.4	1.9
C3	2.1	1.2	1.6	1.7	0.80	1.2	1.6	1.5	1.5
C4	2.7	1.4	1.9	2.0	.79	1.2	3.1	1.0	1.8
C5				1.7	.54	1.1	2.0	0.76	1.3
C6				1.3	.89	1.1	3.5	1.5	2.4
C7				1.1	.93	1.0	2.6	1.2	2.0
C9				2.0	.58	1.3	2.4	1.0	1.6
C10				1.7	.61	1.2	2.4	1.3	1.8
C11				2.0	.83	1.4	2.6	1.6	2.1
C12				3.7	.59	1.8	6.0	1.7	3.3
	139–140 Days			228 Days			248 Days		
S1	1.7	1.5	1.6	2.1	0.70	1.5			
S2	2.9	1.8	2.3	3.4	.90	2.4	3.9	1.9	3.0
S3	4.9	1.8	3.2	4.6	.65	3.1	5.6	1.1	4.3

[1] Maximum value of R/R_0.
[2] Minimum value of R/R_0.

Elements C1 through C4 were produced in the same deposition; C1 and C2 were removed from the vacuum chamber before C3 and C4 were subjected to the post-deposition bombardment and, thus, were not subjected to the post-deposition bombardment. Elements C5 through C12 were produced in a single deposition. Elements S1 through S3 were produced by depositing the barium fluoride film over Nichrome V metallic film electrode configurations provided by a commercial source.

The deviations, in percent RH, of the post-storage calibration points from curves drawn through the prestorage calibration points are tabulated in table 2. The deviations are predominantly of negative sign, indicating that resistance had increased in storage. The arithmetic means of the absolute values of deviations corresponding to a storage period of approximately 5 months for elements C3 through C12 (elements which had been subjected to the post-deposition bombardment) range from 2.9 to 9.2 percent RH. The arithmetic means of the absolute values of deviations corresponding to a storage period of 7½ months for the S-series elements range from 5.8 to 9.8 percent RH.

The post-storage resistance values obtained for the individual elements were adjusted by multiplication by the inverse of the arithmetic mean values of the resistance ratio, R/R_0, for the individual elements. The effect of this operation, which is related to the "lock-in" procedure in the operational use of radiosonde humidity elements, is to bring the post-storage humidity indications into the vicinity of the prestorage calibration curves. The deviations in percent RH, of the adjusted resistance values about the arbi-

TABLE 2. *Deviations (in % RH) of the indications for stored elements from curves drawn through the prestorage calibration points.*

Results for 12%, 33%, 53.5%, 75.5%, and 92% relative humidity points only have been included.

Element	Max [1]	Min [2]	(−) [3]	(+) [4]	$\overline{\lvert d \rvert}$ [5]	Max [1]	Min [2]	(−) [3]	(+) [4]	$\overline{\lvert d \rvert}$ [5]	Max [1]	Min [2]	(−) [3]	(+) [4]	$\overline{\lvert d \rvert}$ [5]
	27 Days					70–75 Days					154–157 Days				
C1	−3.0	−10.5	4	0	6.1	−2.0	−11.5	5	0	6.5	−3.0	−15.5	4	0	9.4
C2	−3.0	−4.5	4	0	3.8	−1.5	−6.0	5	0	3.5	−2.5	−9.5	5	0	7.1
C3	−1.0	−5.0	4	0	2.9	+2.0	−3.5	3	2	2.1	−1.5	−8.5	5	0	4.7
C4	−2.0	−7.0	4	0	4.4	+3.0	−2.5	1	3	1.8	0.0	−7.5	4	0	3.8
C5						+1.0	−8.0	4	1	4.7	−1.0	−8.0	5	0	2.9
C6						+0.5	−2.5	2	1	0.7	−1.0	−10.0	3	0	4.2
C7						+0.5	−1.0	2	1	0.4	−2.5	−10.0	4	0	6.2
C9						+4.5	−8.5	3	2	4.3	0.0	−10.5	4	0	4.1
C10						+3.0	−7.0	3	2	3.3	−2.0	−11.5	5	0	5.4
C11						+1.5	−8.5	3	1	3.8	−1.5	−12.0	5	0	6.6
C12						+3.5	−13.0	4	1	5.5	−3.0	−18.0	5	0	9.2
	139–140 Days					228 Days					248 Days				
S1	+1.0	−8.5	3	1	4.1	+5.5	−10.0	3	1	5.8					
S2	−5.0	−9.5	4	0	7.2	+1.0	−11.5	3	1	7.2	−5.0	−13.0	4	0	9.4
S3	−5.0	−14.5	4	0	9.8	+2.5	−16.0	3	1	9.8	−1.0	−20.0	4	0	12

[1] Most positive or least negative deviation.
[2] Most negative deviation.
[3] Number of negative deviations.
[4] Number of positive deviations.
[5] Arithmetic mean of the absolute values of the deviations.

trary curves drawn through the pre-storage data are tabulated in table 3. The arithmetic mean of the absolute values of the deviations ranges from 0.3 to 4.6 percent RH, with values of 2.5 and 2.8 percent RH for the two elements stored for 248 days.

The following conclusions can be drawn from the data for the elements produced by the modified procedures:

(a) The modified procedures resulted in the production of elements which were more stable, i.e., elements with reduced drift of calibration in storage

(b) The adjustment operation was effective in providing a correction for aged element resistance values to provide a calibration in the vicinity of the prestorage calibration curves. This result implies that the shift of calibration to higher resistances with time in storage

TABLE 3. *Deviations (in % RH) of the indications for stored elements, adjusted by multiplying the resistance values by the inverses of the appropriate mean resistance ratios, from curves drawn through the prestorage calibration points*

Element	Max[1]	Min[2]	(−)[3]	(+)[4]	$\overline{\lvert d \rvert}$[5]	Max[1]	Min[2]	(−)[3]	(+)[4]	$\overline{\lvert d \rvert}$[5]	Max[1]	Min[2]	(−)[3]	(+)[4]	$\overline{\lvert d \rvert}$[5]
	27 Days					70–75 Days					154–157 Days				
C1	+1.0	−1.5	1	1	0.8	+3.5	−2.0	1	4	1.8	+4.0	−3.0	2	2	2.3
C2	+2.5	−1.0	2	1	1.0	+1.0	−5.0	2	2	1.8	+2.5	−7.0	4	1	2.5
C3	+4.5	−5.5	1	2	2.2	+3.5	−3.0	3	2	2.2	0.0	−1.0	2	0	0.3
C4	+1.5	−5.5	1	2	1.5	+5.5	−2.0	1	4	3.3	+4.5	−2.0	1	3	2.0
C5						+6.0	−6.5	3	2	3.8	+4.0	−4.0	2	3	3.0
C6						+1.5	−2.0	1	3	0.9	+4.5	−4.0	2	2	2.5
C7						+0.5	−0.5	2	1	0.3	+0.5	−2.5	3	1	1.2
C9						+6.0	−6.0	2	3	4.1	+3.5	−5.5	1	2	1.9
C10						+4.0	−5.0	2	2	3.1	+2.0	−4.5	2	3	1.8
C11						+3.5	−4.5	2	3	2.7	+1.0	−3.5	2	2	1.4
C12						+7.5	−7.5	2	3	4.6	+4.5	−6.5	3	2	3.5
	139–140 Days					228 Days					248 Days				
S1	+0.5	−2.5	1	1	0.8	+3.5	−5.5	2	2	3.5					
S2	+2.0	−1.5	1	3	1.4	+7.0	−3.0	2	2	3.0	+3.5	−3.0	2	2	2.5
S3	+3.5	−1.5	1	3	2.5	+7.0	−4.0	2	1	3.6	+6.0	−2.0	2	1	2.8

[1] Most positive or least negative deviation.
[2] Most negative deviation.
[3] Number of negative deviations.
[4] Number of positive deviations.
[5] Arithmetic mean of the absolute values of the deviations.

is not, in general, accompanied by a significant change in the *shape* of the calibration curve. From a practical point of view, it would be possible to use the original calibration curves with aged elements, the post-storage resistance values of which had been adjusted.

4. Investigation of a Diffusion Pumping Fluid as a Possible Source of Calibration Drift

The effectiveness of the modified procedures in producing more stable elements is thought to be due to the reduction of contamination of the elements. If a source of contamination is pumping fluid vapor in the vacuum evaporator, as appears probable from the discussion of section 2, then shielding of the substrates from direct electron bombardment from the negative glow discharge electrode would be expected to have reduced the amount of material deposited by electron bombardment in the presence of pumping fluid vapors (item 4 of section 2). The post-deposition bombardment could have removed physically adsorbed organic vapors (item 1 of section 2) from the barium fluoride film. The liquid-nitrogen-cooled mechanical pump trap served to reduce the backstreaming of oil vapor from the mechanical pump into the vacuum chamber during the post-deposition bombardment. The data does not, however, show a statistically significant difference between elements produced with and without the post-deposition bombardment.

On the basis of these results, several experiments were performed to test the hypothesis that contamination by diffusion pumping fluid is a source of the drift of the calibration of the barium fluoride element. These experiments were patterned after similar experiments reported by Holland (1963).

Barium fluoride elements were produced by the deposition of the barium fluoride film on a substrate which had been exposed to the negative glow discharge electrode, and which was presumed therefore to have been bombarded by electrons in the glow discharge prior to the deposition of the barium fluoride film. The resistance of the element was measured at various times at room temperature at 33 percent RH (considered to be an optimum value of RH for detection of calibration shift) during storage over BaO. In figure 5, the resistance ratio, R/R_0, and the logarithm of R/R_0, at 33 percent RH are plotted against time in storage for a typical element, C38.

Another set of elements was produced by the deposition of barium fluoride on substrates which had

been exposed to the negative electrode in glow discharge; dishes containing a diffusion pumping fluid, Octoil S, had been placed in the vacuum chamber and remained there during the bombardment and during the deposition of the film. Results of resistance measurements for a typical element, C43, at 33 percent RH during storage over BaO are plotted in figure 5. The curve designated CR500F applies to an element which exhibited exaggerated drift and was included in figure 5 for comparison purposes.

As can be seen in figure 5, both sets of elements, produced on electron-bombarded substrates, increased in resistance at 33 percent RH during storage over BaO. Over the time period studied, the increase in resistance was greater for the elements produced in the presence of the intentionally introduced pumping fluid vapor.

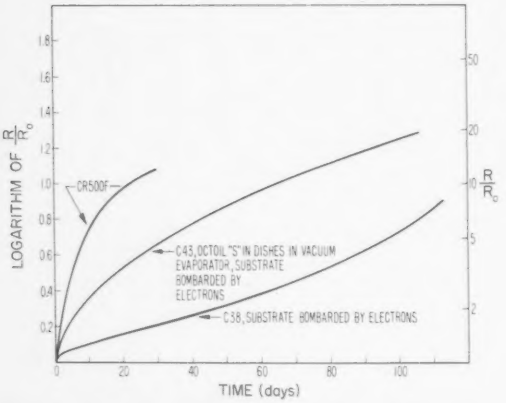
LOGARITHM OF $\frac{R}{R_0}$
$\frac{R}{R_0}$
CR500F
C43, OCTOIL "S" IN DISHES IN VACUUM EVAPORATOR, SUBSTRATE BOMBARDED BY ELECTRONS
C38, SUBSTRATE BOMBARDED BY ELECTRONS
TIME (days)

FIGURE 5. *Example of the effects of storage over* BaO *on the resistance ratio at 33 percent RH for elements for which the substrates had been exposed to electron bombardment, in the absence and presence of Octoil S in the vacuum chamber.*

Another set of elements was produced on substrates which were shielded from direct electron bombardment in the predeposition glow discharge and in a post-deposition bombardment. After subsequent room temperature calibration, the elements were returned to the vacuum evaporator and exposed to a dish containing Octoil S. Spots appeared on the film, presumably due to bursting of bubbles which formed in the oil at the reduced pressure. The resistance ratio for a typical element, C33, was found to be 13. The elements were then degreased in a vapor degreaser in which the solvent was isopropyl alcohol. Spots were no longer visible to the unaided eye and R/R_0 decreased to 1.9. The elements were returned to the vacuum chamber and exposed to a dish containing Octoil S; a shutter placed above the surface of the oil prevented the formation of spots on the film. R/R_0 at 33 percent RH was 8.7 after this second exposure to Octoil S. After storage overnight over BaO, after which R/R_0 at 33 percent RH was 4.8, the elements were degreased and then exposed to glow discharge, shielded from direct electron bombardment, in the vacuum chamber. R/R_0 at 33 percent RH was 3.1 after the bombardment. The elements were then stored in a sealed container over BaO for 109 days. R/R_0 at 33 percent RH increased to a value of 83 at the end of the storage period. These results are plotted in figure 6. The numbers on the circles indicate the sequence of events.

The results plotted in figure 6 can be interpreted in the following way. The rise in R/R_0 after exposure to Octoil S in the vacuum evaporator can be attributed to contamination of the barium fluoride film by liquid oil and oil vapor, resulting in a loss of surface available for the adsorption of water vapor. The subsequent degreasing removed part of the oil contaminant, uncovering relatively active surface for the adsorption of water vapor and the resistance ratio consequently decreased. The second exposure to Octoil S contaminated the surface again with adsorbed vapor and, consequently, the resistance ratio increased to a value somewhat less than that in the presence of spots on the surface. Vapor degreasing and bombardment removed part of the contaminant and subsequent storage over BaO resulted in increasing R/R_0 throughout the 109-day storage period, perhaps due to the diffusion of the contaminant to an increasingly large area of the active surface.

The results of these experiments, although not definitive, are consistent with the hypothesis that contamination by diffusion pumping fluid is a source of the drift of the calibration of the barium fluoride element.

5. Effects of Repeated Bombardment and Prolonged Bombardment on Calibrations for Aged Elements

Returning now to the effects of glow discharge bombardment on the calibration of elements which

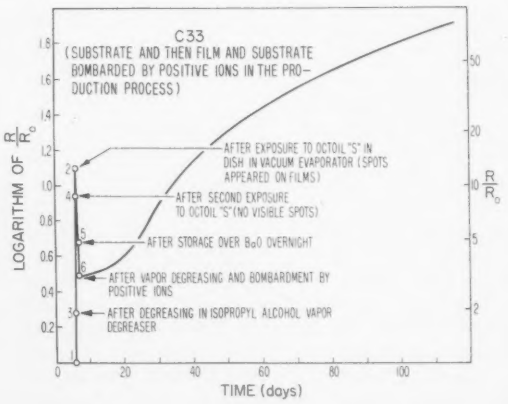
C33
(SUBSTRATE AND THEN FILM AND SUBSTRATE BOMBARDED BY POSITIVE IONS IN THE PRODUCTION PROCESS)
LOGARITHM OF $\frac{R}{R_0}$
$\frac{R}{R_0}$
AFTER EXPOSURE TO OCTOIL "S" IN DISH IN VACUUM EVAPORATOR (SPOTS APPEARED ON FILMS)
AFTER SECOND EXPOSURE TO OCTOIL "S" (NO VISIBLE SPOTS)
AFTER STORAGE OVER BaO OVERNIGHT
AFTER VAPOR DEGREASING AND BOMBARDMENT BY POSITIVE IONS
AFTER DEGREASING IN ISOPROPYL ALCOHOL VAPOR DEGREASER
TIME (days)

FIGURE 6. *Example of the results for an experiment designed to investigate the effects of Octoil S contamination on resistance ratio at 33 percent RH.*

had been stored for 6 years, it was observed that a second bombardment after an intervening period of approximately 5 months of storage over BaO (during which time the resistance had increased) resulted in a shift in calibration to resistances lower than those for the original prestorage calibration. This significant result will be discussed later. The calibration curve after the second bombardment is shown in figure 7.

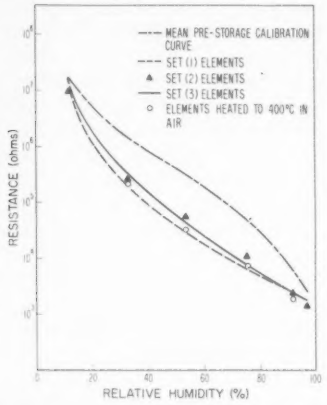

FIGURE 7. *Plots of calibration data for three sets of elements: (1) aged elements exposed to a second glow discharge, (2) aged elements exposed to glow discharge for 8 hours, and (3) elements produced by procedures modified to minimize contamination. The mean prestorage curve and data for elements heated to 400 °C in air are shown for comparison.*

In consideration of the possibility of diffusion of contaminants on the elements, other elements which had been stored for at least 6 years were subjected to prolonged glow discharge bombardment for periods as long as 8 hr. The elements were placed on a plate over the diffusion pump port and were bombarded using aluminum electrodes in an assembly similar to that described by Holland (1958, 1961). In this assembly the negative electrode is shielded and it is therefore assumed that the elements were exposed to positive species of the discharge. The power in the glow discharge was adjusted to attain and maintain a temperature on the elements of approximately 150° C. The elevated temperature was expected to facilitate diffusion. The geometric mean of the measured resistances for 11 elements at each RH for the post-bombardment calibration are plotted in figure 7. These values were found to be lower than the corresponding values for the typical prestorage calibration curve also shown in the figure 7. After 10 days in storage over BaO, the calibration curve had shifted significantly toward higher resistances. Also, an apparent hysteresis effect was observed when the resistance was measured at 33 percent RH, then at 97 percent RH, and again at 33 percent RH. The second measurement at 33 percent RH was found to be lower than the first by a factor of approximately 4. These results will be discussed in a later section.

6. Modification of Production Procedures to Minimize Possibility of Contamination of Elements

On the basis of the results of various experiments in this work and the considerations concerning the possibility that contamination by diffusion pumping fluid is a source of the drift of the calibration of the barium fluorine element, the procedures for the production of barium fluoride elements were again modified as follows:

(1) Liquid nitrogen was maintained in both the mechanical pump cold trap and the oil diffusion pump trap throughout the production process.

(2) The distance between the evaporation (barium fluoride) source and the substrates was reduced from 38 cm to 19 cm.

(3) The substrates were exposed to a glow discharge for approximately 76 min during which time the substrate temperature increased to approximately 160 °C. The glow discharge was produced by the electrode assembly used for the prolonged glow discharge exposure of aged elements in section 5, presumably exposing the substrates to positive species in the discharge, and reducing if not eliminating electron bombardment.

(4) The deposition of the barium fluoride was started within 3 min after the glow discharge power supply had been turned off. The substrate temperature during the deposition was, therefore, near 160 °C.

(5) The time of deposition was reduced from 300 sec to 180 sec.

(6) Argon was introduced into the evaporator as soon as practicable after the deposition of the film to bring the pressure to ambient in the relative absence of oxygen.

(7) The elements were not subjected to a post-deposition glow discharge bombardment.

It should be noted that the pumping fluid in the diffusion pump was DC705 silicone and the bell jar gasket was made of Viton.

These procedures permitted the deposition of the barium fluoride film on substrates which had been bombarded by positive (assumed) ions for a relatively extended period of time and on which the temperature was maintained at about 160 °C to inhibit sorption of silicone vapor and other vapors present in the vacuum evaporator, with a minimum of time during which the substrates and film might be exposed to contaminants in the vacuum evaporator, and with cooling of the elements in a relatively inert atmosphere during the return to ambient pressure.

A room temperature calibration curve for elements produced under these modified procedures is plotted in figure 7. The curve was drawn through points representing the geometric mean of the resistances for 4 elements at each RH point. It can be seen that this curve falls below (in resistance) the mean curve for elements produced by the conventional procedures.

On examination of figure 7, the similarity in shape of calibration curves for three sets of elements: (1) the set of aged elements which were exposed to a second glow discharge bombardment, (2) the set of aged elements which were exposed to glow discharge bombardment for 8 hr, and (3) the set of elements produced by the modified procedures of this section, is conspicuous. Also, the fit of the points for set (2) to the curve for set (3) is good. These results are especially significant considering the large displacements of the data for these sets of elements from the mean calibration curve for elements produced by the conventional procedures. It is, therefore, reasonable to inquire as to what these three sets of elements had in common. On the basis of the hypothesis that contamination of the barium fluoride elements by diffusion pumping fluid (and other contaminants) is a source of the drift of the calibration of the elements, one possible answer to the question is the conjecture that the surfaces of the three sets of elements were relatively free of contamination. It is to be recalled that the apparent effect of glow discharge exposure of aged elements was to essentially (and temporarily) reverse the effect of aging on the calibration of the elements. On the basis of the working hypotheses stated in section 2 it was conjectured that the effect of the glow discharge exposure could be to provide active surface free (or relatively so) of contaminants (or of a specific contaminant). Therefore, it can be conjectured that the second glow discharge bombardment and the 8-hr glow discharge bombardment were more efficient in providing active surface free of contaminants than was a single exposure to bombardment, thereby accounting for the lower resistances for sets (1) and (2) compared with prestorage values. Also, the modified procedures under which set (3) elements were produced were specifically formulated to minimize contamination of substrates and elements. Again, this could account for the lower resistances for set (3) elements. That the calibration curves for the three sets of elements should be similar in shape and relatively close together on figure 7, is, therefore, a not unexpected result. It is interesting to note that the open circles, corresponding to room temperature calibration points for elements which, in earlier work [Jones and Wexler, 1960], had been heated to 400 °C in air in a muffle furnace, fit the curve for set (1) elements over the range 33 percent to 92 percent RH.

The apparent hysteresis phenomenon observed for set (2) elements was also observed for set (3) elements. It is not known whether such a phenomenon existed for set (1) elements. The investigation of this and other properties of set (3) elements is continuing, and therefore, the results presented here for these elements must be considered to be preliminary.

It seems appropriate at this point to make some remarks regarding hysteresis in physical adsorption systems, since it has been hypothesized (working hypothesis 1 in section 2) that the dominant process in the functioning of the barium fluoride film electric hygrometer element is physical adsorption. Hysteresis, both reversible and irreversible, in the physical adsorption process has been studied by many investigators and several theories have been advanced. Hysteresis is said to be reversible if the adsorption isotherm is completely reproduced on repetition of the adsorption-desorption cycle and is said to be irreversible if repetition of the cycle results in a different curve [Brunauer, 1945]. In the case of the barium fluoride element, for which the calibration curve can be considered to be related to an adsorption isotherm [Jones, 1962a], the hysteresis has been found to be irreversible. Brunauer asserts that according to Zsigmondy's (1911) view hysteresis is not a property of the adsorbing system but is due to an extraneous effect, impurities, and that the desorption branch represents adsorption on an adsorbent from which impurities have been removed and therefore is the true equilibrium curve. It is not asserted here that Zsigmondy's theory best accounts for hysteresis, but rather only that the results in the present work fit into this theory rather well. The relatively large hysteresis effect observed for elements with presumably more active surfaces (i.e., elements of sets (2) and (3)) might be attributable to higher sensitivity of these more active surfaces to contamination by components of laboratory air at low relative humidity.

7. The Element as a Research Tool

Although possible use on a routine basis has been limited by aging of the element, a situation which the results of the present work substantially relieves, the element has shown promise for immediate use as a research tool. Such application has been made in the following areas, the results for which are as yet unpublished:

(1) Aircraft cloud physics studies. Thirteen flights of elements mounted on the exterior fuselage of an aircraft have been made.

(2) Atmospheric turbulence and radio refractive index structure studies.

(3) Studies of evaporation and evaporation reduction from a fresh water lake.

(4) Determination of water vapor flux from natural surfaces. Preliminary studies of the applicability of the element have been made and, at this writing, application in a micrometeorological field experiment is imminent.

(5) Tropospheric humidity distribution studies. In addition to the series of radiosonde flights mentioned above [Jones, 1963], an element provided the only tropospheric humidity measurements on a manned balloon flight.

In all of these areas the results have been encouraging.

8. Conclusions

(1) The work reported here has substantially improved the storage stability of the barium fluoride film electric hygrometer element.

(2) The potential of the element as a research tool, primarily due to its rapid response, has begun to be realized in several fields.

This work was sponsored by the Atmospheric Sciences Laboratory of the U.S. Army Electronics Command, Fort Monmouth, New Jersey.

9. References

Bateson, S., Aluminium reflecting films applied to glass and plastics by thermal evaporation, Vacuum **2**, 365, 1952.

Brunauer, S., in The Adsorption of Gases and Vapors, p. 394 (Princeton University Press, Princeton, N.J., 1945).

Holland, L., Sources of surface contamination in vacuum evaporation systems, Vacuum **13**, 173, 1963.

Holland, L., and S. K. Bateman, A low pressure evaporation plant for rapid operation, in 2nd International Conf. Vac. Sci. Technol., p. 1201 (Pergamon Press, New York, London and Paris, 1961).

Holland, L., Problems in the construction and operation of bakeable and non-bakeable vacuum systems, in 7th National Sym. Vac. Technol. Trans. (Pergamon Press, New York, London and Paris, 1960).

Holland, L., and S. K. Bateman, Effects of oil vapour contamination on the adhesion of zinc sulphide films to glass and silica, Brit. J. Appl. Phys. **11**, 382, 1960.

Holland, L., The cleaning of glass in glow discharge, Brit. J. Appl. Phys. **9**, 410, 1958.

Jones, F. E., Performance of the barium fluoride film hygrometer element on radiosonde flights, J. Geophys. Res. **68**, 2735, 1963.

Jones, F. E., Evaporated-film hygrometer elements, J. Res. NBS **66C** (Engr. and Instr.), No. 3, 209 (1962a).

Jones, F. E., Hygrometer elements, U.S. Patent 3,059,079, 1962b.

Jones, F. E., and A. Wexler, A barium fluorode film hygrometer element, J. Geophys. Res. **65**, 2087, 1960.

Zsigmondy, R., über die struktur des gels der Kieselsäure. Theorie der entwässerung, z. anorg. Chem. **71**, 356, 1911.

(Paper 71C3–255)

JOURNAL OF RESEARCH of the National Bureau of Standards—C. Engineering and Instrumentation
Vol. 71C, No. 3, July–September 1967

Torsion Creep of Circular and Noncircular Tubes*

Leonard Mordfin [1]

(March 21, 1967)

A torsion creep theory for noncircular tubes was developed by applying a multiaxial creep theory to a derived generalization of Bredt's equations.

A review of the literature revealed no torsion creep data on noncircular tubes. Hence, to evaluate the theory, a test program was carried out on twelve specimens of aluminum alloy structural tubing, of four configurations, at 400 °F.

Observed discrepancies between the torsion creep theory and experiment are smaller than variations in the measured creep properties of the specimen material from one tube configuration to another and are not appreciably greater than discrepancies between elastic torsion theory and experiment. Most of the observed discrepancies are consistent with measured anisotropy in the tubes, while other discrepancies are ascribed to nonhomogeneity in creep properties and a hydrostatic stress effect in multiaxial creep.

For the calculation of torsion stresses in circular tubes the thin-wall approximation is adequate for thickness-to-radius ratios up to one-tenth. For straight-sided tubes equivalent accuracy is obtained for effective ratios up to only one-twentieth. These criteria apply to creep conditions as well as to elastic conditions.

Key Words: Creep, primary creep, shear, shell, stress analysis, thin wall, torsion, tube.

1. Introduction

Torsion testing of thin-walled tubes furnishes a number of advantages over tensile testing in the determination of creep properties. The most significant of these is that the measurement of strain in torsion tests is essentially unaffected by the thermal expansions and contractions which accompany minor temperature fluctuations. Also, if the wall thickness is small compared to the diameter, the shear stress across the section may be regarded as uniform and, for a constant torque, this stress remains constant throughout the duration of the test. A final advantage, for certain research purposes, is that it is comparatively easy to reverse the stress direction.

In spite of these advantages most laboratory creep testing is carried out in tension. On the other hand, most structural members are subjected to multiaxial stress conditions. It is necessary, therefore, to relate creep behavior under multiaxial stress states to the uniaxial creep behavior that is usually obtained in the laboratory. The purpose of this paper is to develop a means of calculating the torsion creep behavior of noncircular tubes from the tensile creep properties of the tube materials.

The first recorded torsion creep tests of hollow tubes were carried out by Bailey [1, 2][2] in 1929. Other pioneers in this area of research include Everett [3, 4] and Lea [5]. A. E. Johnson [6–10] has probably done more work in this field than anyone else and, indeed, with the exception of one related investigation [11], Johnson was the only researcher of record engaged in torsion creep studies between 1940 and 1960. Recently, however, there has developed a mounting international interest in the subject as evidenced by the appearance of six papers [12–17] in the last three years. This is attributable, in part at least, to anticipated creep deformation problems in the wings of supersonic aircraft.

The tubular specimens used in the above investigations were, in every case, circular. This investigation is believed to be the first study of torsion creep in noncircular tubes.

Most of the torsion creep tests cited in the literature

*The results reported in this paper were used in parts of a dissertation submitted to the University of Maryland in partial fulfillment of the requirements for a Ph. D. degree. The initial phase of the work was supported by the National Aeronautics and Space Administration. An invited paper.

[1] Present address: Headquarters, Office of Aerospace Research (RROSG), 1400 Wilson Blvd., Arlington, Va. 22209.

[2] Figures in brackets indicate the literature references on page 220.

were performed on miniature test specimens having diameters of about ½ in and gage lengths of about 2 in. In fact, until recently [17] no torsion creep data had been reported on any tubular specimen longer than 8 in or larger than 1.6 in in diameter.

2. Theory

The theory of elastic torsion in thin-walled tubes, as developed by Bredt [18] in 1896 represents an approximation to Saint-Venant's general elastic torsion theory. Bredt's analysis was based on certain assumptions regarding the nature of the stress distribution and results in two familiar equations. The first of these, which gives the stress distribution, is

$$\tau = \frac{T}{2Ah} \tag{1}$$

where

τ = shear stress
T = torque
A = area enclosed by the midthickness curve C of the tube cross section
h = wall thickness.

This equation is derived strictly from equilibrium considerations and is, therefore, assumed to be applicable to creep conditions as well as to elastic conditions.

Bredt's second equation, which gives the angle of twist of the tube, is applicable only to elastic materials. However, a generalized version of Bredt's second equation is derived in appendix A and is applicable to material obeying any constitutive equation. This generalized version of Bredt's second equation is

$$\theta = \frac{\gamma_m P}{2A} \tag{2}$$

where

θ = angle of twist per unit length
γ_m = mean shear strain
P = perimeter of C.

It is only necessary to insert the proper expression for γ_m in this equation to make it applicable to the particular material behavior under consideration.

For the present case, let it be assumed that the tensile creep behavior of the tube material can be expressed in the common form

$$\epsilon = k\sigma^m t^n \tag{3}$$

where

ϵ = tensile creep strain
σ = uniaxial tensile stress
t = time

and k, m, and n are constants which depend only on the material and the temperature. This equation applies only to constant stress, constant temperature conditions.

If the octahedral shear stress theory of multiaxial creep is invoked, it can be shown that for a material obeying eq (3) the shear creep characteristics are given by

$$\gamma = \sqrt{3}k(\sqrt{3}\tau)^m t^n \tag{4}$$

where

γ = shear creep strain

and k, m, and n are the tensile creep constants defined by eq (3). Substituting eq (1) into eq (4) gives

$$\gamma = \sqrt{3}k\left(\frac{\sqrt{3}}{2}\frac{T}{Ah}\right)^m t^n.$$

For the case of a thin-walled tube in torsion, a mean value for the shear creep strain may be obtained by performing a contour integration of this expression around C. That is,

$$\gamma_m = \int_c \frac{\gamma ds}{P} = \sqrt{3}\frac{k}{P}\left(\frac{\sqrt{3}}{2}\frac{T}{A}\right)^m t^n \int_c \frac{ds}{h^m} \tag{5}$$

where

ds = incremental arc length of C.

Equation (5) can now be inserted into eq (2) to give the angle of twist,

$$\theta = \frac{\sqrt{3}}{2}\frac{k}{A}\left(\frac{\sqrt{3}}{2}\frac{T}{A}\right)^m t^n \int_c \frac{ds}{h^m}. \tag{6}$$

This represents the creep counterpart of Bredt's second equation. If the tube in question has a uniform wall thickness h, eq (6) simplifies to

$$\theta = \frac{\sqrt{3}}{2}\frac{P}{A}k\left(\frac{\sqrt{3}}{2}\frac{T}{Ah}\right)^m t^n. \tag{7}$$

For a circular tube with mean radius r_m this equation may be written as

$$\theta = \sqrt{3}\frac{k}{r_m}\left(\frac{\sqrt{3}}{2}\frac{T}{Ah}\right)^m t^n. \tag{8}$$

Whereas eq (7) is approximate in the sense that it was derived with Bredt's assumptions regarding the nature of the stress distribution, eq (8) is exact in the sense that it coincides with a solution (appendix B) which does not require these assumptions.

3. Test Program

A test program was designed to evaluate the applicability of eq (7) to several shapes of thin-walled tubes. Tension creep tests of the tube materials were carried out to determine k, m, and n, and torsion creep tests of the tubes were performed to provide experimental data for comparison with eq (7).

3.1. Specimens

Drawn seamless 2024–T3 aluminum alloy tubing was acquired for use as test specimens. This alloy was selected because of its reported adherence to the octahedral shear stress theory [19, 20] and because of its applicability to airframes. Four tubes of each of four different shapes were obtained: circular, square with rounded corners in two thicknesses, and rectangular with rounded corners. The diameter of the circular tubes, the sides of the square tubes, and the longer side of the rectangular tubes were all nominally 3 in. and the lengths of the tubes were each 7 ft. The nominal dimensions of the four shapes are shown in figure 1. For any single tube, variations in the outside dimensions and in the thicknesses did not exceed 0.01 in and 0.004 in, respectively.

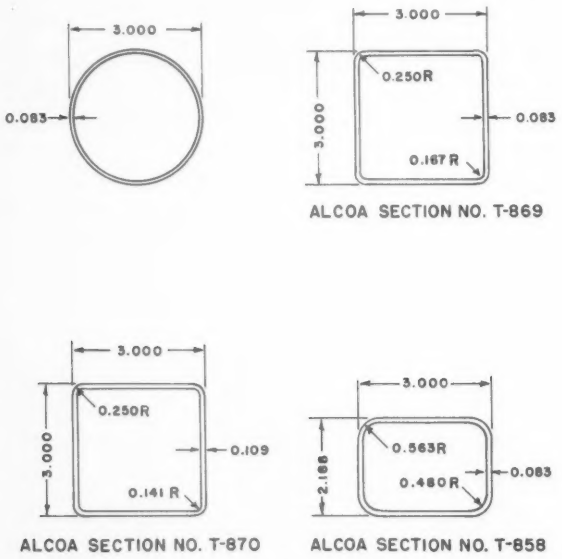

FIGURE 1. *Nominal dimensions of tube specimens, in inches.*

3.2. Tension Creep Tests

Four tension creep specimens were cut longitudinally from one tube of each of the four shapes. Using a conventional dead weight, lever arm testing machine, creep tests of approximately 50-hr duration were carried out on these specimens at 400 °F. The stress levels ranged from 9,100 to 22,500 lb/in². Using 14 data points from each test, a least squares approach was set up to find appropriate values of k, m, and n for the material of each tube shape. The resulting tension creep equations, in the form of eq (3), are as follows: For the circular tube material

$$\epsilon = 13.4\sigma^{1.05}t^{0.38} \times 10^{-6}. \tag{9a}$$

For the 0.083-in wall square tube material

$$\epsilon = 2.54\sigma^{1.60}t^{0.28} \times 10^{-6}. \tag{9b}$$

For the 0.109-in wall square tube material

$$\epsilon = 6.49\sigma^{1.33}t^{0.36} \times 10^{-6}. \tag{9c}$$

For the rectangular tube material

$$\epsilon = 2.43\sigma^{1.57}t^{0.30} \times 10^{-6}. \tag{9d}$$

In these equations σ is in kips/in² and t is in hours.

A comparison between eq (9b) and the experimental tension creep curves for the specimens cut from the 0.083-in wall square tube is given in figure 2. The discrepancies appear to be random and are attributed to the usual scatter in creep behavior. The discrepancies obtained with the specimens cut from the other tube shapes are similar to that shown in figure 2.

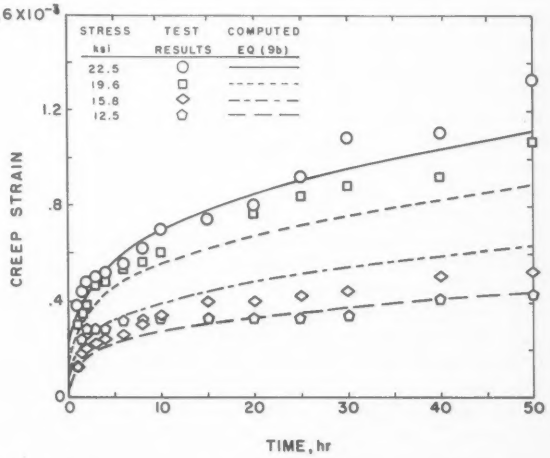

FIGURE 2. *Tension creep behavior of specimens cut from 0.083-in wall square tube.*

To compare the tensile creep properties of the four tube materials, creep curves were calculated from eqs (9) for a stress of 15,000 lb/in². These are given in figure 3. It may be seen that significant differences exist between the creep curves for the materials of two of the tube shapes as compared to those for the

265-343 O-67—3

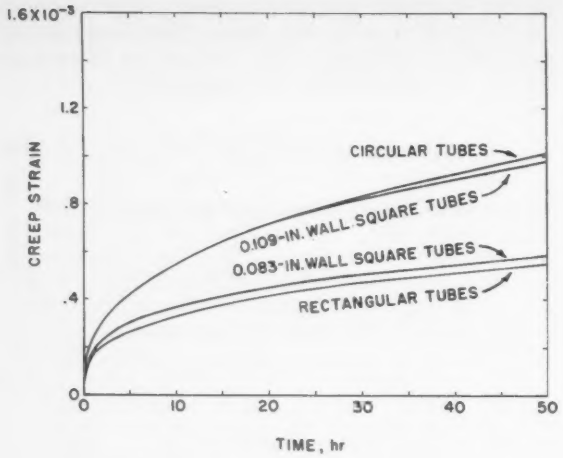

FIGURE 3. *Tension creep curves for the tube materials at 15,000 lb/in² according to eqs (9).*

materials of the other two tube shapes. These differences may be attributable to variations in chemical composition or heat treatment, or to differences in the degree of cold work resulting from the respective drawing operations.

3.3. Torsion Creep Tests

Twelve torsion creep tests were carried out at 400 °F, three on each of the four tube shapes shown in figure 1. Each tube specimen was seven feet long and was mounted such that it passed symmetrically through a six-foot test furnace. Twist measurements were made over a three-foot gage length at the center. The twist measuring system had errors not exceeding one percent and individual measurements were repeatable to better than 3×10^{-6} radians per inch. Temperatures were constant within 1 °F throughout each test and uniform, over the gage length, within 3 °F. The testing equipment, the test procedure, and the calibration technique are described in appendix C.

Table 1 lists the specimen designations, the torques, and the stress levels computed from eq (1) for each test. The experimental creep data are plotted in figures 4, 5, 6, and 7 in terms of angle of twist against time. Also given in the figures are the theoretical torsion creep curves calculated with eq (7). For the circular tubes, figure 4, and the rectangular tubes, figure 7, agreement between theory and experiment is good for the lowest stress level. At the higher stress levels the theory predicts considerably less creep than was observed in the tests. For the 0.083-in wall square tubes, figure 5, the theory predicts less creep at all stress levels than was actually obtained, while for the 0.109-in wall square tubes, figure 6, the theory predicts significantly more creep at all stress levels than was actually obtained. Although the relationship between experiment and theory is reasonably consistent for each tube shape, no dominant relationship is apparent from all of the data taken together.

TABLE 1. *Torsion creep tests*

Specimen No.	Torque	Shear stress	Stress error
	in-lb	*lb/in²*	*Percent*
Circular tubes			
1	9,930	8,940	+2
2	11,800	10,600	−25
3	10,900	9,820	−23
0.083-in wall square tubes			
4	11,800	8,080	−15
5	13,800	9,380	−18
6	15,600	10,700	−12
0.109-in wall square tubes			
7	16,600	8,920	+31
8	18,500	9,940	+30
9	14,700	7,900	+23
Rectangular tubes			
10	11,800	11,800	−13
11	9,350	9,350	0
12	12,800	12,800	−23

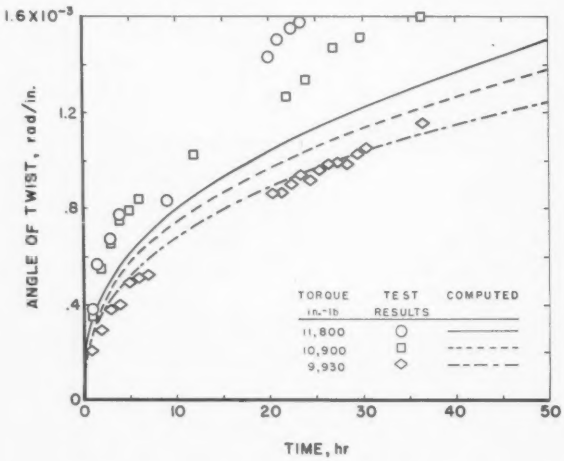

FIGURE 4. *Torsion creep behavior of circular tubes.*

The discrepancies between calculated and experimental results were evaluated in terms of stress. That is, for each test the stress that would have brought the calculated curve into approximate coincidence with the experimental data was computed. The difference between this value and the theoretical stress, expressed as a percentage, is given in table 1 as the "stress error."

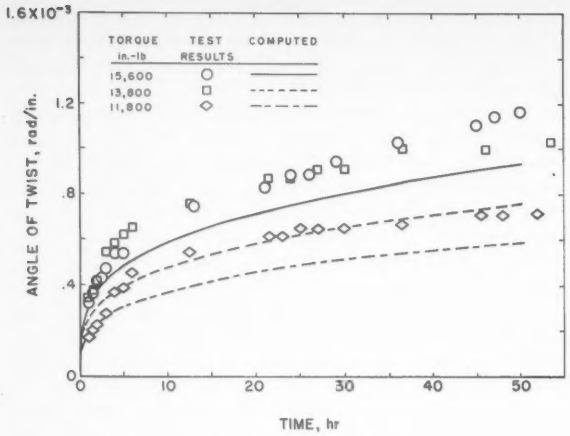

FIGURE 5. *Torsion creep behavior of 0.083-in wall square tubes.*

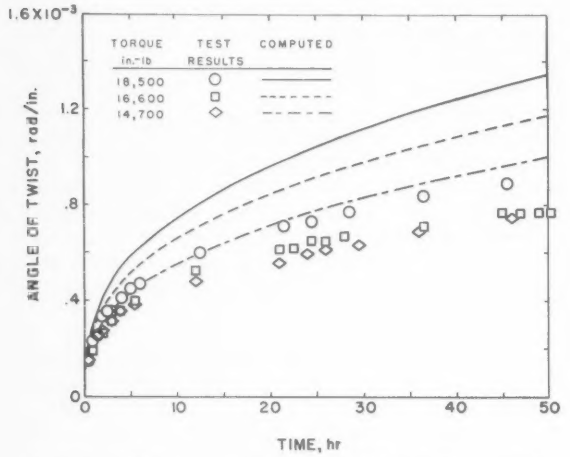

FIGURE 6. *Torsion creep behavior of 0.109-in wall square tubes.*

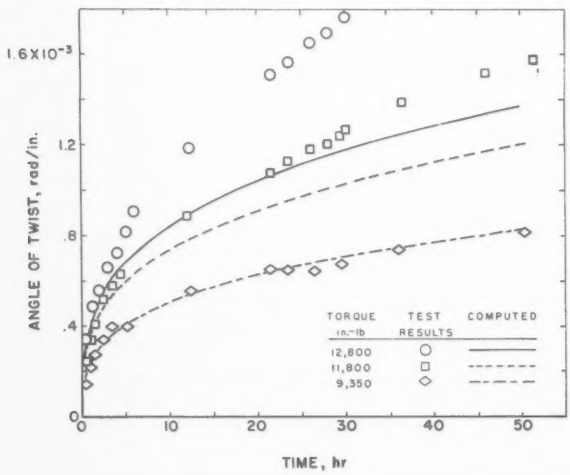

FIGURE 7. *Torsion creep behavior of rectangular tubes.*

4. Analysis of Results

The discrepancies between the theoretical and experimental creep curves are not significantly greater than the discrepancies that are obtained when Bredt's equations are applied to elastic tubes at room temperature [21–24]. This, however, does not explain the reasons for the discrepancies and, therefore, gives no indication of the limits of applicability of the theory.

In order to explain the observed discrepancies between theory and experiment, it is desirable to reexamine the justifications for the numerous assumptions which were involved in the theory. These assumptions may be divided into three categories. The first category includes those common assumptions regarding the idealization of the specimen materials which are necessary to make them amenable to mathematical treatment. These assumptions are:

1. The material is continuous.[3]
2. The material is homogeneous. (See footnote 3.)
3. The material is isotropic.

In the next category are the additional assumptions inherent in the Saint-Venant torsion theory.

4. Ends are free to extend or contract in the lengthwise direction.
5. Ends are loaded by a pure torsional couple with no resultant force.
6. There is no restraint of warping.
7. There are no reentrant corners or other areas of severe stress concentration.

Finally, there are the assumptions required by Bredt's approximation to the Saint-Venant theory.

8. The shear stress parallel to the surface is uniform throughout the wall thickness.
9. The shear stress normal to the surface is zero throughout the wall thickness.

4.1. Material Idealization

a. Continuity

Although it is known that metallic materials are composed of crystals, their dimensions are generally very small in comparison with the dimensions of the specimens. Hence, the mathematical treatment of the material as though it were continuous is generally reasonable. In the present case, however, there was some doubt as to whether the crystals were, in fact, small in comparison with the wall thicknesses of the tubes. To resolve this doubt, small samples were cut from one square tube of each of the two wall thicknesses. For each sample the number of grains in the thickness direction was counted both on a longitudinal surface and on a transverse surface. In all cases the count ranged between 33 and 48 grains. On this basis, it is felt that the assumption of continuity is justified.

[3] For these two characteristics, *continuity* and *homogeneity*, some authors prefer the terms *homogeneity* and *uniformity*, respectively. In the present context *continuity* indicates the nature of a structureless mass and *homogeneity* is the quality of having the same mechanical properties throughout the material, i.e., independent of location.

265-343 O-67—4

b. Homogeneity

It is conceivable that the tubes from which the tensile creep specimens were cut may not have been representative of the tubes which were tested in torsion creep. Therefore, the homogeneity of the specimen materials was checked, as follows, with a hardness survey.

A rectangular plate, approximately 1 in by 2 in, was cut from each torsion creep specimen, from the region which had been between the grips and the test furnace. The material in this region is considered to have suffered the least change in properties due to stressing or heating. In addition, a similar plate was cut from each of the four tubes from which the tension creep specimens had previously been cut.

Table 2 lists the average Vickers hardness numbers

TABLE 2. *Hardness test results*

Specimen No.	Hardness
	VHN
1	146
2	148
3	141
C	143
Average	144
4	147
5	148
6	145
SN	147
Average	147
7	145
8	148
9	142
SK	146
Average	145
10	145
11	140
12	141
R	140
Average	142

for each of the test plates. The plate numbers in the first column refer to the tube specimen numbers (table 1) from which the respective plates were cut. The plates designated by letter symbols refer to those tubes from which the tensile creep specimens had been cut. It can be seen that the variation in hardness within each batch is small, as expected. Unfortunately, the data also indicate that the difference in hardness from batch to batch is also small. Yet, it has been determined (fig. 3) that a significant difference in creep properties exists between different batches. Hence, it must be concluded that the uniformity in hardness within each batch does not necessarily indicate a uniformity in creep properties. The possibility thus remains that the discrepancies between the calculated and experimental torsion creep behaviors may be due to nonhomogeneity.

c. Isotropy

As a result of the cold-working process, drawn tubes are typically orthotropic with the maximum strength properties coinciding with the longitudinal direction. In the present investigation the tension creep properties of the tube materials were determined from specimens cut longitudinally from the tubes. In the torsion tests, however, the principal directions are at 45 deg to the longitudinal axis of the tubes. It is natural, therefore, to question whether the creep properties of the material in the diagonal (45-deg) direction and in the longitudinal direction are equivalent. Unfortunately, the tensile creep properties in the diagonal direction could not be evaluated in the present investigation because the specimen lengths which could be cut diagonally are too short to be satisfactorily accommodated by the available creep testing equipment.

As a compromise, it was decided to secure a general picture of the anisotropy in the tubes by conducting room-temperature tensile tests on miniature specimens which had been cut from a tube in the longitudinal, diagonal and transverse directions. The first set of miniature specimens was taken from the 0.083-in wall square tube from which the tension creep specimens had been cut. In figure 8 the longitudinal, diagonal and transverse stress-strain characteristics are compared. It may be seen that anisotropy does, indeed, exist with the material being stronger in the longitudinal direction than in the transverse direction.

Tensile and yield strengths from these tests are given in table 3, each tabulated value being the average from a pair of tests. The ratio of yield strengths

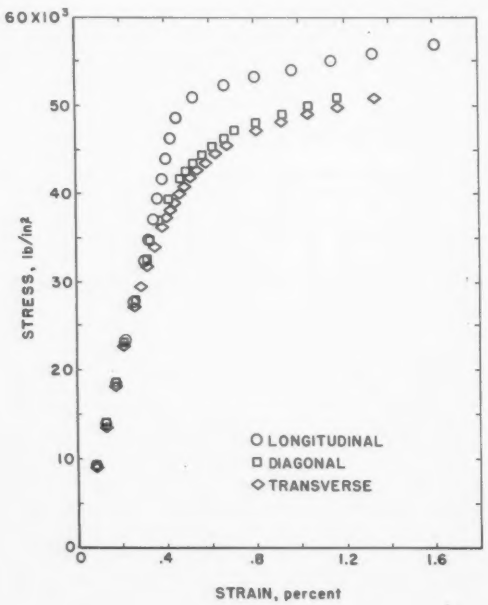

FIGURE 8. *Comparison of tensile stress-strain characteristics of 0.083-in. wall square tube material in three directions.*

TABLE 3. *Tensile properties of 0.083-in wall square tube material*

Direction	Yield strength [a]	Tensile strength
	lb/in²	*lb/in²*
Longitudinal	52,000	72,800
Diagonal	45,200	69,200
Transverse	43,500	67,800

[a] 0.2 percent offset.

in the longitudinal and diagonal directions is 1.15. If this ratio may be taken as a measure of the plastic anisotropy, then an estimate can be made of the effect of anisotropy on the torsion creep behavior of the 0.083-in wall square tubes. On the basis of this ratio it is postulated, for purposes of this estimate, that plastic flow in the diagonal direction may be deduced from the plastic flow properties in the longitudinal direction by considering the stress in the diagonal direction to be 15 percent greater than the true value. Thus, the creep strain in the diagonal direction [4] is taken as [cf eq (3)]

$$\epsilon = k(1.15\sigma)^m t^n.$$

With this modification the torsion creep equation, eq (7), becomes

$$\theta = \frac{\sqrt{3}}{2}\frac{P}{A}k\left(\frac{\sqrt{3}}{2}\frac{1.15T}{Ah}\right)^m t^n. \qquad (10)$$

An independent justification for this form of anisotropy correction is given in appendix D. Torsion creep curves were calculated for the 0.083-in wall square tubes using this equation. These calculated curves are compared with the experimental results in figure 9. It is seen that, on the whole, the agreement between calculated and experimental results is now quite acceptable. The remaining discrepancies appear to be random, rather than systematic, and are apparently within the experimental variability of the creep properties of the material as exhibited by figure 2.

On similar bases it is reasonable to presume that the discrepancies obtained with the circular and rectangular tubes (figs. 4 and 7) can likewise be explained, for the most part, in terms of anisotropy. Unfortunately, however, this type of correction would increase the discrepancies obtained with the 0.109-in wall square tubes (fig. 6) since, in this case, the isotropic theory predicts considerably more creep than was observed in the tests. This situation naturally creates a suspicion that the 0.109-in wall square tubes possess a reverse type of anistropy; that is, one where the material is stronger in the diagonal (and transverse) direction than in the longitudinal direction.

[4] The degree of anisotropy is so small that the angle between the directions of principal stress and principal strain may be ignored.

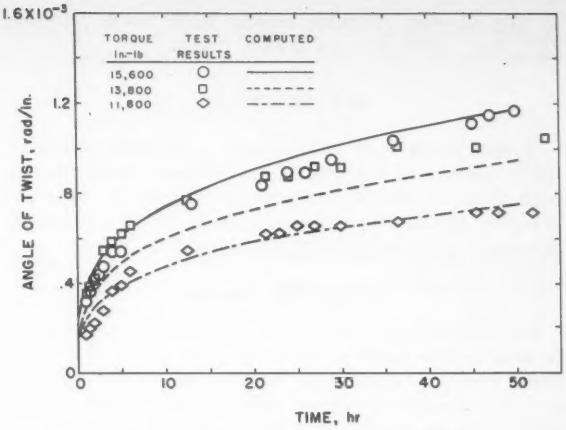

FIGURE 9. *Torsion creep behavior of 0.083-in wall square tubes.* Comparison of experimental data with theory corrected for anisotropy.

To check this, a set of miniature specimens was cut from the 0.109-in wall square tube from which the tension creep specimens had earlier been taken. The stress-strain characteristics determined from these specimens indicate that the anisotropy in this case is qualitatively similar to that obtained with the thinner tube material (fig. 8). It must be concluded therefore, that anisotropy cannot, by itself, explain all of the discrepancies between experimental and calculated torsion creep behavior, and that some other factor or factors, as yet unknown, are operative here.

The tensile and yield strengths for the 0.109-in wall square tube material are given in table 4.

TABLE 4. *Tensile properties of 0.109-in wall square tube material*

Direction	Yield strength [a]	Tensile strength
	lb/in²	*lb/in²*
Longitudinal	55,700	70,900
Diagonal	47,200	69,600
Transverse	43,300	67,500

[a] 0.2 percent offset.

d. Compressive Creep Properties

Another assumption of concern here, which is related to the matter of isotropy, is the equivalence of the creep properties in tension and in compression. This was not listed as a separate assumption but it is inherent in the octahedral shear stress theory of multiaxial creep, which was used in the development of the torsion creep equations. Vawter et al. [25], and Heimerl and Farquhar [26] measured and compared the tensile and compressive creep properties of 2024–T3 aluminum alloy at several temperatures. Although no data were obtained at 400° F their results suggest that at this temperature the creep properties in tension and compression are probably close

to one another. Similar results have been reported [27] for 2024–T4 aluminum alloy.

4.2. End Effects

Assumptions 4, 5, and 6 may be considered collectively under the heading of end effects. Conformance with these three assumptions is required in order to achieve, in the specimen, the state of pure torsional loading which is considered in the theory.

a. Longitudinal Restraint

If a tubular specimen were to manifest a tendency to lengthen or shorten under torsion, and if this tendency were resisted, axial stresses would be induced in the tube. Accordingly, the design of the torsion creep testing equipment incorporated provision for the torquing shaft to slide axially in its bearings. Thus, with exception of some friction, the torqued end of the specimen was free to extend or contract.

b. Applied Stress Distribution

The Saint-Venant solution to the torsion problem concludes that the stress distribution is the same at every cross section. This indicates that, for conformance with the theory, the torque must be applied to the end surface of the cylinder as a system of tractions identical with the shear stress distribution which is thence obtained at every cross section. The restrictive nature of this requirement is eased by the application of Saint-Venant's principle, which is usually satisfactory. In the case of thin-walled members, however, it has been known for some time that Saint-Venant's principle is not universally valid.

With a thin-walled tube in torsion, if the applied system of shear forces is not identical with the derived shear stress distribution, then longitudinal normal stresses are creafed in order to maintain compatability of the deformation at the ends. (This is illustrated later for the case of a square tube.) These normal stresses differ from those induced by the restraint of elongation or contraction in that they are self-equilibrating at any cross section. Nevertheless, these stresses may make themselves felt at longitudinal distances which are many times the depth or diameter of the tube.

Thus, assumption No. 5, which is adequate for solid cylinders is inadequate for thin-walled tubes. Instead, strict conformance with the Saint-Venant torsion theory requires that the torque be applied in such a way that the applied distribution of shear forces is identical with the derived distribution of shear stresses. In a practical sense, deviations can be tolerated only if the induced longitudinal stresses are comparatively small.

The dissipation of the longitudinal normal stresses with distance from the ends was calculated by Vlasov's method [28] for the square and rectangular tubes of the present investigation. The results of the calculations are given in figure 10, which shows the variation

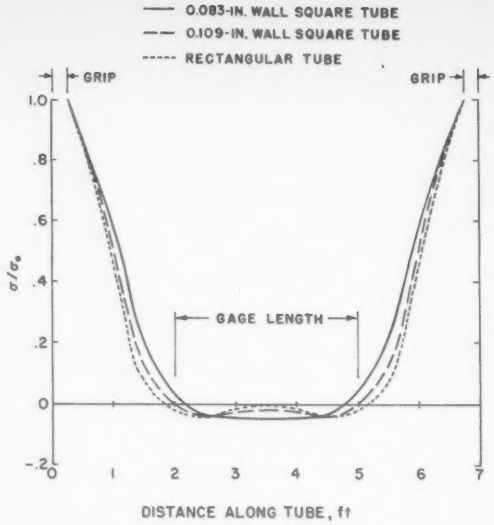

FIGURE 10. *Dissipation of longitudinal normal stresses.*

of the longitudinal normal stresses σ as a fraction of the indeterminate value σ_0 at the ends. It may be seen that, owing to the fact that 21-in lengths of tube were provided between the grips and the gage length, the longitudinal stresses within the gage length have dissipated to less than five percent of the values at the ends of the tubes. This indicates that the conversion of the applied shear stress distribution into the Saint-Venant shear stress distribution is essentially accomplished. Only in an infinitely long tube would this conversion be complete.

The absence of significant longitudinal normal stresses within the gage length was checked experimentally with strain gages, as described in appendix C.

c. Warping

In the case of rectangular tubes, longitudinal normal stresses are also introduced by the restraint of warping. The effects of these stresses on torsional stiffness were calculated by von Kármán and Chien [29]. From their results it was determined that, for the rectangular tubes tested in the present investigation, the restrained warping causes a noticeable effect on the angle of twist for distances of only an inch or two from the grips. Thus, within the gage length, the warping may be considered to be unrestrained, as required by assumption No. 6.

4.3. Stress Concentration

The square and rectangular tubes used in the present investigation were selected with rounded corners in order to minimize the stress concentrations. These stress concentrations were evaluated from Huth's charts [30] as follows:

For the 0.083-in wall square tubes, $k_c = 1.02$;
for the 0.109-in wall square tubes, $k_c = 1.15$;
for the rectangular tubes, $k_c = 1.00$.

It may be seen that the stress concentrations are, indeed, small. The largest value, for the 0.109-in wall square tubes, cannot reasonably explain the discrepancies observed between the theoretical and experimental torsion creep results. If anything, the stress concentration would tend to cause greater experimental deformations than the theory predicts whereas, in fact, the opposite was observed with the 0.109-in wall square tubes.

4.4. Thickness Effects

Assumptions 8 and 9, which are required by Bredt's analysis, may be discussed under the subject of thickness effects since, to a large extent, these assumptions are justified if the wall thickness is small enough.

a. Stress Gradient

Curiously, there is no well-known criterion or rule-of-thumb which defines the maximum thickness or other limiting condition for application of thin-wall torsion theory. On the other hand, for pressure vessels there is a widely quoted criterion that defines a thin cylinder as one in which the wall thickness is less than one-tenth of the radius. It is interesting to examine this criterion with a view toward establishing a similar one for torsion.

(1) *Circular Tubes.* In an internally pressurized circular tube the tangential stresses vary through the wall thickness, reaching a maximum at the inside surface. Under elastic conditions the maximum stress, as given by Lame's equation, may be written as

$$\sigma_{max} = p\left(\frac{1}{\alpha}+\frac{\alpha}{4}\right)$$

where p is the pressure and α is the ratio of the wall thickness h to the mean radius r_m. For thin-walled tubes the tangential stress is considered to be uniform through the thickness with a value of

$$\sigma_{thin} = \frac{pr_i}{h} = p\left(\frac{1}{\alpha}-\frac{1}{2}\right)$$

where r_i is the inside radius. The ratio

$$\frac{\sigma_{max}}{\sigma_{thin}} = \frac{\dfrac{1}{\alpha}+\dfrac{\alpha}{4}}{\dfrac{1}{\alpha}-\dfrac{1}{2}} \qquad (11)$$

is an index of the error of the thin-wall approximation for any specific value of α.

For elastic torsion of a circular tube the shear stresses vary through the thickness, reaching a maximum at the outside surface. The maximum stress, as given by Saint-Venant's theory, may be written as

$$\tau_{max} = \frac{T}{4\pi r_m^3}\,\frac{1+\dfrac{\alpha}{2}}{\dfrac{\alpha}{2}+\dfrac{\alpha^3}{8}}$$

where T is the torque. For thin tubes the shear stress is considered to be uniform through the thickness with a value

$$\tau_{thin} = \frac{T}{2Ah} = \frac{T}{2\pi r_m^3}\left(\frac{1}{\alpha}\right).$$

The ratio of the maximum shear stress to the shear stress given by the thin-wall theory is

$$\frac{\tau_{max}}{\tau_{thin}} = \frac{1+\dfrac{\alpha}{2}}{1+\dfrac{\alpha^2}{4}}. \qquad (12)$$

Equations (11) and (12) are plotted in figure 11. It is seen that the error involved in the thin-wall approximations is greater for the pressure case than for the torsion case. Hence, a criterion applicable to the pressure case is reasonable for the torsion case as well. When $\alpha = 0.1$ the error is slightly more than five percent for the pressure case and slightly less than five percent for the torsion case. For the circular tubes tested in the present investigation, $\alpha = 0.057$, which corresponds to an error of less than three percent.

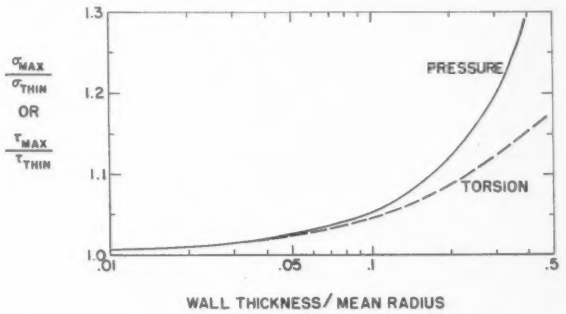

FIGURE 11. *Effect of wall thickness on the thin-wall approximation of the stress.*

(2) *Straight-Sided Tubes.* For elastic torsion of square or rectangular tubes the situation is not as favorable. If a mean radius for straight-sided tubes is defined by

$$r_m = \frac{2A}{P} \qquad (13)$$

and if the stress concentrations at the corners are

neglected, then the maximum shear stress at the outer surface is [24, 31]

$$\tau_{max}=\frac{T}{2Ah}\ (1+\alpha).$$

Therefore,

$$\frac{\tau_{max}}{\tau_{thin}}=1+\alpha.$$

Using the criterion of five percent error that was used above it appears that, for straight-sided tubes in torsion, thin-wall theory is applicable only if α is less than 0.05, rather than 0.1, which is the case for circular tubes. The following values of α apply to the square and rectangular tubes tested in the present investigation:

For the 0.083-in wall square tubes, $\alpha=0.057$;
for the 0.109-in wall square tubes, $\alpha=0.074$;
for the rectangular tubes, $\alpha=0.066$.

Clearly, the wall thicknesses for these tubes exceed the limit within which thin-wall torsion theory is accurate. However, this limit applies only to the stresses. It has been shown [32, 33] that the thin-wall requirement is far less restrictive for the calculation of angle of twist than it is for the calculation of stresses. Hence, the use of the thin-wall approach is acceptable for present purposes.

(3) *Effect of Creep.* For the case of circular tubes the exact creep stress distribution is given by eq (B.3) in appendix B. As an illustration of this stress distribution, this equation, with $r_m=1$ and $h=0.1$, is plotted in figure 12 for creep exponents of $m=1$, $m=2$, and $m=\infty$. The curve for $m=1$ represents the elastic stress distribution. The curve for $m=2$ represents a creep stress distribution where elastic strains are negligible in comparison with the creep strains. For a real case where a combination of elastic and creep strains exist the distribution would lie somewhere between the curves for $m=1$ and $m=2$. The curve for $m=\infty$ represents the uniform stress distribution assumed by Bredt's thin-wall theory. Thus, it is seen that in creep the stress distribution is actually closer to the thin-wall approximation than it is under elastic conditions. It may be concluded, therefore, that any criterion which defines a limiting wall thickness for elastic torsion is acceptable for creep conditions, too.

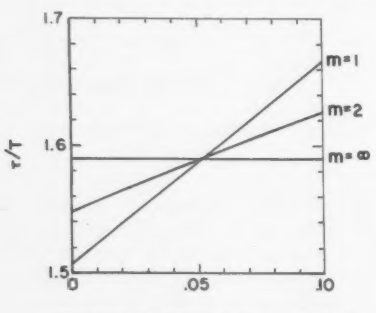

FIGURE 12. *Variation of shear stress through the wall of a circular tube in torsion.*

b. Stress Direction

Assumption No. 9 requires that all shear stresses be parallel to the surface of the tube. Thinking in terms of the hydrodynamic analogy, this appears to be a reasonable assumption for tubes of smooth contour, such as circles, but it can be demonstrated that it is somewhat erroneous for tubes with corners.

Consider, for example, torsion of a thin-walled tube of length L having a cross section in the form of a square with sides of length u and thickness h. This is shown diagramatically in two views in figure 13(a). According to the assumption, the shear stresses τ in each side of the square are parallel to the surface. If these are considered to be the only stresses acting, the only deformation which could take place is pure shear with displacements δ as shown in figure 13(b). (Only one face is shown in the left view, for simplicity. The broken lines indicate the original, undeformed shape.) The angle γ is simply the shear strain τ/G', where G is the modulus of rigidity and the prime is added for generality; G' and γ may be considered time-dependent to allow for creep. Displacement δ is equal to γL.

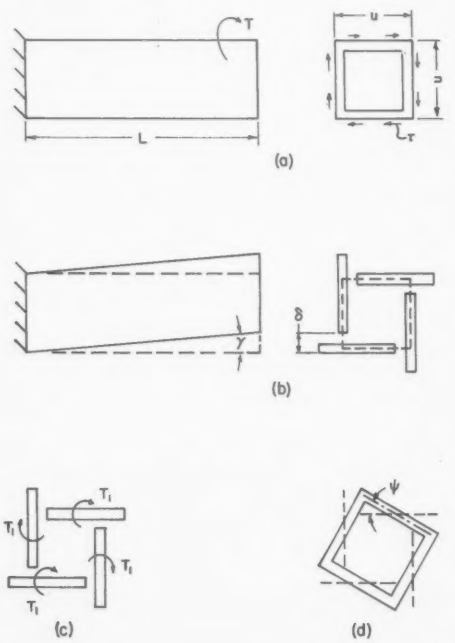

FIGURE 13. *Deformation of a square tube in torsion.*

This deformation pattern is clearly unacceptable by itself. What is required to restore compatability to the tube shape is a torsion of each face about its own longitudinal axis, as indicated by the torques T_1 in figure 13(c). The final configuration is shown in figure 13(d), where the required angle of twist is

$$\psi=\frac{2\delta}{u}=\frac{2\gamma L}{u}=\frac{2\tau L}{G'u}.$$

The torques T_1 are comprised of shear stresses near the corners which act normal to the surface although they are necessarily zero at the surface. The magnitude of T_1 is simply the torque required to twist a flat strip through angle ψ. That is,

$$T_1=\left(\frac{\psi}{L}\right)JG'=\frac{2\tau}{G'u}\,\frac{uh^3}{3}\,G'=\frac{2}{3}\,\tau h^3$$

where J is the torsional constant.

The condition of moment equilibrium can now be imposed. The four torques T_1 plus the moment of the shear stresses τ [fig. 13(a)] must equal the applied torque T. That is,

$$T=4T_1+4(\tau hu)\,\frac{u}{2}=\frac{8}{3}\,\tau h^3+2\tau hu^2$$

from which

$$\tau=\frac{T}{2h\left(\frac{4}{3}\,h^2+u^2\right)}.$$

According to Bredt's equation, however, the shear stress is

$$\tau=\frac{T}{2Ah}=\frac{T}{2hu^2}.$$

The difference, expressed as a fraction of the Bredt stress is

$$\frac{\Delta\tau}{\tau}=\frac{1}{1+\frac{3u^2}{4h^2}}.$$

This quantity is negligible for the square tubes tested in the present investigation and, in fact, amounts to less than one percent for h/u ratios up to one-tenth.

The presence of shear stresses normal to the surface of the tube introduces another source of error, namely, distortion of the cross-sectional shape in its own plane. This distortion changes the enclosed area and, therefore, the stresses as well. This problem was studied in detail by Ikeda [34] for square, thin-walled tubes. Using the results of his analysis it was determined that the effect on the stresses is less than one percent for the square tubes tested in the present investigation.

5. Discussion

The foregoing analyses have demonstrated that the assumptions introduced by Bredt's approximation to the Saint-Venant torsion theory are applicable to the torsion creep problem studied in this investigation. In the area of material idealization, however, some aspects of questionable applicability were revealed. Specifically, it was found that the materials of the tubes tested were not isotropic. However, with an approximate correction for anisotropy, satisfactory coincidence between theory and experiment was shown to be attainable. Unfortunately, this was not the case for the 0.109-in wall square tubes.

The studies carried out were inadequate to demonstrate that the specimen materials are homogeneous insofar as creep properties are concerned. Therefore, the discrepancies between theory and experiment could logically—although tentatively—be ascribed to nonhomogeneity; little can be done with such a problem unless the actual distribution of creep properties in the specimen is known. Intuitively, however, this is an unsatisfactory conclusion. The discrepancies (fig. 6) appear too large and too consistent to be attributed to a negative characteristic such as an absence of homogeneity. The fact that the discrepancies are not appreciably greater than those obtained under elastic conditions does not mitigate the need for a more satisfactory explanation, and at least one other possible explanation does exist.

In the preceding sections most of the assumptions involved in the development of the theory were justified or evaluated by measurements or calculations applicable to the problem at hand. The justifications for two of the assumptions, however, were based on references to data in the literature. These two assumptions, which are related, are the octahedral shear stress theory of multiaxial creep, and the equivalence of tensile and compressive creep. The failure of the torsion creep theory to describe the behavior of the 0.109-in wall square tubes is reason enough to reexamine the adequacy of these justifications. Although the octahedral shear stress theory is reported to be the one most commonly used at the present time [35] and also most favored by the weight of evidence in the literature [36], careful experimental measurements have been presented, in recent years, which are inconsistent with it [12, 37].

Some investigators are inclined to the belief that inconsistencies with the octahedral shear stress theory are somehow attributable to an effect of hydrostatic stress. The theory neglects such an effect but a difference between tensile and compressive creep properties would indicate that the effect is not negligible. Finnie [12] attempted to evaluate this effect experimentally and found that it could not be characterized by any simple modification of the octahedral shear stress theory. By means of a literature search, he also concluded that the hydrostatic stress effect becomes significant only when the absolute test temperature

exceeds half the absolute melting temperature of the test material, and proposes this as an explanation for the belief (which was widespread until recently) that the hydrostatic stress effect is negligible. In this context it is significant that the tests in the present investigation were conducted at a temperature which does, in fact, exceed half the absolute melting temperature of the specimen material.

The current state of knowledge regarding creep under multiaxial stresses was adequately summed up by Manson [35] in his discussion of the octahedral shear stress formulation:

> Whether the quantitative discrepancies that occur . . . are due to the inadequacy of the formulation still remains to be established. If modifications are to be made, the question must still be resolved as to whether they should be in the form proposed by Wahl [38], or by a suitable correction which includes hydrostatic stress, or whether still another interpretation is best.

It appears that an improved torsion creep theory for noncircular tubes must await the development of an improved multiaxial creep theory.

6. Conclusions

A theory for the torsion creep behavior of thin-walled tubes was developed by applying the octahedral shear stress theory of multiaxial creep to a generalized version of Bredt's equations. The theory was compared with experimental results obtained by tests on 12 large circular and noncircular aluminum alloy tubes at 400 °F. The following principal conclusions, applicable to the material and tube configurations tested herein, were obtained:

1. In most cases the theory can provide usable results when suitable allowances or corrections are made for anisotropy.

2. Aside from the effects of anisotropy, differences between theory and experiment have been tentatively ascribed to (a) a shortcoming in existing theory of multiaxial creep behavior which is related to the inequality of tensile and compressive creep properties, or (b) nonhomogeneity in creep properties.

3. The largest differences between theory and experiment were obtained with the 0.109-in wall square tubes. These differences were conservative and are smaller than the differences in the measured creep properties of the material from batch to batch. Also, the differences between theory and experiment are not appreciably larger than the discrepancies obtained when Bredt's equations are used to predict the torsion behavior of elastic tubes at room temperature.

Other conclusions of interest which were obtained in the course of the investigation are:

1. The existence of nonhomogeneity in creep properties at elevated temperatures is not, necessarily, revealed by measurements of other mechanical properties at room temperature.

2. For the calculation of stresses in circular tubes the thin-wall approximation may be considered adequate for thickness-to-radius ratios up to one-tenth. For straight-sided tubes equivalent accuracy is obtained for ratios up to only one-twentieth, where the effective radius is defined as in eq (13). These criteria are applicable under creep conditions as well as under elastic conditions. For the calculation of twist angles the thin-wall approximation presumably is less restrictive than it is for the calculation of stresses.

3. A simple and unique analysis is presented for evaluating the shear stresses which act normal to the surface of square tubes under torsion. It is shown that the effect of these stresses, on the overall stress distribution, is negligible for thin-walled tubes.

7. References

[1] R. W. Bailey, Creep of steel under simple and compound stresses and the use of high initial temperature in steam power plant, Trans. Tokyo Sectional Meeting, World Power Conf. **3**, 1089 (1929).

[2] R. W. Bailey, The utilization of creep test data in engineering design, Proc. Inst. Mech. Eng. **131**, 131 (1935).

[3] F. L. Everett, Strength of materials subjected to shear at high temperatures, Trans. Am. Soc. Mech. Eng. **53**, 117 (1931).

[4] F. L. Everett and C. L. Clark, Report on torsion creep tests for comparison with tension creep tests on a carbon-molybdenum steel, Proc. Am. Soc. Testing Materials **39**, 215 (1939).

[5] F. C. Lea, discussion of [2], Proc. Inst. Mech. Eng. **131**, 334 (1935).

[6] H. J. Tapsell and A. E. Johnson, Creep under combined tension and torsion, part 1, the behavior of a 0.17 percent carbon steel at 455 deg C., Engineering (London) **150**, 24 (1940).

[7] A. E. Johnson, Behavior of cast steel at elevated temperatures, Engineer (London) **188**, 126 (1949).

[8] A. E. Johnson, The creep of a nominally isotropic aluminum alloy under combined stress systems at elevated temperatures, Metallurgia (Manchester) **40**, 125 (1949).

[9] A. E. Johnson, The creep of a nominally isotropic magnesium alloy at normal and elevated temperatures under complex stress systems, Metallurgia (Manchester) **42**, 249 (1950).

[10] A. E. Johnson, Creep under complex stress systems at elevated temperatures, Proc. Inst. Mech. Eng. **164**, 432 (1951).

[11] G. Gerard and A. C. Gilbert, A critical strain approach to creep buckling of plates and shells, J. Aero/Space Sci. **25**, 429 (1958).

[12] I. Finnie, An experimental study of multiaxial creep in tubes, Proc. Joint Intern. Conf. on Creep, p. 2/21 (Inst. Mech. Eng., London, 1963).

[13] J. L. Gubser, O. M. Sidebottom and M. R. Shammamy, Creep torsion of prismatic bars, Proc. Joint Intern. Conf. on Creep, p. 2/99 (Inst. Mech. Eng., London, 1963).

[14] V. P. Sdobyrev, Creep and durable strength under combined tensile and torsional stress, Engineering J., No. 2, p. 391 (NBS Joint Publ. Research Service, 1963). Translated from Inzhenernyy Zhurnal (Moscow) **3**, 413 (1963).

[15] S. Taira, R. Koterazawa and R. Mamiya, Creep under the changing combined tension-torsion stress system, Proc. 7th Jap. Cong. Testing Materials, p. 56 (1964).

[16] N. R. Bauld, Jr., and O. M. Sidebottom, Experimental and theoretical evaluation of several creep theories for creep torsion of circular bars, Developments in Theoretical and Applied Mechanics **2**, 557 (1965).

[17] E. Z. Stowell and R. K. Gregory, Steady-state biaxial creep, Trans. Am. Soc. Mech. Eng. [E] **32**, 37 (1965).

[18] R. Bredt, Critical observations on elastic torsion (in German), Z. Ver. Deut. Ingenieure **40**, 785 (1896).

[19] G. I. Taylor and H. Quinney, The plastic distortion of metals, Trans. Roy. Soc. London [A] **230**, 323 (1931).

[20] W. T. Lankford, J. R. Low and M. Gensamer, The plastic flow of aluminum alloy sheet under combined loads, Trans. Am. Inst. Mining Met. Eng. **171**, 574 (1947).
[21] P. Kuhn, The torsional stiffness of thin duralumin shells subjected to large torques, NACA TN 500 (1934).
[22] W. Hovgaard, Torsion of rectangular tubes, J. Applied Mech. **4**, A131 (1937).
[23] S. Levy, A. E. McPherson and W. Ramberg, Torsion test of a monocoque box, NACA TN 872 (1942).
[24] R. L. Moore and D. A. Paul, Torsion tests of 24S-T aluminum-alloy noncircular bar and tubing, NACA TN 885 (1943).
[25] F. J. Vawter, G. J. Guarnieri, L. A. Yerkovich and G. Derrick, Investigation of the compressive, bearing, and shear creep-rupture properties of aircraft structural metals and joints at elevated temperatures, Wright Air Development Center Tech. Rep. 54-270, Part 2 (1956).
[26] G. J. Heimerl and J. Farquhar, Compressive and tensile creep of 7075-T6 and 2024-T3 aluminum-alloy sheet, NASA TN D-160 (1959).
[27] O. K. Salmassy, R. J. MacDonald, R. L. Carlson and G. K. Manning, An investigation of the interchange of tensile creep for compressive creep, part 1, types 2024-T4 and 1100-0 aluminum, Wright Air Development Center Tech. Rep. 56-26, Part 1 (1956).
[28] V. Z. Vlasov, Thin-walled elastic beams, 2d ed., pp. 244-249 (Israel Program for Scientific Translations, Jerusalem, 1961). Translation of Tonkostennye uprugie sterzhni (Gosudarstvennoe izdatelstvo fiziko-matematicheskoi literatury, Moscow, 1959).
[29] T. von Kármán and W. Z. Chien, Torsion with variable twist, J. Aeron. Sci. **13**, 503 (1946).
[30] T. H. Huth, Torsional stress concentration in angle and square tube fillets, J. Applied Mech. **17**, 388 (1950).
[31] D. Williams and J. Taylor, Variations of shear stress in thin-walled tubes under torque, Aeron. Research Comm. (London) Rep. & Mem. No. 1812 (1938).
[32] P. Kuhn, Stresses in aircraft and shell structures, p. 14 (McGraw-Hill Book Co., Inc., New York, 1956).
[33] R. M. Koper, Twist and shear in thin-walled bars under torsion, Product Eng. **34**, No. 22, 92 (Oct. 28, 1963).
[34] K. Ikeda, Failure of non-circular thin tubes in torsion, calculations and experiments about square thin tubes (in Japanese with English abstract), J. Soc. Aeron. Sci. Nip. **7**, 426 (1940).
[35] S. S. Manson, Design considerations for long life at elevated temperatures, Proc. Joint Intern. Conf. on Creep **2**, D29 (Inst. Mech. Eng., London, 1965).
[36] G. H. Rowe, J. R. Stewart and K. N. Burgess, Capped end, thin-wall tube creep-rupture behavior for type 316 stainless steel, Trans. Am. Soc. Mech. Eng. [D] **85**, 71 (1963).
[37] A. M. Wahl, G. O. Sankey, M. J. Manjoine and E. Shoemaker, Creep tests of rotating disks at elevated temperature and comparison with theory, Trans. Am. Soc. Mech. Eng. **76**, 225 (1954).
[38] A. M. Wahl, Application of the modified Bailey equations for creep under biaxial tension stress, Proc. 4th U.S. Nat. Cong. Applied Mech., p. 1167 (Am. Soc. Mech. Eng., 1962).
[39] I. Finnie and W. R. Heller, Creep of engineering materials, pp. 147-148 (McGraw-Hill Book Co., Inc., New York, 1959).
[40] L. M. Kachanov, Theory of creep (in Russian), p. 90 (Fizmatgiz, Moscow, 1960).

Appendix A. Generalized Version of Bredt's Second Equation

Consider a cylindrical shell of closed section having a length L and faces normal to the cylinder axis. See figure 14. Under an applied torque T an originally longitudinal element AB of the midsurface rotates to an orientation AB'. Angle BAB' is the shear strain γ. Displacement $\overline{BB'}$ is equal to $L\gamma$ and it is assumed that the strains are sufficiently small that this displacement is perpendicular to the radius r from the axis of torsion.

The angle of twist, viewed from this axis, is

$$\psi=\frac{\overline{BB'}}{r}=\frac{L\gamma}{r} \tag{A.1}$$

and the angle of twist per unit length is

$$\theta=\frac{\psi}{L}=\frac{\gamma}{r}. \tag{A.2}$$

It is clear that this quantity does not remain constant as midthickness curve C is traversed. Yet it is common and desirable to assign a single value to the quantity known as angle of twist per unit length. Generally, this question is ignored and θ is computed either by the membrane analogy or by a strain energy approach, both of which yield an effective mean value θ. A mean value is also sought here, but the membrane analogy and the strain energy method will not be used since these approaches apply principally to elastic materials.

A mean radius can be deduced from the relation

$$r_m=\frac{2A}{P} \tag{A.3}$$

where P is the perimeter of C and A is its enclosed

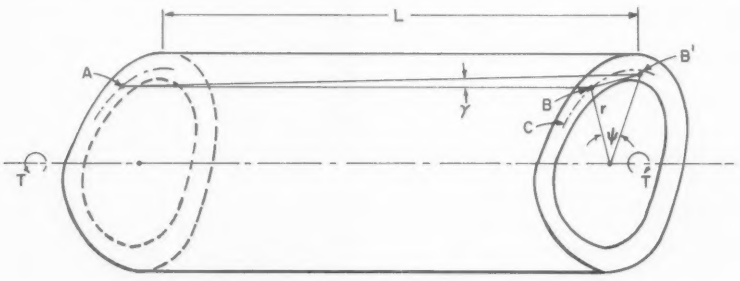

FIGURE 14. *Derivation of generalized version of Bredt's second equation.*

area. Then, designating the mean shear strain as γ_m leads to the following expression for angle of twist.

$$\theta=\frac{\gamma_m}{r_m}=\frac{\gamma_m P}{2A}. \tag{A.4}$$

This equation may be regarded as a generalized version of Bredt's second equation.

Appendix B. Torsion Creep of Circular Tube

Consider a hollow circular rod in torsion with inside radius a and outside radius b. The shear creep properties of the material are given by eq (4). Then, neglecting elastic strains for the moment,[5] the shear stress at any radius r is shown [39, 40] to be

$$\tau=\frac{\left(3+\frac{1}{m}\right)T}{2\pi b^3\left[1-\left(\frac{a}{b}\right)^3+\frac{1}{m}\right]}\left(\frac{r}{b}\right)^{1/m}. \tag{B.1}$$

The shear strain distribution is obtained by substituting eq (B.1) into eq (4), giving

$$\gamma=\sqrt{3}\,k\,\frac{r}{b}\left[\frac{\sqrt{3}\left(3+\frac{1}{m}\right)T}{2\pi b^3\left[1-\left(\frac{a}{b}\right)^{3+1/m}\right]}\right]^m t^n.$$

Then the angle of twist is

$$\theta=\frac{\gamma}{r}=\frac{\sqrt{3}\,k}{b}\left[\frac{\sqrt{3}\left(3+\frac{1}{m}\right)T}{2\pi b^3\left[1-\left(\frac{a}{b}\right)^{3+1/m}\right]}\right]^m t^n. \tag{B.2}$$

For a thin-walled circular tube let the mean radius be r_m and the wall thickness be h so

$$b=r_m+\frac{h}{2}\text{ and }a=r_m-\frac{h}{2}.$$

Then the stress distribution, eq (B.1), becomes

$$\tau=\frac{\left(3+\frac{1}{m}\right)T}{2\pi r_m^3\left[\left(1+\frac{h}{2r_m}\right)^{3+1/m}-\left(1-\frac{h}{2r_m}\right)^{3+1/m}\right]}\left(\frac{r}{r_m}\right)^{1/m}. \tag{B.3}$$

Since $\frac{h}{2r_m}\ll 1$, the quantity in brackets in the denominator reduces to approximately $2\left(3+\frac{1}{m}\right)\frac{h}{2r_m}$. Thus, the stress distribution may be written as

$$\tau=\frac{T}{2\pi r_m^2 h}\left(\frac{r}{r_m}\right)^{1/m}. \tag{B.4}$$

[5] The effect of the elastic component is discussed in section 4.4a(3).

Using a similar approach, the angle of twist, eq (B.2), may be rewritten as

$$\theta=\frac{\sqrt{3}k}{r_m}\left(\frac{\sqrt{3}T}{2\pi r_m^2 h}\right)^m t^n$$

or

$$\theta=\frac{\sqrt{3}k}{r_m}\left(\frac{\sqrt{3}T}{2Ah}\right)^m t^n. \tag{B.5}$$

This is identical with eq (8) which was derived with the generalized Bredt equation. Note also that the shear stress at the mean radius, from eq (B.4), is

$$\tau_m=\frac{T}{2\pi r_m^2 h}=\frac{T}{2Ah}$$

which is the value of the uniform shear stress according to Bredt's first equation.

Appendix C. Details of Torsion Creep Tests

C.1. Equipment

An overall view of the torsion creep testing equipment is shown in figure 15. Close-up views of the left and right ends of the setup are given in figures 16 and 17, respectively.

The ends of the specimen (A, figs. 15 and 16) are reinforced with close-fitting plugs to a depth of three inches. The specimen is mounted such that it passes through the test furnace (B, figs. 15, 16 and 17). The plugged left end of the specimen is rigidly bolted to a welded lug on a building column. The right end of the specimen is fastened, by means of a keyed shaft passing through the end plug, to a large sprocket wheel (C, figs. 15, 16 and 17). The shaft is supported by three journal bearings used at only a small fraction of their load capacity. The horizontal positions of the bearings are adjustable, both longitudinally and laterally, to permit proper alinement of the shaft with the fixed end mounting. The sprocket wheel, which has a pitch diameter of 38.2 in, applies torque to the

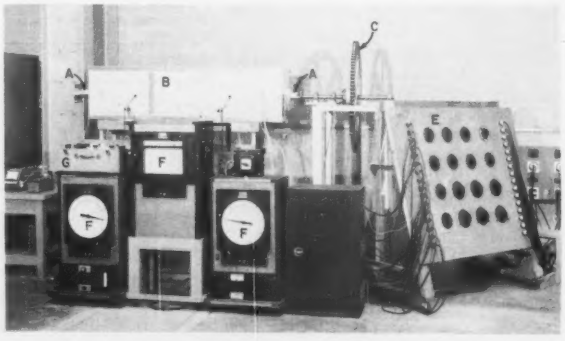

FIGURE 15. *Overall view of torsion creep testing setup.*

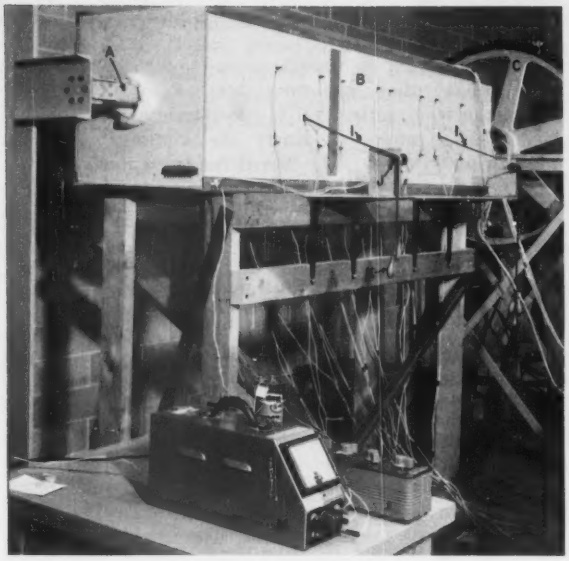

FIGURE 16. *Torsion creep testing setup.*
View from left side.

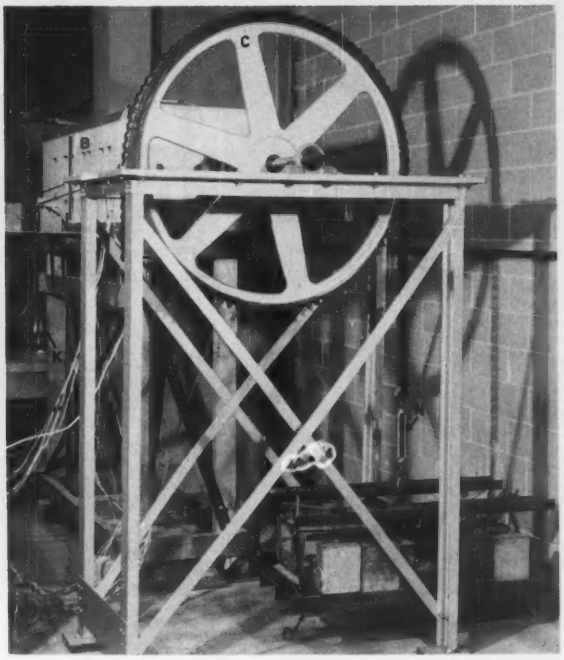

FIGURE 17. *Torsion creep testing setup.*
View from right side.

test specimen by means of a weight pan (D, fig. 17) suspended from the sprocket chain.

The test furnace is fabricated of transite, with steel reinforcement at the edges. The side of the furnace which faces the wall in figure 15 is hinged. Figure 18 is a view of the furnace, in a different location, with the hinged side opened to reveal the interior. Heat is supplied by 32 tubular infrared lamps rated at 120 V and 500 W. The lamps are wired in parallel pairs, the voltage to each pair being adjustable by one of a bank of variable autotransformers (E, fig. 15). Power is regulated by three time-proportioning, potentiometer-type temperature controllers (F, fig. 15), each controlling the temperature over approximately one-third of the furnace. Nine chromel-alumel thermocouples were spot welded to the outer surface of each torsion specimen, at various locations within the three-foot gage length. Three of these thermocouples served as the sensors for the temperature controllers and their outputs were continuously recorded. Outputs of the other six thermocouples were monitored with a calibrated millivolt potentiometer (G, fig. 15), which was also used to periodically check the calibration of the temperature recorders.

Thermocouples cannot normally be spot welded to the structural aluminum alloys with portable, laboratory-type spot welding apparatus. However, the usual alternative mounting technique, clamping, was considered to be particularly undesirable for this type of specimen since the clamps would have to be large as well as numerous and, therefore, deleterious to the attainment of a uniform temperature distribution. Hence, a new technique was devised for spot welding thermocouple beads to 2024-T3 aluminum alloy, which turned out to be completely successful. The technique, in brief, consists of spot welding a small piece of 0.004-in gold foil, about 1 mm square, to the aluminum and then spot welding the thermocouple bead to the foil.

Twist was measured with a troptometer [6] developed specifically for this investigation. Steel sprockets (H, fig. 18) having a pitch diameter of 5.73 in were concentrically attached to the specimen at each end of the three-foot gage length. Sprocket chains (I, figs. 16 and 18) passed over these sprockets and out of the furnace through small holes and thence over a pair of small sprockets (J, figs. 16 and 17) having a pitch diameter of 0.81 in. Each small sprocket is mounted on the shaft of a precision, one-turn, resistance potentiometer rated at 10,000 Ω ± 1 percent with a linearity tolerance of ± 0.50 percent. The ends of the chains are weighted (K, figs. 16 and 17) to keep them taut.

Torsion of the specimen causes rotation of the 5.73-in sprockets mounted on it. This rotation is transferred, by means of the sprocket chains, to the resistance potentiometers, and magnified by the sprocket ratio. The difference in rotation of the two 5.73-in sprockets, measured as the difference in resistance between the two potentiometers, is the angle of rotation of the specimen over the three-foot gage

[6] trop.tom.e.tər, n. An instrument for measuring the angular distortion of a bar or piece undergoing a torsion test (Webster). From the Greek *tropos*, turn and *metron*, measure. This word is clearly preferable to any of the existing words used for this purpose in the current literature.

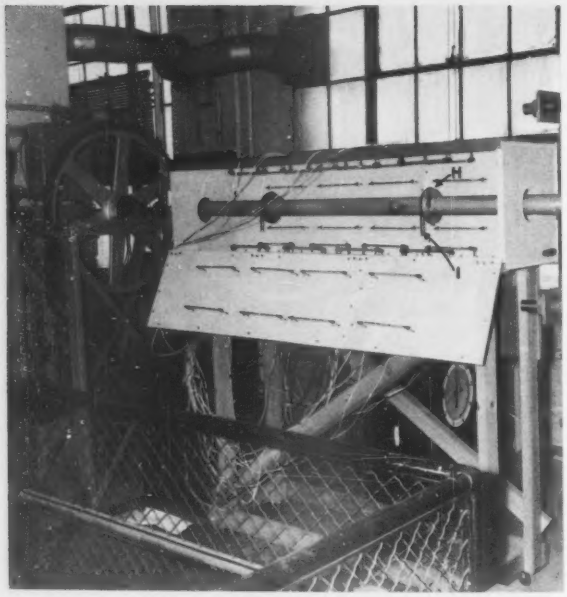

FIGURE 18. *Torsion creep testing setup in a different location with furnace door open.*

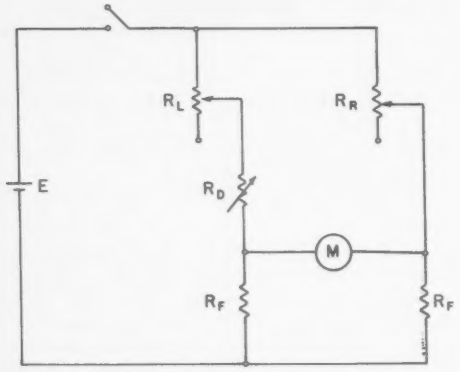

FIGURE 19. *Troptometer bridge circuit.*
E. Dry cell, 1½ V.
M. Null indicator, Honeywell 104 W1G.
R_D. Decade resistance box, 0 to 11,110 Ω.
R_F. Precision fixed resistor, 5,000 Ω.
R_L. Left potentiometer, 0 to 10,000 Ω.
R_R. Right potentiometer, 0 to 10,000 Ω.

length. A bridge circuit, figure 19, is used to measure the difference in resistance between the left and right potentiometers. The decade resistance box (L, fig. 16 and R_D, fig. 19) is periodically adjusted to give a null indication on the meter (M, figs. 16 and 19) and the box setting is then equal to the desired resistance difference. The sensitivity of the null indicator is equivalent to a fraction of an ohm and resistance measurements were made to the nearest ohm. With the sprocket ratios and potentiometers used, one ohm corresponds to an angle of twist of 2.42×10^{-6} radians per inch.

Since an exact solution is available for elastic torsion of circular tubes, a torsion test of a circular tube specimen was carried out at room temperature, within the elastic range, to verify the loading and twist measuring systems. The shear modulus derived from this test was 3.98×10^6 lb/in^2 which agrees with the nominal value of 4.0×10^6 lb/in^2 for 2024-T3 aluminum alloy.

C.2. Procedure

Twelve torsion creep tests were carried out at 400 °F, three on each of the four tube shapes shown in figure 1.

Alinement of each specimen was visually achieved by adjusting the positions of the bearings which support the torque shaft. (This procedure was verified with one 0.083-in wall square tube specimen using resistance strain gages. Thirteen gages were cemented onto the outer surface of the specimen, at various locations, in the longitudinal direction. Torques were applied, within the elastic range, at room temperature. The strain measurements did not reveal the presence of any significant bending or axial force in the specimen.) The weight pan was supported on a platform such that the sprocket chain was unloaded, and weights of the desired amount were stacked upon it. Specimens were heated to the test temperature, 400 °F, in approximately 1 hr, and were kept at this temperature for another hour to permit temperatures to equalize prior to the start of the creep test. The test was started by smoothly raising the weight pan from its platform with a turnbuckle (N, fig. 17) and then removing the platform.

Twist and temperature measurements were made at closely spaced intervals following the start of a test and less frequently thereafter. Twist readings were found to be repeatable within 1 Ω on the decade box (which is equivalent to an angle of twist of less than 3×10^{-6} radians per inch) and temperatures were constant within 1 °F throughout the tests and uniform within 3 °F.

Tests were terminated after approximately 50 hr.

Appendix D. Anisotropic Torsion Creep Theory for Noncircular Tubes

Effects of anisotropy in plastic deformation are commonly included by using a modified expression for the octahedral shear stress, such as

$$\bar{\tau} = \frac{1}{3}\left[\zeta_1(\sigma_x - \sigma_y)^2 + \zeta_2(\sigma_y - \sigma_z)^2 + \zeta_3(\sigma_z - \sigma_x)^2 + 6\zeta_4\tau_{xy}^2 + 6\zeta_5\tau_{yz}^2 + 6\zeta_6\tau_{zx}^2\right]^{1/2} \qquad \text{(D.1)}$$

where x, y, and z are Cartesian coordinates which denote the principal axes of orthotropy and ζ_i are con-

stants. Coordinate x is parallel to the longitudinal axis of the tube. In this form $\bar{\tau}$ does not have physical significance as the shear stress on the octahedral plane unless all the ζ_i are unity; it is simply a measure of the propensity for plastic flow (in this case creep). The octahedral shear creep strain is, as usual,

$$\bar{\gamma}=\frac{2}{3}\left[(\epsilon_x-\epsilon_y)^2+(\epsilon_y-\epsilon_z)^2+(\epsilon_z-\epsilon_x)^2 + \frac{3}{2}\gamma_{xy}^2+\frac{3}{2}\gamma_{yz}^2+\frac{3}{2}\gamma_{zx}^2\right]^{1/2}. \quad \text{(D.2)}$$

Using eqs (D.1) and (D.2) it may be seen that in uniaxial tension with $\sigma_x=\sigma$ and $\epsilon_x=\epsilon$, and assuming Poisson's ratio is one-half,

$$\bar{\tau}=\frac{\sqrt{\zeta_1+\zeta_3}}{3}\sigma \text{ and } \bar{\gamma}=\sqrt{2}\epsilon. \quad \text{(D.3)}$$

Similarly, for pure shear with $\tau_{xy}=\tau$ and $\gamma_{xy}=\gamma$

$$\bar{\tau}=\sqrt{\frac{2\zeta_4}{3}}\tau \text{ and } \bar{\gamma}=\sqrt{\frac{2}{3}}\gamma \quad \text{(D.4)}$$

Solving eqs (D.3) and (D.4) simultaneously and substituting eqs (1) and (3) therein gives

$$\gamma=\sqrt{3}k\left(\frac{\sqrt{3}}{2}\frac{ZT}{Ah}\right)^m t^n$$

where

$$Z=\sqrt{\frac{2\zeta_4}{\zeta_1+\zeta_3}} \text{ is the anisotropy parameter.}$$

Performing a contour integration to evaluate γ_m and substituting into eq (2) gives, for a tube of uniform wall thickness

$$\theta=\frac{\sqrt{3}}{2}\frac{P}{A}k\left(\frac{\sqrt{3}}{2}\frac{ZT}{Ah}\right)^m t^n.$$

When $Z=1$, this agrees with the isotropic twist equation, eq (7), and when $Z=1.15$ it agrees with the anisotropic version, eq (10).

(Paper 71C3–256)

JOURNAL OF RESEARCH of the National Bureau of Standards—C. Engineering and Instrumentation
Vol. 71C, No. 3, July–September 1967

Digitized Low-Frequency Phasemeter Assembled from Logic Modules

John E. McKinney

Institute for Basic Standards, National Bureau of Standards, Washington, D.C. 20234

(April 27, 1967)

A digital phasemeter is described which is capable of operating from arbitrarily low frequencies to 10 kHz, for which the lower limit depends essentially upon the time available to the operator to make the measurement. The phasemeter involves a logic circuit which can be assembled easily from commercially available logic modules without the necessity of a proficiency in electronics. The output of the logic circuit is read into a conventional digital preset frequency-ratio meter. The determination is absolute and utilizes a time base. Accordingly, no calibration against a phase standard is necessary. The agreement between this phasemeter and a quality phase shifter was found to be within $\pm 0.01°$ at 400 Hz, which is the accuracy specified by the manufacturer of the phase shifter. Considerable ability to ignore signal imperfections is inherent in this device.

Key Words: Digital, phasemeter, logic circuit, low frequency, measurements, phase.

1. Introduction

This work is concerned with the description of a highly accurate digital phasemeter capable of operating from any arbitrarily low frequency up to 10 kHz continuously. The lower limit on frequency depends essentially upon the time available to make the measurement. The demand for a device of this type often arises in certain types of rheological measurements on substances manifesting very long relaxation times. Apparently most, if not all, commercial production phasemeters have a low-frequency cutoff in the low audio range, at best, and the more accurate ones are capable of measuring at only a single frequency. The device described here utilizes logic[1] circuitry, which can be assembled easily from commercially available logic modules[2] without the necessity of a proficiency in electronics. The output of the logic circuit is applied to a conventional digital preset frequency-ratio meter. The prototype without the frequency-ratio meter is shown in figure 1.

For two periodic signals of the same waveform, but relatively displaced in time, a phase angle may be defined as the angular separation between a pair of corresponding[3] points selected arbitrarily. Thus, using a suitable level detector, a measurement may be obtained on a time base, which has a great advantage because measurements in time may be taken to very high resolution. In the phasemeter to be described zero crossings (with both derivatives) were selected as the characteristic points. This choice is appropriate because the first derivative of a sine function is a maximum when the value of the function is zero. Thus, maximum resolution in the time of the level crossing is obtained. Consequently, only two basic ingredients are necessary to measure phase under ideal conditions, a stable level detector (for example, a high gain, or open loop, operational amplifier, or a voltage comparator) and an accurate time base generator, which is activated by the level detector. If τ is the time interval between corresponding zero crossings and ν is the frequency, the phase angle φ in radians as defined above is

$$\varphi = 2\pi\nu\tau. \tag{1}$$

The nature of errors often encountered over a one cycle measurement using a digital time interval meter (counter) is discussed in reference [2].[4]

An alternative method is to measure the output of a suitable level detector with a voltmeter over many cycles of input signal. Also, a so-called "coincident slicer" [3] has been used in this connection. Some discussion on modifying the logic circuit to use a digital integrating voltmeter in place of the frequency ratio meter is included later in this paper.

[1] "Logic" as commonly used in computer technology, applies to compatible electronic components, which when interconnected appropriately, can implement digital arithmetic and Boolean functions. For a treatise on this subject, see for example reference [1].

[2] For a list of makers of logic modules, consult the current Electronic Engineers Master Catalog, United Technical Publications, Inc., New York (annual periodic publication).

[3] Any point on a sine wave of unit amplitude is uniquely characterized over a period by the value of the function and its first derivative. Points on two different sine waves correspond if they have identical characteristic values.

[4] Figures in brackets indicate the literature references at the end of this paper.

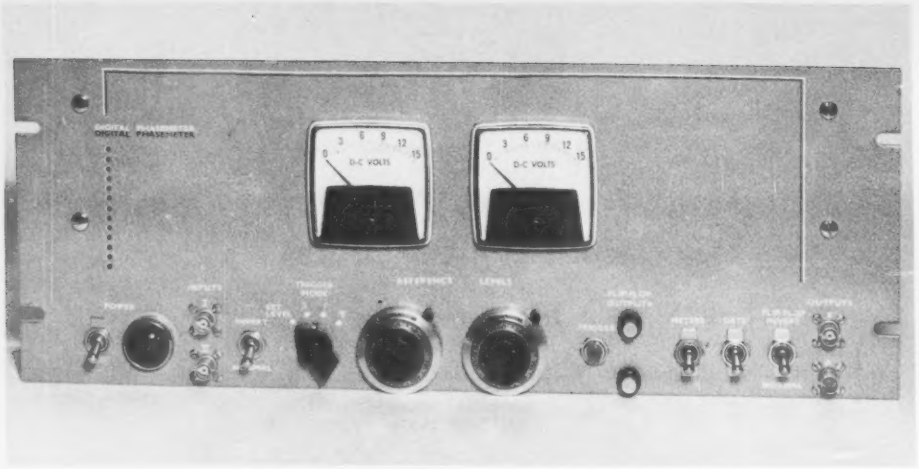

FIGURE 1. *Prototype containing the logic circuit.*

In practice ideal sine waves are never encountered, and in general the quality of the signals will not be as good as desired. Accordingly, the course which was followed in this work was to analyze the effect of signal imperfections on the shift of the zero crossings from those of ideal sine waves, and then to attempt to develop an instrument which would essentially ignore these imperfections and other potential systematic errors.

The results of this work are considered to be very satisfactory. The determination is absolute in the sense that it does not have to be calibrated against a phase standard, but may be referred to the basic frequency standard. It involves only one adjustment which can be made without the use of auxiliary equipment and which may be omitted with only a slight loss in accuracy. On comparison with a quality phase standard operating at 400 Hz with an accuracy within $\pm 0.01°$ claimed by the manufacturer, agreement was found to be slightly better than the accuracy claimed for the above instrument.

2. Design Considerations

2.1. Errors Encountered Using Zero Crossing Detectors

If the frequency of the fundamental is constant, a signal may be considered to consist of the fundamental sine wave plus imperfections, which include d-c offset, noise, and harmonic distortion. With a zero-crossing detector these imperfections will usually influence the position of the zero crossings of an otherwise ideal sine wave. Clearly, if the waveforms of the two signals are the same (including the imperfections), the zero crossings of each signal will be displaced from those of the fundamental by the same amount with no corresponding error in the apparent [5] phase angle. Unfortunately, in practice, the imperfections accompanying the fundamentals of the two signals usually will be significantly different. The imperfections which are considered are d-c offset, noise, including periodic disturbances incommensurable [6] with the signal frequency, and harmonic distortion. Also considered is frequency instability, which is a special case for which the "sine wave" itself does not exist. In order to simplify the analysis, one of the signals will be considered hypothetically to be a pure sine wave, while the other will be considered to contain only one of the following designated imperfections.

a. D-C Offset

Unless a transformer coupled output is used, the presence of a significant d-c offset voltage accompanying the signal is very likely. This is particularly true at low frequencies because of the necessity of using either direct coupled stages with "bucking" voltages, or very large electrolytic capacitors with significant dissipation.

The effect of an offset voltage on the apparent phase angle is easy to analyze. For a given offset voltage, E_{DC}, the positions of the actual zero crossings are the solutions of the equation

$$E_1 \sin \omega t + E_{DC} = 0.$$

For offset voltages small in comparison to signal amplitude, the corresponding phase error using positive-going crossings is

$$\Delta\varphi \approx -\frac{E_{DC}}{E_1}. \tag{2}$$

Accordingly, the error introduced here may be very serious. For example, if one wishes to make a measure-

[5] In this usage "apparent" applies to the angle given by the phasemeter.

[6] Two frequencies are "commensurable" only if their ratio is a rational number. Thus, two signals with incommensurable frequencies can never have more than one common zero crossing.

ment to within 0.01°, the offset voltage may not exceed 175 μV with a 1 V signal. Since offsets of this magnitude or more are usually encountered in low-frequency measurements and their magnitudes are usually not known or even constant, it is desirable, if not necessary, for accurate measurements to incorporate a technique in the design of the phasemeter to cancel or essentially eliminate errors from this source. Two methods of accomplishing this will be mentioned in later sections. One of these is to utilize both positive- and negative-going crossings for triggering.

The effect of long time instability in level detectors may also be treated in the same fashion as offset voltages accompanying the signals.

b. Noise

Noise may be considered to be a randomly varying offset voltage for which the integral tends to go to zero over large values of the argument, time. Through reasoning similar to that in the last section, a bound on the error in the apparent phase angle measured over one cycle may be approximated by

$$|\Delta\varphi| \sim 1/r \tag{3}$$

where r is the signal to noise ratio. Since noise is usually random in character, and since the errors in time are essentially an odd function of the instantaneous noise, one would expect the phase error to be effectively cancelled if the measurement is taken over many periods of sine wave. This is accomplished by using a preset frequency-ratio meter.

Periodic fluctuations, such as 60 Hz hum, for which the frequency is incommensurable with the signal frequency have an effect similar to noise. Although these fluctuations are not random, by the specific nature of their regularity and incommensurability (with respect to the input signal frequency), the contributions of all the errors in time should cancel providing the measurement is taken over many cycles of both input signal and periodic disturbance. Commensurable periodic imperfections other than harmonics are not considered because the possibility of encountering them is remote in this application.

c. Harmonic Distortion

With phasemeters based on zero crossings, harmonic distortion appears to be the most annoying imperfection. In general, there is apparently no obvious and reliable method to remove or even significantly reduce the corresponding errors in the apparent phase angle. Oscillators with less than 0.02 percent harmonic distortion are not common; therefore, significant harmonics are usually introduced into a network which is to be investigated. Since both the phase shift and attenuation of any network are generally frequency dependent, the character of the harmonic content with respect to the fundamental will be modified so that effective cancellation of zero crossing errors is nonexistent. The only reliable solution to this problem is to reduce harmonic distortion at the source as much as possible and to maintain the network input voltage sufficiently low to linearize response. This procedure is, of course, not always possible.

In order to analyze the errors introduced by harmonic distortion, the character of the distortion must be known with respect to the amplitudes and phase relations of the significant harmonics. This kind of information is nearly impossible to obtain. The following argument reveals some semiqualitative information which may be useful, in particular, when knowledge of the harmonic content is limited.

In general, ignoring the d-c component, which was treated earlier as an offset, a periodic signal with repeat frequency $\omega/2\pi$ may be expressed in terms of its Fourier components as follows:

$$E(\omega t) = E_1 \sin \omega t + \sum_{m=2}^{M} E_m \cos m\omega t + \sum_{n=2}^{N} E_n \sin n\omega t, \ (E_1 > 0)$$

where the first term on the right is the undistorted signal, again arbitrarily taken as a sine function. The positions of the zero crossings are given by the solutions of the following equation in which the cosine terms have been resummed to distinguish between odd and even harmonics.

$$E_1 \sin \omega t + \sum_{j=1}^{J} E_j \cos (2j+1)\omega t + \sum_{k=1}^{K} E_k \cos 2k\omega t + \sum_{n=2}^{N} E_n \sin n\omega t = 0.$$

For small harmonic distortion the behavior at the positive-going zero crossing may be approximated by

$$E_1\omega t + \sum_{j=1}^{J} E_j + \sum_{k=1}^{K} E_k = 0.$$

The corresponding phase error is accordingly

$$\Delta\varphi = -\left[\sum_{j=1}^{J} E_j + \sum_{k=1}^{K} E_k\right]/E_1. \tag{4}$$

The response in the vicinity of the negative-going zero crossings may be evaluated by replacing the argument ωt by $\omega t + \pi$ and again evaluating the behavior at small ωt. The negative-going crossings are, accordingly, the solutions of the equation

$$E_1 \sin (\omega t + \pi) + \sum_{j=1}^{J} E_j \cos (2j+1)(\omega t + \pi) + \sum_{k=1}^{K} E_k \cos 2k(\omega t + \pi) = 0.$$

Using multiple angle formulas and the approximations used previously, the following phase error is obtained:

$$\Delta\varphi = -\left[\sum_{j=1}^{J} E_j - 2\sum_{k=1}^{K} E_k\right]/E_1. \tag{5}$$

Equations (4) and (5) pertain to positive- and negative-going zero crossings with indices j and k pertinent to odd and even cosine harmonics. Obviously, if both zero crossings are used for triggering, the errors in phase are additive. In this case the phase error is

$$\Delta\varphi = -2\sum_{j=1}^{J} E_j, \tag{6}$$

which indicates that under the conditions imposed on this evaluation, only the cosine terms of odd order contribute to phase errors when contributions at all zero crossings are considered.

When the amplitudes of the significant harmonics are known without any knowledge with respect to their sign and zero crossings (as obtained from a wave analyzer), a useful bound on the phase error is

$$|\Delta\varphi| \leq \sum_{q=2}^{Q} |E_q|/E_1 \tag{7}$$

where q is the harmonic number. In practice the phase error is usually considerably less than that given by eq (7) because the sine terms essentially do not contribute to phase errors.

Some additional discussion on phase angle error introduced by harmonics is presented by Epstein [4] in his description of a similar device. Also, a technique which is supposed to compensate errors from even harmonics is suggested, although errors resulting from odd, out of phase, harmonics are, again, not compensated by his technique.

d. Frequency Stability

Since the apparent phase angle is linearly dependent upon the frequency (eq (1) with constant τ), the frequency must be known and stable to within the desired accuracy of the phase angle during the course of the measurement. Accordingly, for an error in frequency by the amount $\Delta\nu$, the relative error in phase is

$$\frac{\Delta\varphi}{\varphi} = \frac{\Delta\nu}{\nu}.$$

If the frequency instability is random with time, an average and more reproducible value of the phase angle may be obtained by taking the measurement over many cycles.

2.2. Principle of Operation

Basically this phasemeter is a timing circuit which obtains the information necessary to evaluate the phase angle by measuring the average time intervals between appropriate pairs of zero crossings of the two signals over an integral number of cycles. Triggering modes involving all zero crossings, or one pair per cycle, may be used. If the latter mode is used, the zero crossings may be corresponding[7] or noncorresponding. The choice of the mode is often arbitrary, but for maximum performance, depends upon the character of the signals. The following description is based upon the utilization of all zero crossings, which is the most common mode of operation for this instrument, and, for brevity, the phase angles are restricted to the first and second quadrants.

A gate which interrupts a clock signal is controlled by two devices (one for each signal) which respond to all zero crossings of the signals. The output of the gate is connected to the numerator input of a preset digital frequency-ratio meter. Another device which generates a pulse for each zero crossing of one of the signals is connected to the denominator input of the frequency-ratio meter. Accordingly, the display on the frequency-ratio meter gives the total number of clock pulses accepted by the gate for a duration of $N/2$ periods of input (the active time of the frequency-ratio meter), where N is the value of the denominator, which is preset on the frequency-ratio meter. The value of N is arbitrary, but for maximum performance, depends upon the signal frequency and the signal to noise ratio. The determination of the phase angle requires two measurements. The first, essentially determines the time between pairs of corresponding zero crossings of the two signals, whereas the second, measures the period, or frequency. (If the frequency is already known to sufficient accuracy, the second may be omitted.) In the first measurement zero crossings of one signal activate the gate while zero crossings of the other signal inactivate it. The gate is, therefore, active, two times per cycle, each for a duration of φ/ω. This procedure continues for exactly $N/2$ cycles after which the frequency-ratio meter is inactivated. Thus, the gate is active for a total duration of $N\varphi/\omega$ while the frequency-ratio meter is active. When the second measurement is taken, the gate is always held active, and its total effective active time is $\pi N/\omega$. Since both measurements are referred to the same clock, the above durations are related to the digital displays by the same factor. Accordingly, the phase angle in radians is

$$\varphi = \pi R, \qquad 0 < \varphi < \pi$$

where R is the display ratio for the first and second measurements.

Since all zero crossings are used to obtain the information, the measured phase angle is ambiguous by π. When the phase angle is in the third or fourth quadrants, φ appearing in all the durations above should be replaced by $\varphi - \pi$. Accordingly, the phase angle is

$$\varphi = \pi(R+1), \qquad \pi < \varphi < 2\pi.$$

[7] For corresponding zero crossings, the time derivatives of the fundamental have the same sign, and conversely, for noncorresponding zero crossings, have opposite signs.

As will be explained in a later section, the flip-flop switching becomes spurious using this mode when the phase angles approach 0 or π. For this reason these values are excluded from the above inequalities.

The explanation based on the utilization of one pair of zero crossings per cycle is similar. In this case the gate is only activated once per cycle, and only one pulse per cycle is applied to the denominator input of the frequency-ratio meter. Using pairs of corresponding zero crossings, the total effective active times of the gate for the first and second measurements are $N\varphi/\omega$ and $2\pi N/\omega$. The phase angle is

$$\varphi = 2\pi R.$$

Using noncorresponding zero crossings, φ appearing in the above active times should be replaced by $\varphi - \pi$. The phase angle is then

$$\varphi = \pi(2R + 1).$$

It is apparent that changing between these last two modes is equivalent to introducing a phase shift of π to one of the input signals. In these modes there is no ambiguity in the phase angle, as with the utilization of all zero crossings. The merits and limitations of the various modes are discussed further in a later section.

When the frequency is known to sufficient accuracy, the frequency-ratio meter may be preset appropriately to read the phase angle directly in degrees in the first reading. The obvious requirement is that the ratio of the clock frequency to the signal frequency should be such that the value calculated for N should be an integer. Since, in general, the frequencies of these two signals are probably not commensurable, the calculated value for N should be sufficiently close to an integer to obtain the desired accuracy in the measurement.

2.3. Interconnection of the Logic Modules

In this section the logic circuit is described, which is capable of performing in the manner described in the last section. Figure 2 is the schematic diagram of the logic input to the frequency-ratio meter giving the arrangement of the designated logic modules.[8] Figure 3 gives the time or angular dependent waveforms corresponding to the points designated in figure 2 using all zero crossings. With the particular line of modules used, both logic levels are negative and are activated by positive-going pulses (positive logic) with appropriate heights and rise times only.

The two signals to be compared in phase are applied to the two essentially identical channels for appropriate processing. The initial stage of each channel is a voltage comparator. Whenever the input signal is slightly positive with respect to an arbitrary d-c reference, the comparator goes to the more positive logic level, and whenever the input signal goes slightly negative with respect to the reference, the output goes to the more negative logic level. Typically, a signal input swing of 20 mV is sufficient to swing the output to saturation at both logic levels. In order to obtain good resolution in time, however, the imput amplitude should exceed by far that need to saturate the logic levels over the course of a cycle. The excess amplitude depends, of course, upon the character of the signals, for example, the signal to noise ratio. For the performance evaluation, described later, 1 V amplitude was found to be more than sufficient.

In order to obtain a d-c reference voltage for the comparator, the simplest course is to connect the reference terminal to "common"; however, this method may introduce a slight bias, which will be, in effect, the same as a small d-c offset accompanying the signal. In general, a more satisfactory method is to apply a well regulated d-c voltage[9] necessary (usually several millivolts) to establish the comparator output at a voltage midway between the logic levels with the input shorted. This adjustment, which comprises the only one necessary in this device, is accomplished by shorting the inputs to ground and connecting the voltmeters shown in figure 2. In place of compara-

[8] The logic symbols used here are taken from reference [5].

[9] A suitable reference voltage may usually be obtained from the center tap of a multiturn voltage divider connected to the well regulated power supply such as one obtained from the manufacturer of the modules.

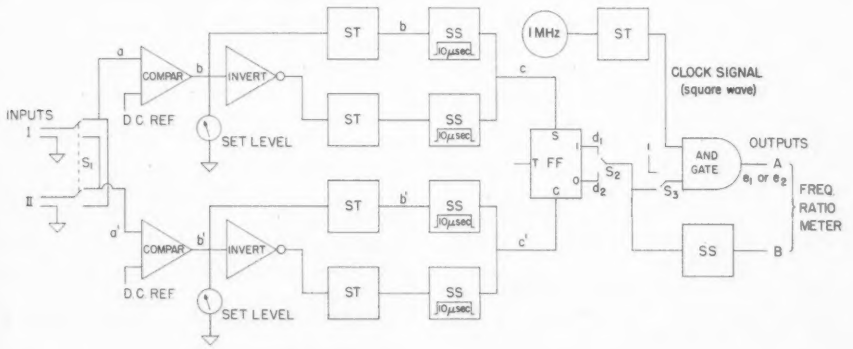

FIGURE 2. *Schematic diagram of the logic circuit.*

265-343 O-67—5

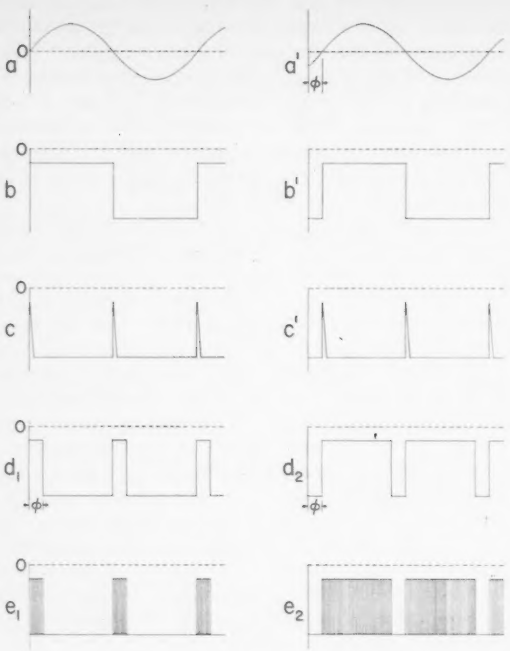

FIGURE 3. *Angular dependent wave forms at the points designated in figure 2 using all zero crossings.*

tors other types of level detectors, including certain operational amplifiers, could probably be used as well, provided they are sufficiently stable and compatible with subsequent stages. The choice of type of module or component here and certain other places in this circuit is often a matter of convenience depending upon the line of modules used, and the imput requirements.

In order to obtain information from both positive- and negative-going zero crossings, the circuit branches at the comparator outputs, as shown, with one of the branches in each channel being applied to an inverting amplifier. The next stages in each of the branches are bistable squaring circuits or Schmitt Triggers (designated ST), which decrease the rise and fall times from the comparator and inverter outputs, in particular at the lower frequencies. At the outputs of the Schmitt Trigger these times are essentially independent of the input signal frequency and now compatible with the requirements of subsequent stages or modules. The direct inputs of the Schmitt Triggers should be used here and set to trigger at a voltage approximating the average of the logic levels. This is easily accomplished by fixed biasing in accordance with the instructions supplied by the manufacturer.

The following stages are "single shots" (monostable multivibrators, designated SS). The reason for the 10 μsec pulse width shown is to reduce the occurrence of spuriousness from noise as explained in the next section.

The outputs from the "single shots" are combined as shown to form the channel outputs, which are applied to the "set" and "clear" (designated S and C) inputs of a flip-flop (bistable multivibrator, designated FF). Pulses at both flip-flop inputs correspond to all zero crossings of input signals (both positive- and negative-going). The "single shot" outputs may be disconnected appropriately in order that flip-flop is active only once per cycle and controlled by either corresponding or noncorresponding pairs of zero crossings, which are used for phase angles in the vicinity of π and 0, respectively. The merits and limitations of the above triggering modes are discussed in the following subsection. It is desirable to connect high impedance indicator lamps [10] at the flip-flop outputs to detect spuriousness or malfunctioning if either should occur. Connection to the trigger input (designated T) is not necessary for this application.

The pulses received by the flip-flop will be delayed from their corresponding zero crossings of input nearly equal to the sum of the rise times of the preceding stages. Clearly, if these delays are the same in both channels, no corresponding error will appear in the apparent phase angle. Since significant differences may appear in these delays, the corresponding error may be effectively cancelled by repeating the measurement with the channels interchanged by switching S_1 and S_2 and taking the average reading. In the prototype, the difference in these delays was found to approximate 1 μsec.

The output of the flip-flop is split into two branches. One of these is applied to the input of a "single shot" which generates pulses corresponding to zero crossings of input. These pulses are used to activate and inactivate the frequency-ratio meter. (In order to prevent spuriousness from noise, it is necessary to use this "single shot" to gate the frequency-ratio meter rather than to use any of the four "single shot" outputs which control the flip-flop.) The other branch is applied to one of the inputs of an "And" gate [11] which gates a clock signal for a duration proportional to the phase angle, with S_3 in the lower position as shown. When S_3 is in the upper position, the corresponding gate input is held at the active level (designated by 1), which means that the gate output is controlled by the clock signal only. Either passive or active "And" gates may be used here; however, the passive gates used were found to have faster rise and fall times. In order to generate the clock signal, a sufficiently stable oscillator at an appropriate frequency (depending somewhat on the anticipated signal frequency range) may be used. Usually it is desirable and convenient to use the oscillator of the frequency-ratio meter (usually 1 MHz) for this purpose. The Schmitt Trigger following the clock oscillator may be necessary depending upon input rise time requirements of the "And" gate.

Outputs A and B are applied to the A/B inputs of a

[10] Compatible transistorized or electronic high impedance indicator lamps are usually available from the manufacturer of the logic modules.

[11] The output of an "And" gate is active only when all inputs are active.

suitable preset digital frequency-ratio meter. The "preset" feature is important because it makes possible a measurement over N arbitrarily selected periods of input. Taking the measurement over a large number of periods effectively averages the influence of noise on the positions of the zero crossings and improves the phase resolution which would be limited by the clock frequency. If the "preset" feature is not available, it may be incorporated by constructing a frequency divider by appropriately interconnecting a suitable number of flip-flops.

At very low frequencies one may not wish to spend the time necessary to average the effect of noise by taking the measurement over many cycles of input. Birnboim [6] has suggested and tried a method utilizing tunnel diode level detectors to control a gate. In complete absence of noise a given tunnel diode will switch rapidly only once per sine wave zero crossing. In the presence of noise the tunnel diode may switch several times in the vicinity of the fundamental zero crossing turning "on" and "off" according to the actual sign of the input in a manner similar to a voltage comparator, but with much faster transient times. According to Birnboim, the active time of the output is nearly the same with or without noise with this method, even though the measurement is taken over only one cycle of input. Extreme caution must be taken, however, with measurements over only one cycle of input, in that long transient times in the signal are damped so that a steady state is acquired. Even at very low frequencies a network which manifests an appreciable phase angle will often manifest a long transient time of magnitude comparable to the period.

In some cases it appears possible to prevent the coincidence of pulses by introducing a small phase shift in one of the signals with an appropriate phase shifting network before one of the comparators. It is not necessary to know the exact value of the phase shift because its effect can be canceled by taking a second measurement with the channels interchanged utilizing switches S_1 and S_2 (fig. 2), which is the normal procedure even without this phase shifter. This is probably feasible at the higher frequencies; however, at very low frequencies the phase shifter would probably produce a large transient which would not damp out within the time desired to take the measurement. Accordingly, it may be desirable or necessary to use only one zero crossing per cycle which imposes certain other limitations, as discussed in the next section.

2.4. Single Versus Double Triggering

As mentioned earlier, several modes of operation are possible with this phasemeter. The phase angle can be measured by utilizing information from all zero crossings, or from one pair per cycle involving either corresponding or noncorresponding zero crossings. In this section the merits and limitations of each mode are discussed. The terms "single" and "double" triggering refer to whether the gate is active once per cycle and controlled by either corresponding or noncorresponding pairs of zero crossings, or active twice per cycle controlled by all zero crossings, respectively.

The most accurate measurements are taken with double triggering, as will become apparent; however, a limitation in this mode of operation is that phase angles must be sufficiently remote from either 0 or π. From figures 2 and 3 it is apparent that the flip-flop "set" and "clear" input pulses approach coincidence as the above angles are approached. The degree to which these angles can be approached depends upon the amount of noise present at the input, the input level detector stability, and the flip-flop response times.

A minor disadvantage of double triggering is that there is an ambiguity between the angle φ and $\varphi+\pi$. Usually a phase angle is known to within $\pm\pi/2$ before the measurement is commenced; however, if this approximate information is not known, an initial measurement with single triggering, which is not ambiguous in this respect, is useful to determine the proximity of the angle before commencing with the more accurate measurement using double triggering.

Whenever the phase angle is sufficiently remote from 0 or π, double triggering is the preferable mode and is very reliable, even when moderate amounts of noise are present in the input signals. Under these conditions, there may be more than one actual zero crossing per zero crossing of fundamental. Accordingly, the input stages, including comparators, inverters, and Schmitt Triggers, will chatter with a corresponding burst of pulses appearing at the flip-flop inputs. If the flip-flop is set by a pulse corresponding to the first zero crossing of one signal, all subsequent crossings will be ignored until the flip-flop is cleared by a pulse corresponding to the first zero crossing of the other signal. Since all zero crossings are used, no spuriousness can result from an actual zero crossing being opposite in sign from that of the fundamental in this vicinity. The noise will still perturb the positions of the zero crossings; however, when the measurement is taken over many cycles, the effect of noise on the measurement should be effectively canceled because of the random nature of noise. As will be explained in the next paragraph, complete freedom from spuriousness from noise is not inherent in the single triggering mode.

When the phase angle approximates 0 or π, and when the double triggering mode is used, the pulses appearing at the "set" and "clear" inputs of the flip-flop approach coincidence, which makes the output spurious, as mentioned earlier. Under these conditions one must proceed with single triggering using pairs of corresponding or noncorresponding zero crossings when the phase angles approach π and 0, respectively. Unfortunately, with single triggering, if the noise is sufficiently large, the output will, again, be spurious. In this mode there are unused, or ineffective, zero crossings. If a burst of noise appears in the vicinity of a zero crossing intended to be ineffective, the actual signal may reverse slope opposite to that of the fundamental one or more times within the critical region over which the circuit responds to fluctuations. Thus, zero

crossings which are supposed to be ineffective become effective in an irregular manner with a corresponding spuriousness in the measurement. For a given signal to noise ratio, it has been found that spuriousness from noise was encountered more at the lower frequencies. (For example, with a one volt signal with a signal to noise ratio of 100, spuriousness was detected using the single triggering mode at frequencies less than 10 Hz.) Presumably, this is because the time of the critical region is longer at the lower frequencies. The increased pulse widths, or increased active times, of the "single shots" shown in figure 2, will in some cases eliminate the effect of this disturbance. The longer pulse simply prevents the flip-flop from chattering from more than one crossing of input in the vicinity of each zero crossing of fundamental for a duration equal to the active time of the "single shots." Ideally, this time should depend upon the signal frequency with the limitations being that it should be small in comparison with the input period and slightly larger than the duration of the critical region over which the circuit responds to fluctuations. A given pulse width on the "single shot" outputs is obtained by connecting the appropriate capacitor as instructed by the manufacturer of the logic modules. Variation of these capacities with frequency may be accomplished by suitable manual switching. This feature was not incorporated in the prototype. Since this type of spuriousness does not appear with double triggering, there is no need to increase these pulse widths, except to assist in visual display on an oscilloscope, if this need should occur.

In the author's anticipated applications for this phasemeter the occurrence of phase angles in the vicinity of 0 or π is not anticipated. Accordingly, all of the measurements are to be taken using double triggering, and not much has been done to improve the performance in the neighborhood of these angles where single triggering is necessary. Extension of performance to improve reliability in the neighborhood of these angles might be accomplished by the capacitor switching scheme mentioned above, or by incorporating in the circuit some sort of a stable trigger hysteresis limiter. Such possibilities, which could be modified to be compatible with the logic line used, are given in reference [7].

One of the principal advantages of double triggering is that errors from d-c offset voltages are canceled, providing the waveforms are symmetric about their peaks. The obvious limitation is, of course, that the offset voltage must be less than the amplitude. This cancellation is verified by the following argument. Consider an even function which obeys the above symmetry requirement,

$$F(\omega t) = F(-\omega t),$$

which has an extremum at $\Delta t = 0$. It is desired to find the change in the apparent phase angle $\Delta\varphi$ resulting from shifts of the zero crossings Δt from an offset voltage E_{DC}. Using the closest zero crossings on each side of $\omega t = 0$, we take

$$F[\omega(t+\Delta t_1)] + E_{DC} = F[-\omega(t+\Delta t_2)] + E_{DC},$$

which can be true only for

$$\Delta\varphi = \omega(\Delta t_1 - \Delta t_2) = 0.$$

It is not necessary to equate both sides of the penultimate equation to zero because the relation is valid for any pairs of values of an even function chosen by setting the argument $\omega t = -\omega t$.

The above result is illustrated in figure 4, which reveals the phase angle errors introduced from d-c offset using single triggering: (a) gives the time dependence of the symmetric input waveforms, which, for the purpose of argument, are sine waves, and the time between any pair of corresponding points is φ/ω. One of the signals with amplitude E_1 is offset by the amount E_{DC} for which the time between actual zero crossings is shifted by the amount

$$\Delta t \approx E_{DC}/\omega E_1.$$

(b) gives the corresponding wave form for the control input of the gate, which, in this case, is controlled by only positive-going zero crossings of (a). The dashed line shows what the gate input would be in the absence of offset. Clearly, the apparent phase angle is in error by the amount $\omega\Delta t$. (c) gives the gate input waveform

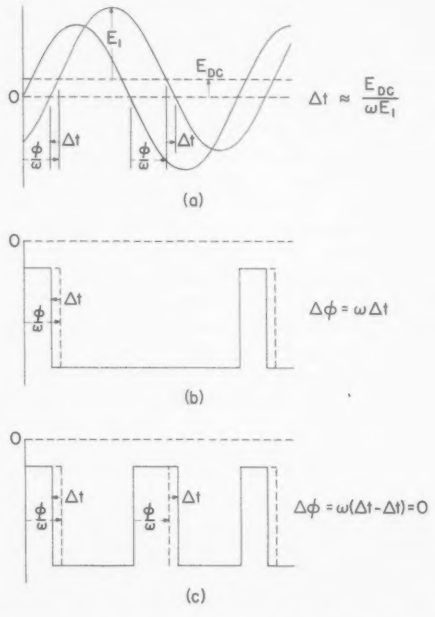

FIGURE 4. *Comparison of the effect of d-c offset voltages between single and double triggering.*

(a) Input signals, one of which is offset by the amount E_{DC}. (b) Gate control input using single triggering (positive-going zero crossings). (c) Gate control input using double triggering (all zero crossings).

using all zero crossings of (a). For symmetrical input waveforms, the errors introduced by each pair of zero crossings cancel as shown.

In addition, as illustrated in section 2.1c, the phase errors introduced by even, out of phase, harmonics are effectively eliminated only when double triggering is used.

2.5. Modification for Integrating Voltmeter

Depending on the nature of the application of the phasemeter and the availability of certain types of equipment, one may wish to use a digital integrating voltmeter in place of the digital frequency-ratio meter. A phasemeter using this technique has been described by Heydemann [8]. In order to modify the logic circuit to be used in conjunction with an integrating voltmeter, the flip-flop shown in figure 2 should be replaced by two as shown in figure 5, similar to the circuit developed by Heydemann. This arrangement converts the two logic levels, A and B, into three, A − B, 0, and −(A − B). The principal reason for doing this is for the zero output to correspond to a zero (or π) shift in phase. The flip-flop output waveforms corresponding to the designated points in figure 5 are shown in figure 6 as a function of ωt. a and b are the outputs at points a and b in figure 5 and $a-b$ is the differential input of the integrating voltmeter. The apparent phase angle φ in terms of the voltages shown is

$$\varphi = \frac{\int_0^{2\pi N} e\,d(\omega t)}{4\pi NE}$$

where N is the integral number of periods, selected arbitrarily, over which the measurement is taken, e is the instantaneous voltage, and E is the magnitude of the two active levels. For angles $0 < \varphi < \pi$, the output is positive as shown in (a), and for angles $0 > \varphi > -\pi$, the output is negative as shown in (b). A reversible [12] integrating digital voltmeter is preferable to the more common absolute-value type because with the former the sign of the phase angle is given as well as its magnitude. In figure 6 this distinction is illustrated by taking φ and $-\varphi$ by simply reversing the inputs as shown at the top of the figure. The author has not assembled a prototype employing an integrating voltmeter.

It is apparent that the integrating voltmeter technique might have advantages compared to the frequency-ratio meter technique at high frequency. It is not limited by the finite resolution imposed by the clock frequency and may tend to more effectively cancel errors resulting from finite flip-flop output rise and fall times. However, at low frequencies the frequency-ratio meter technique should be advantageous. For example, at a frequency of 1 Hz it is easy to establish the period, or any interval within the period, to within $\pm 10^{-6}$ sec. Under ideal conditions this would introduce a corresponding error of $\pm 0.00036°$. Comparable accuracies using voltage measurements at this frequency are difficult to obtain. With the scheme shown on figure 5 the output is not affected by offset voltages, providing the waveforms are again symmetric about their peaks, as illustrated in reference [8]. However, the possibility of spuriousness from noise is not completely removed as it is with the frequency-

[12] A reversible (sometimes called "count-up, count-down") meter integrates the signed value over a preselected time interval and indicates the sign of the definite integral in the readout. An absolute-value meter integrates the magnitude of the function over a preselected interval without respect to sign. Hence, in this application, an absolute-value meter will give the correct magnitude of the phase angle, but with no information with respect to lag or lead, whereas, the reversible meter completely specifies the phase angle.

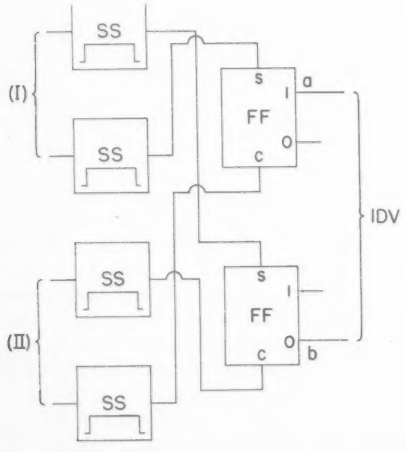

FIGURE 5. *Proposed modification of the logic circuit to use a reversible digital integrating voltmeter in place of a frequency-ratio meter.*

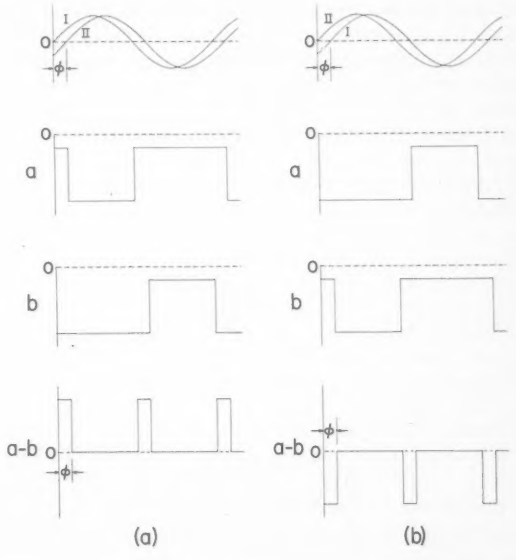

FIGURE 6. *Angular dependent wave forms at points designated in figure 5.*
(a) II leading I (b) II lagging by same amount.

ratio technique using double triggering at phase angles sufficiently remote from 0 or π.

3. Performance Evaluation

This section includes the description of tests by which the apparent phase angles obtained by this phasemeter are compared to those generated by reliable sources.

Using common laboratory techniques, it is difficult to obtain a phase "standard" operating continuously over the audio range to better than 10 min. The limitation seems to be mostly in the quality of sinewave generators because of distortion and frequency stability. Ironically, variable frequency oscillators, such as frequency synthesizers, which have excellent frequency stability, usually have considerable harmonic distortion, and those which have good wave form usually lack the stability desired for this test. If one is willing to make a comparison at a single frequency, there is at least one commercially available phase shifter capable of generating two very pure coherent sine waves from which a continuously adjustable phase angle (over 2π) can be defined to within $\pm 0.01°$.

Accordingly, two tests were used to evaluate the performance of this phasemeter. The first used a phase shifter constructed from ordinary laboratory equipment from which a phase angle can be established to within several tenths of a degree over a wide range of frequencies, and the second used a quality phase shifter of very high accuracy at a single frequency.

In order to obtain an approximate check over a frequency band, an "operational" phase shifter was assembled from available components as shown in figure 7. The decade resistors and fixed capacitor (1 μF) had accuracies specified to within 0.025 percent by the manufacturer. Two different oscillators were used: a frequency synthesizer, with a harmonic distortion of less than 1 percent, which was found to be stable in frequency to better than 1 part in 10^{-7} over the course of any of our measurements; and an RC oscillator, for which the corresponding numbers are 0.5 percent and 1 part in 10^4. Using hypothetical, pure sine waves, neglecting leakage resistances and stray capacitances, the magnitude of the phase angle δ evaluated from the circuit in figure 7 is

$$|\delta| = \frac{\omega R_f C}{1 + \frac{R_i}{R_f}(1 + \omega^2 R_f^2 C^2)}.$$

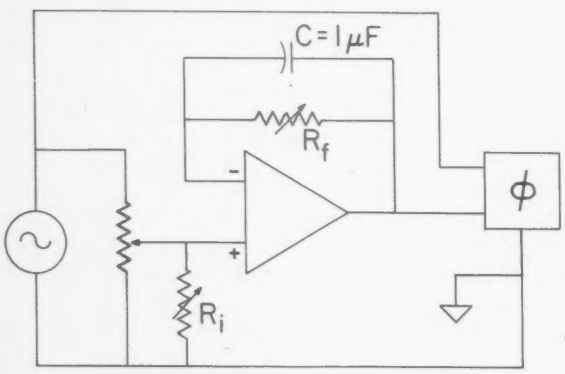

FIGURE 7. *Schematic diagram of the phase shifter circuit used to evaluate the digital phasemeter over a wide frequency band.*

Measurements were made at arbitrarily selected phase angles within the first quadrant at decade intervals in frequency from 0.1 to 10,000 Hz. Agreement was always obtained to within 0.2° up to 1,000 Hz. The apparent phase angle differed by as much as 0.17° under the same settings between the two oscillators. This disagreement is attributed to their differences in harmonic content. At 10,000 Hz the agreement was within 0.7°; however, a 0.01 μF capacitor had to be substituted here in place of the 1 μF to generate an appreciable phase shift at this frequency. In this case anticipated stray capacities of approximately 100 pF could produce 0.7° difference between the observed value and that calculated from eq (8). Since all of the measured values fell within the bounds predicted from the uncertainty of the phase shifter, this is not a very meaningful test with respect to accuracy. However, this evidence does indicate reasonable performance and the absence of spuriousness except in the vicinity of 0 and π as discussed in the last section.

The second comparison was made using a high quality commercial phase shifter operating only at a single frequency. According to the manufacturer's specifications, this instrument is capable of producing two sine waves of sufficient quality to define any phase angle (0 to 2π) to within $\pm 0.01°$ at 400 Hz. With careful adjustment it is the opinion of this author that a precision to within $\pm 0.005°$ can be obtained. The manufacturer's specifications list the harmonic distortion as within 0.05 percent, and the frequency to within 4×10^{-7} over 24 hr.

The results of typical comparison are included in the following table. The first column gives the phase settings on the phase shifter. The second column gives the apparent phase angle evaluated from two sets of data. In the first set an angle δ is set on the phase shifter and the apparent phase angle φ is observed. In the second, the angle $2\pi - \delta \sim -\delta$ is set on the phase shifter, the input leads to the phasemeter are reversed, and the apparent phase angle is observed. In each determination these two apparent phase angles are averaged to give those appearing in the second column. With pure sine waves the phasemeter should see no distinction between the two methods by which these values are obtained. However, between these two sets, the apparent phase angles were found to disagree consistently with replicate measurements at a particular phase setting by as much as 0.01°, which, incidentally, is the accuracy claimed by the manufacturer

TABLE 1. *Comparison between the quality commercial phase shifter and the digital phasemeter at 400 Hz*

Setting $\delta \pm 0.01$	Apparent phase angle φ	Disagreement $\varphi - \delta$
deg.	*deg.*	*deg.*
1.5	1.503	0.003
30	30.004	.004
60	60.003	.003
90	90.006	.006
120	120.001	.001
150	150.000	.000
178.5	178.500	.000
181.5	181.501	.001
210	210.002	.002
240	239.999	−.001
270	269.997	−.003
300	299.996	−.004
330	329.995	−.005
358.5	358.498	−.002
Average error.....		0.0004

of the phase shifter. These biased differences may be attributed to the difference in harmonic content between the primary and shifted signal of the phase shifter. The last column gives the disagreement between the corresponding values of the first two columns with the average error. The trend, in which the errors reverse sign at angles larger than 210°, also reveals the presence of a small, biased systematic error; however, the disagreement did not exceed 0.006°.

From the above evidence it is apparent that the accuracy of the digital phasemeter at 400 Hz is at least as good as that of the commercial phase shifter, which, according to the manufacturer, is $\pm 0.01°$. This uncertainty corresponds to a time interval of 0.069 μsec. Considering that the clock pulses are spaced by 1 μsec and the rise times of the components are 1 μsec or slightly less, an error in time of 0.069 μsec is probably not excessive in spite of the averages that are taken by appropriate switching and measuring over many cycles of sine wave. If the principal errors (using ideal sine waves) are from the finite resolution of the clock pulses and finite rise times, as expected, the accuracy should improve as the frequency is decreased.

4. Concluding Remarks

In evaluating the performance of a prototype of an absolute measuring technique for which all known anticipated systematic errors have been evaluated or eliminated, it is usually desired to compare the apparent values of the quantities the instrument is capable of measuring against the "true" values obtained from a suitable "standard." In this usage the meaning of a "true" value is that obtained from a well established standard for which the resolution is far superior to that of the prototype in that errors generated by the standard are essentially insignificant compared to those from the prototype. The exact "true" values of a quantity are never known except for some of the more basic standards for which the values are selected arbitrarily. In order to prevent the possibility of a mutual occurrence of an unanticipated systematic error, it is desirable for the two techniques to be disparate but still capable of measuring the same quantity.

In this particular comparison in which the digital phasemeter was compared to the commercial phase shifter used as a standard, the agreement was found always to be within $\pm 0.006°$, which is even better than the $\pm 0.01°$ accuracy specified by the manufacturer of the commercial phase shifter. One should not ignore the possibility of a coincidence that the same biased systematic errors are common to both instruments. However, this possibility is considered to be extremely unlikely since the methods of measurement are very distinct. The commercial phase shifter is based on frequency division and coincidence of Lissajous patterns, whereas the digital phasemeter refers the information to a time base. Also, the commercial phase shifter utilizes all pairs of corresponding points, whereas the digital phasemeter utilizes only zero crossings ignoring all intermediate information.

In view of the agreement between these two absolute measurements, utilizing quite different principles of operation and presumably subject to different types of systematic error, it seems reasonable to claim that both this new instrument and the commercial phase shifter are accurate to something better than 0.01° at 400 Hz. As noted above, the new instrument described here should have about this same accuracy up to a frequency of about 1,000 Hz and even better accuracy at frequencies lower than 400 Hz providing the systematic errors are principally caused by uncertainties in time intervals between zero crossings. If the signals were perfect sine waves and no other systematic errors entered, an error of 0.01° at 400 Hz would correspond to an error in the measurement of time of 0.7 μsec, certainly an easily attainable accuracy. The tests described above seem to indicate that the systematic errors of the instrument described here are within this limit, and that any greater "error" is associated not with the measurement itself, but with imperfections in the signals used. One could reasonably say that this instrument measures phase angles defined as the angular separation between an arbitrary pair of corresponding points to better than 0.01° on two periodic signals of identical waveform but displaced in time. For periodic signals with the same frequency but different waveform, there is, of course, no unique definition of a phase angle. The definition based on the angular separation of zero crossings seems to be appropriate for many uses; for others a definition involving comparison over a complete cycle might be preferred. The consideration of the most commonly encountered imperfections indicates, however, that if one defines the phase angle between two voltages consisting of sine waves plus imperfections as the phase between the two pure sine waves, this phase measured here will be in error by no more than the ratio of the amplitude of the distortion to the amplitude of the basic sine

wave, plus the product of the angular frequency and the timing error. This latter factor should not exceed 0.01° at 400 Hz and will be proportional to frequency.

The author acknowledges and appreciates the assistance from Edward J. Hayes of the Engineering Electronics Company for his suggestions with respect to design of the phasemeter and selection of its components, from Carson Meadors for the physical arrangement of the components and construction of the prototype, and from Miss H. V. Belcher for making the drawings contained in this paper.

4. References

[1] Yaohan Chu, Digital Computer Design Fundamentals, McGraw-Hill Book Co., New York, 1962.
[2] H. Koppe, Inst. Practice **18,** 350 (1964).
[3] Y. P. Yu, Electronics, **31,** 99 (1958).
[4] W. S. Epstein, J. Res. NBS **68C** (Engr. and Instr.) No. 4, 223 (1964).
[5] Military Standard, Graphic Symbols for Logic Diagrams, MIL-STD-806B, Feb. 26, 1962.
[6] M. H. Birnboim, private communication, to be published.
[7] Typical Oscilloscope Circuitry, Tektronix, Inc. Beaverton, Oregon (1961).
[8] P. Heydemann, Acustica **13,** 421 (1963).

(Paper 71C3-257)

JOURNAL OF RESEARCH of the National Bureau of Standards—C. Engineering and Instrumentation
Vol. 71C, No. 3, July–September 1967

Publications of the National Bureau of Standards*

Selected Abstracts

Recrystallization and melting of partially melted stark rubber, D. E. Roberts, *J. Res. NBS* **71A** (*Phys. and Chem*), *No. 3, 231–235 (May–June 1967).*
Two specimens from a piece of stark rubber which had a melting temperature originally at 41 °C were partially melted at 38 °C and allowed to stand for 11 years, one at about 25 °C, the other at 38 °C. The first showed a continuous slow decrease in specific volume, while the second increased slowly in volume for 5 months and remained constant for about 5 months more before showing the continuous slow decrease. The melting temperature of the first increased to 45 °C and the melting range was broadened. The melting temperature of the second became 52 °C and the range was narrowed. Perfecting or enlarging of crystals and the effect of higher recrystallization temperatures have influenced the melting temperatures. The effect of heating rate is discussed in connection with slow increases in volume, attributed to relaxation of oriented regions, during melting.

Key Words: Crystallized rubber, crystal size, heating rate, melting range, melting temperature, oriented, partial melting, recrystallization, rubber, slow melting, stark rubber.

Effects of a distribution of volume relaxation times in the annealing of BSC glass, P. B. Macedo and A. Napolitano, *J. Res. NBS* **71A** (*Phys. and Chem.*), *No. 3, 237–244 (May–June 1967).*
The influence of a distribution of relaxation times is studied in annealing experiments. A two-relaxation time model is proposed which permits the calculation of the distribution of relaxation times from the crossover data of Spinner and Napolitano as well as Ritlands. This model also characterizes the structure of any glass in terms of two parameters. Thus quenched equilibrium as well as nonequilibrium glass were compared with rate cooled glasses in their behavior upon further annealing as well as their conductivity at low temperatures with excellent agreement.
Borosilicate crown glass was found to have a narrow distribution of relaxation times particular to associated liquid manomers rather than polymers. The results can be explained in terms of a topological model for the distribution of relaxation times. The temperature dependence of the viscosity is due to a true activation energy rather than a free volume effect.

Key Words: Annealing of glass, borosilicate crown glass, distribution of relaxation times, glass, index of refraction, relaxation times, two-relaxation time model, volume relaxation.

Heat treatment and properties of iron and steel, T. G. Digges, S. J. Rosenberg, and G. W. Geil, *Mono. 88 (Nov. 1, 1966), 35 cents. (Supersedes Circular 495 and Mono. 18).*
This Monograph is a revision of the previous NBS Monograph 18. Its purpose is to provide an understanding of the heat treatment of iron and steels, principally to those unacquainted with this subject. The basic principles involved in the heat treatment of these materials are presented in simplified form. General heat treatment procedures are given for annealing, normalizing, hardening, tempering, case hardening, surface hardening, and special treatments such as austempering, ausforming, martempering and cold treatment. Chemical compositions, heat treatments, and some properties and uses are presented for structural steels, tool steels, stainless and heat-resisting steels, precipitation-hardenable stainless steels and nickel-maraging steels.

Abscissas and weights for Gaussian Quadrature for $N=2$ to 100, and $N=125, 150, 175, 200,$ C. H. Love, *Mono. 98 (Dec. 28, 1966), 55 cents.*
The abscissas and weights for Gaussian Quadrature of order $N=2$ to 100, and $N=125$, 150, 175, and 200 are given. The abscissas are given to twenty-four places and the error is estimated to be no more than 1 unit in the last place. The weights are given to twenty-three places and the error is estimated to be no more than 1 unit in the last place.

Key Words: Integration, Gaussian, quadrature.

Scanning electron probe microanalysis, K. F. J. Heinrich, *Tech. Note 278 (Feb. 3, 1967), 30 cents.*
The combination of electron microprobe x-ray emission spectrometry with the scanning techniques first developed for the scanning electron microscope permits using the scanning electron probe as a microscope sensitive to elemental composition. This technique is particularly useful in the many applications in which spatial distribution of one or more elements in a specimen is more important than local composition. Although oscilloscope representation of probe scanning is usually obtained by the simple technique of producing a dot of light for each arriving photon, more sophisticated scanning techniques such as expanded contrast registration and concentration mapping can provide more quantitative information. Signals other than x-rays, such as target current, electron backscatter, or cathodoluminescence may be used for image formation. Electron beam scanning can also be performed in a discontinuous fashion, so that the electron beam irradiates in succession a number of spots arranged in a square or rectangular pattern, and the number of photons registered in each position is retained in the memory of a multichannel analyzer. The application of these diverse scanning techniques is illustrated.

Key Words: Electron probe, microanalysis, x-ray spectrometry, scanning electron microscopy, electron backscatter, cathodoluminescence.

A new near-zone electric field-strength meter, F. M. Greene, *Tech. Note 345 (Nov. 15, 1966), 35 cents.*
The National Bureau of Standards has recently completed the development of prototype instrumentation for measuring the electric-field components of complex, high-level, near-zone electromagnetic fields from 0.1 to 1000 volts per meter, at frequencies from 150 kHz to 30 MHz with a present uncertainty of less than ± 2 dB. The design of the NBS meters is based on the use of a novel form of telemetry, employing a completely nonmetallic electrical transmission line, which apparently has not been fully exploited heretofore. This avoids the perturbing effects on the field being measured, usually caused by field-strength meters employing metallic RF transmission lines. The design and performance of the meter are discussed in some detail.

Infrared reflectances of metals at cryogenic temperatures—a compilation from the literature, P. F. Dickson and M. C. Jones, *Tech. Note 348 (Oct. 14, 1966), 40 cents.*
Spectral and total reflectances for metals at cryogenic temperatures in the infrared wavelength region are compiled from the literature. Information concerning sample preparation and purity, radiation source, and methods of reflectance measurement

are also presented. Observations regarding the effects on reflectance of temperature, oxide layer, wavelength, and sample preparation are given.

Key Words: Compilation, cryogenic, infrared, metals, reflectance.

The design and operation of a high-voltage calibration facility, W. W. Scott, Jr., *Tech. 349 (Nov. 10, 1966), 25 cents.*
The high-voltage calibration facility, in operation for seven years at the National Bureau of Standards, Radio Standards Laboratory (RSL) but now at NBS Washington, is described with emphasis on several novel construction features and calibration techniques. The more usual calibration techniques are also outlined for the assistance of those personnel in standards laboratories assigned the task of calibrating with high accuracy, electrostatic voltmeters, resistive dividers, and potential transformers at high voltage. Precautions, based on experience in the calibration and use of high voltage standards, are given so that certain errors may be avoided by the users.

Key Words: Alternating-current, calibration, direct-current, high-voltage, ratio, safety, standards enclosure, transformer, voltage-divider, voltmeter.

Radiochemical analysis: activation analysis, instrumentation, radiation techniques, and x radioisotope techniques July 1965 through June 1966, ed. J. R. DeVoe, *Tech. Note 404 (Sept. 30, 1966), $1.25.*
This is the third summary of progress of radiochemical analysis which encompasses the work of both the Radiochemical Analysis and Activation Analysis Sections of the Analytical Chemistry Division at the National Bureau of Standards.
Pertinent information on the irradiation facilities of the nuclear reactor, Linac, and Cockcroft-Walton generator are described. A number of analyses of standard reference materials by activation analysis are described (e.g., Cu in cast iron, SRM 82b; Se in selenium steel, SRM 1170; Al in steel, SRM 14e; and V in stainless steel, SRM 73c). Various aspects of the technical problems in activation analysis such as its use for homogeneity testing, production of suitable flux monitors, and experimental design with respect to increasing selectivity (such as by using variable neutron energy) and reducing systematic and random errors, are presented. A realistic procedure for estimating sensitivity and for designing the analysis to optimize the detection limit is described. A computer program that resolves complex decay curves utilizes parameter changes convenient for the conversational aspect of "time sharing" digital computers. A highly specific radiochemical separation for copper using a type of amalgam exchange is described.
Description of specialized data handling equipment as well as information on a fast rise preamplifier, solid state detector system, and other special instruments such as a pneumatic transport system rabbit sensor, are presented.
A description of the laboratories used in Mössbauer spectroscopy is presented. Special problems in radiation detection for use in a spectrometer are also described. The Standard Reference Material Program for chemical shift in Mössbauer spectroscopy is discussed with particular reference to the search for a tin standard. The computer program, "Parlors M," that is used for resolving complex Mössbauer spectra is presented in its entirety in Appendix II.
The use of thin layer chromatography in conjunction with radioactive reagent analysis for trace elements is described. Substoichiometric radioisotope dilution continues to be studied by evaluating systematic and random errors, as well as by developing the technique from physico-chemical principles such as controlled potential coulometry.

Key Words: NBS reactor, NBS Linac, Cockroft-Walton generator digital computers, activation analysis, standard reference materials, photo-neutron reactions, flux monitors, Cu, Se, Al, V in irons and steels; homogeneity testing, pneumatic rabbit sensor, Mössbauer spectroscopy, tin standard for chemical shift, PARLORS program for Mössbauer spectra, Mössbauer instrumentation, Mössbauer laboratories, radiometric trace chromatography, radioisotope dilution, substoichiometry by controlled potential coulometry, radiochemical separations, theoretical detection limits for activation analysis, CLSQ program for multicomponent decay, solid state detectors, electronic data handling.

Microwave attenuation measurements and standards, R. W. Beatty, *Mono. 97 (Apr. 3, 1967), 25 cents.*
A comprehensive and commentarial review of microwave attenuation measurement methods and standards is presented. In addition, a relatively new and more precise way of representing and analyzing an attenuation measurement is presented. This in turn permits more rigorous definitions and error analyses than were previously possible. Expressions for both mismatch and connector errors are presented. The referral of microwave attenuation measurements to standards operating at lower frequencies is discussed with particular attention to the errors in the referral processes as well as the errors in the standards themselves. Standards operating at d-c, audio frequencies, and higher frequencies are included in this discussion which covers waveguide-below-cutoff attenuators and rotary vane attenuators. Desirable characteristics are listed for attenuators which are suitable for calibration, and examples of these are given.
Measurement methods are classified and described, giving greatest emphasis to the intermediate-frequency substitution method using a waveguide-below-cutoff standard attenuator, and to d-c substitution techniques. Methods for measurement of small attenuations as well as methods not requiring reference to any standard attenuators are covered.
Comments are made on the accuracy and convenience of various methods, and references are given which cover most of the basic and important research in this field.

Key Words: Microwave, attenuation, measurements, standards, tutorial.

ASTM metric practice guide, *Handb. 102 (Mar. 10, 1967), 40 cents.*
To continue to serve the best interests of science and industry the American Society for Testing and Materials is actively cooperating with other standardization organizations in the development of simpler and more universal metrology practices. In some industries both here and abroad, U.S. customary (and British) units are gradually being replaced by those of a modernized metric system known as Système International d'Unités (SI). Recognizing this trend, the Society considers it important to prepare for broader use of the modernized metric system through coexistence of these two major systems. This policy involves no change in standard dimensions, tolerances, or performance specifications. Current "inch-pound" units will therefore be published as before along with their modern metric (SI) equivalents, but conversions in the opposite directions will be avoided.
This Guide is offered primarily to provide the technical committees of ASTM with conversion procedures and factors to implement this Society policy.

Legibility of alphanumeric characters and other symbols, II. A reference handbook, D. Y. Cornog and F. C. Rose, *Misc. Publ. 262–2 (Feb. 10, 1967).*
The major psychological findings and data in the field of the legibility of alphanumeric characters and other symbols are provided in this detailed Reference Handbook. Summaries and extracts of information for 203 experimental, developmental, review, and other legibility reports are presented and are multiply indexed in depth by (1) a matrix, cross-reference index (article versus functional variables-environmental typographical), (2) author indexes (alphabetical and chronological), and (3) a character-face-name index. These Handbook entries are further indexed by the permuted title index in NBS Miscellaneous Publication No. 262–1, "Legibility of Alphanumeric Characters and Other Symbols: I. A Permuted Title Index and Bibliography." Selected samples of several important experimental and other faces are presented in an appendix.

Key Words: Alphanumeric characters, displays, handbook, human factors, legibility, psychology, readability, standards, symbols, type faces, typography, visibility.

Bibliography on flame spectroscopy. Analytical applications 1800 to 1966, R. Mavrodineanu, *Misc. Publ. 281 (Feb. 23, 1967), $2.00.*
Flame spectroscopy, especially in its analytical applications, continues to be an active field of study. Its literature is growing

steadily, and the use of flame photometry in many specialized applications calls for a comprehensive indexed bibliography. This collection consists of 5,113 references to works on flame spectroscopy, selected with emphasis toward analytical measurements. It covers the period from 1800 to 1966. Subject indexes, keyed by number to the references cited, precede most of the sections.

Key Words: Flame, spectroscopy, analytical emission, atomic absorption, electrical discharge, bibliography, indexed.

Bibliography of low energy electron collission cross section data, L. J. Kieffer, *Misc. Publ. 289 (Mar. 10, 1967), 50 cents.*

A bibliography of low energy electron collission cross section data is presented. Only references which report original measurements or calculations of electron collission cross sections are included. The cross section data for each process are listed by atomic species in order of their atomic number. The data for molecules are listed in arbitrary order.

Key Words: Atom, molecule, electron, collission cross section.

Tables of molecular vibrational frequencies. Part 1., T. Shimanouchi, *NSRDS–NBS6 (Mar. 1, 1967), 40 cents.*

A compilation of vibrational frequency data for selected molecules is being conducted at the University of Tokyo in cooperation with the National Standard Reference Data Program of the National Bureau of Standards as a part of an international effort to compile and evaluate physical and chemical data. This report, first of a series of annual reports, contains fundamental vibrational frequencies of 59 molecules together with vibrational assignments, sources of data, brief comments, and citations of references. The fundamental frequencies are obtained mainly from the infrared and Raman spectra. When these are not available, other experimental data such as microwave results are taken into account. The selection of vibrational fundamentals from observed spectral data is based upon careful studies of the spectral data and comprehensive mathematical analyses. These tables were designed to provide a concise summary needed for the computation of ideal gas thermodynamic properties. They may also provide a convenient source of information to those who require vibrational energy levels and related properties in molecular spectroscopy, analytical chemistry, and other fields of physics and chemistry.

Key Words: Molecular, vibrational, frequencies, data, tables, force, constants, spectral.

Procedures for precise determination of thermal radiation properties, November 1964 to October 1965, J. C. Richmond, G. J. Kneissl, D. L. Kelley, and F. J. Kelly, *Tech. Note 292 (Feb. 10, 1967), 50 cents.*

An error analysis of the shallow cavity technique for measuring total normal emittance of ceramic materials at very high temperatures showed that there was an error due to the translucency of the specimens that was as much as +60% for alumina, and a second error due to thermal gradients in the specimen that was on the order of −10%. Two new techniques were devised in the hope of greatly reducing the translucency error. Progress was made in developing codes to compute and correct for the thermal gradients present in the specimen. The laser-source integrating sphere reflectometer for measuring reflectance of specimens at very high temperatures was extensively redesigned to eliminate errors due to flux reaching the detector on the first reflection, and to convert the reflectometer from the substitution to the comparison mode. A literature search was made of techniques for measuring thermal radiation properties of solids at temperatures above 2500 °K (4000 °F).

Key Words: Emissivity, emittance, high temperature reflectance, infrared reflectance, radiation properties, reflectance, spectral emittance, spectral reflectance, thermal radiation, total emittance.

A survey of ionization vacuum gages and their performance characteristics, W. G. Brombacher, *Tech. Note 298 (Feb. 3, 1967), 40 cents.*

The design of various types of ionization gages is outlined, with particular attention to the design elements important to performance. The performance and the many factors affecting the performance of the various gages are reviewed. Methods of calibration are discussed in some detail, including the use of volumetric pressure dividers, conductance pressure dividers and constant rate of pressure change methods. About 365 references to the literature are cited.

Key Words: Bayard-Alpert gages, cold cathode vacuum gages, conductance pressure dividers, hot cathode vacuum gages, ionization gages, vacuum gage calibration systems, vacuum gages, volumetric pressure dividers.

Methods for performance-testing of electromechanical pressure transducers, P. S. Lederer, *Tech. Note 411 (Feb. 9, 1967), 25 cents.*

This publication describes methods in one particular program at NBS for the performance-testing of electromechanical pressure transducers (such as telemetering transducers used in aerospace testing). It covers static and dynamic calibration procedures in detail, delineates environmental and other tests, and describes the test equipment used. Examples of dynamic calibration results are interpreted.

Key Words: Electromechanical, pressure, transducer, calibration, performance, test method, dynamic calibration, telemetering.

Standard sizes of blackboard slate, *PS2–66 (May 15, 1966), 10 cents. Supersedes SPR15–35.*

This recommendation covers dimensions for blackboard slabs and dimensions of blackboard slates for other than wall use. Also included are requirements for thickness, finish, and color and imperfections of natural slate.

TFE-Fluorocarbon (polytetrafluoroethylene) resin skived tape, *PS3–66 (Sept. 1, 1966), 10 cents.*

This standard establishes requirements and methods of test for the material, dimensions, workmanship, and the physical and electrical properties of three grades of skived tape manufactured entirely of TFE-fluorocarbon resin in accordance with good commerical practice. The materials covered range in thickness from 0.002 inch to 0.125 inch, and are normally manufactured by skiving.

Porcelain enameled formed steel plumbing fixtures, *PS5–66, (Nov. 1, 1966), 15 cents. Supersedes CS144–47.*

The standard covers materials, dimensions, construction and methods of inspection, testing, and labeling. Definitions are given for certain trade terms. The types and sizes of fixtures in general use and demand are listed for bathtubs, lavatories, kitchen sinks and sink-and-laundry-tray combinations.

Trim for water-closet bowls, tanks and urinals (dimensional standards), *PS6–66 (Nov. 1, 1966), 10 cents. Supersedes CS172–50.*

The purpose of this standard is to establish a basis for dimensional interchangeability for those items of trim for water-closet bowls, tanks, and urinals known as spuds, lock nuts for spuds, flush valves for stable low tanks, float valves, flush elbows, and coupling nuts. It is also intended to provide a basis for understanding between buyers and sellers for the dimensions and tolerances that govern the fit of trim in the fixtures and connecting parts of trim.

Effect of certain crystalline substances on physical properties of elastomers. I. Stress-strain behavior, F. J. Linnig, E. J. Parks, and R. D. Stiehler, *Rubber Chem. Technol.* **39,** *No. 4, Pt. 1, 1041–1052 (Sept. 1966).*

At present there are two principal theories concerning the nature of reinforcement of rubber with fine particle fillers such as carbon black. One postulates chemical bonds between rubber and filler; the other that reinforcement is a physical phenomenon only. The work reported in this paper suggests strongly that physical forces alone can produce modulus reinforcement of rubber.

Addition of crystalline organic compounds having a β-naphthyl group has been found to increase the modulus of various rubbers to a remarkable degree. Of the compounds used, phenyl-β-naphthylamine (PBNA) produces the greatest effect; five percent of PBNA is comparable in its stiffening effect on rubber on first extension to about 40 phr of a good reinforcing carbon black. Extraction of the

compounds removes the stiffening effect.
Conditions under which reinforcement occurs, and mechanical properties of the resulting products have been examined.

Oxidation products in an oxygen-blown Kuwait asphalt, P. G. Campbell and J. R. Wright, *I&EC Product Res. Devel.* **5,** *No. 4, 319–323 (Dec. 1966).*
A Kuwait asphalt flux, which is ordinarily very difficult to harden, was treated with oxygen to prepare a coating-grade asphalt. Oxidative changes were measured by increase in softening point and by infrared spectroscopy. The infrared spectra of the coating-grade asphalt to which model organic compounds were added were compared with the spectrum of the original asphalt. The principal oxygen-containing products formed during hardening (oxidation), as assigned by infrared analysis, confirmed previous findings with asphalts from other geographical sources.

Studies of molten alumina in the arc-image furnace, J. J. Diamond and A. L. Dragoo, *Rev. Hautes Temper. et Refract.* **3,** *272–279 (1966).*
Aluminum oxide was melted in vacuum and in atmospheres of H_2, He, O_2, N_2, Ar, air and water vapor with an arc-image furnace. Water vapor was found to dissolve rapidly in molten alumina and to boil out vigorously when it was made supersaturated in a water vapor atmosphere. In spite of this solubility water vapor does not appreciably enhance the vaporization of molten alumina. The rate of vaporization of molten alumina in vacuum was determined in the temperature range 2 493° to 2 606° K and the mean third law heat of vaporization found to be 729.0 kcal mol^{-1}, with a standard error of the mean of 0.9 kcal mol^{-1}. Some problems associated with the measurement of the temperature of molten alumina were studied and are discussed.

Key Words: Alumina, arc-image furnace, heat of vaporization, molten alumina, temperature measurement, vapor pressure, vapprization, water in alumina, water vapor.

Temperature measurement in high temperature chemistry: 10000–3000 °C, R. F. Walker, Rev. *Hautes Temper. et Refract.* **3,** *301–308 (1966).*
The uncertainty of temperature measurements is one of the principal causes of error in the measurement of the thermodynamic and kinetic properties of substances above the gold point. In terms of international standards, the ultimate accuracy of temperature measurements depends on the consistency of the International Practical Temperature Scale (IPTS) with the thermodynamic temperature scale. The accuracy achieved in measuring other properties depends on the accuracy of calibration of the temperature measuring instruments in accordance with the IPTS, and on the ability to use the instruments under prescribed physical and chemical conditions. The higher the temperatures, the more difficult it becomes to meet these prescribed conditions.
The present status of the IPTS is reviewed briefly. A summary is given of the precision and accuracy achievable with common temperature measuring instruments. The potential advantages and limitations of newer instruments, such as photoelectric pyrometers, are also indicated. It is concluded that in the field of high temperature chemistry the principal limitation, is the inability to use the instruments under ideal conditions. Higher precision and accuracy would be achievable if additional internal checks, such as, internationally recognized secondary reference points, were available to the experimentalist. Severe problems of both a chemical and physical nature are, however, attendant on the provision of such reference points, and these are briefly discussed.

Key Words: High temperature chemistry, international temperature scale, melting points, pyrometry, secondary reference points, temperature measurement.

An ultrasonic pressure gage, P. L. M. Heydemann, *Am. Soc. Mech. Eng. Publ. No. 66–WA/PT–5 (1966).*
The transit time of short ultrasonic pulses in solid rods is used to measure pressures throughout the fluid range. Self-excited regenerating circuits are used. Measurements to 3500 bar with an uncertainty of .3 bar and to 20 kb with an uncertainty of 2 bar are reported. Further improvements, temperature compensation and stability are discussed.

Key Words: Gage, high pressure, ultrasonics, velocity of sound, delay line, temperature compensation, self-excited pulse repetition, frequency stability.

Progress in nuclear electronics, L. Costrell, *Book, Radioisotopes for Aerospace, Part 1. Advances and Techniques, p. 1–13 (Plenum Press Inc., New York, N.Y., 1966).*
At the conclusion of World War II nuclear instrumentation was to a great extent concerned with detectors that required essentially unsophisticated electronics. The advent of the scintillation counter in the late 1940's called for an order of magnitude improvement in the associated instrumentation. Introduction of the semiconductor radiation detectors with their tremendous energy resolution capabilities stimulated additional sophistication of nuclear electronics.

Key Words: Nuclear instruments, progress, state-of-the-art, standards modules.

The measurement of solar radiation, with principal emphasis on the ultraviolet component, R. Stair, *Air Water Pollut. Int. J.* **10,** *665–688 (1966).*
A review is presented covering much of the scientific work of the past half century relating to the measurement of the spectral distribution of radiant energy (in particular in the ultraviolet region) from the sun. Mention is made of those special solar disturbances that are expected to result in large variations of the ultraviolet solar emission as well as the absorbing medium, ozone, which through its turbulence and distribution further affects greatly the spectral distribution of the solar radiation reaching the earth's surface at any locality. Various instrumentations and the standards employed by the different laboratories are discussed in some detail with emphasis placed upon some of their shortcomings and the great lack of accurate solar spectral data, in particular within the ultraviolet region. Finally, new instrumentation offering promise of considerable usefulness in obtaining rapidly more accurate data in this area is described.

Key Words: Solar radiation, stratospheric ozone, ultraviolet solar radiation.

Accurate microscopical determination of optical properties on one small crystal, C. P. Saylor, *Book, Advances in Optical and Electron Microscopy, Ed. R. Barer and V. E. Cosslett, 1, 41–76 (Academic Press, Inc., New York, N.Y., 1966).*
By rotating a crystal about one axis and using phase, double diaphragm, or interference contrast, refractive indices of a typical crystal can be microscopically determined for any wavelength with an error that is not greater than 0.00002. For such accuracy, the diameter of the crystal must be about 20μ or larger. Precautions involve careful orientation, precise matching of index with that of immersion, fluid, and correct determination of the refractive index of the fluid.

Compressibility, gas, J. M. H. L. Sengers, *Encyclopedia of Physics, p. 118–120 (Reinhold Publ. Corp., New York, N.Y., 1966).*
This is a contribution to the "Encyclopedia of Physics." After defining compressibility, a brief discussion is given of experimental methods for determining this quantity, its experimental behavior and an explanation of this behavior in terms of molecular theory. Same references to recent reviews of experimental and theoretical effort are added.

Pyrometry, optical, H. J. Kostkowski, *Encyclopedia of Physics, p. 563–564 (Reinhold Publ. Corp., New York, N.Y., 1966).*
A summary of optical pyrometry is presented including the description of a disappearing filament optical pyrometer and the manner and accuracy with which this instrument is calibrated and used. Photoelectric pyrometers, total radiation and two color pyrometers are briefly discussed.

X-ray fiber optics, L. Marton, *Appl. Phys. Letters* **9,** *No. 5, 194–195 (Sept. 1, 1966).*
The possibility of the creation of fiber optics for x rays is investigated. While the aims in the creation of such fiber optics are similar

to those in light optics, the technical means for achieving it are quite different.

Key Words: Fiber, optics, x rays.

A pycnometer for small volumes of liquids, S. Marantz and G. T. Armstrong, *Chem. Anal.* **55,** 114–115 (*Oct. 1966*).
The design, calibration, and performance of a small volume (0.1 cm^3) pycnometer is described. The instrument can be used to measure liquid densities to a 0.1 percent accuracy.

Key Words: Pycnometer, density.

Galvanic pitting in metallic coatings, F. Ogburn and M. Schlissel, *Plating* **54,** *No. 1,* 54–62 (*Jan. 1967*).
An electrolyctic cell is described which simulates a corrosion pit extending through a metal coating and permits measurement of the cell currents. Such cells were used to investigate the galvanic currents between coatings of chromium, copper, and nickel and substrates of zinc, iron, nickel, and copper. The investigation included outdoor salt spray and corrodkote exposures; and determinations of the effects of anode size, depth of electrolyte, and proximity of a second anode on cell currents.
An equation for the cell current as a function of the cell parameters is discussed and compared with experiments.

Key Words: Electroplating, pitting, galvanic corrosion, pitting corrosion, corrosion currents, corrosion.

Measurement of the surface area and the heats of wetting of dentin powders, G. M. Brauer (*Proc. Second Workshop on Adhesive Restorative Materials, Charlottesville, Va., December 1965*), *Book, Adhesive Restorative Dental Materials II,* 203–223 (*Department of Health Education, and Welfare, Public Health Service, Washington, D.C. 1966*).
This progress report describes the measurement of the "apparent heats of immersion" of powdered dentin which was characterized by surface area measurements and determination of organic matter. The specific surface of ground dentin which is nearly independent of particle size was found to be around 10 m^2/g. The percentage of volatile matter amounted to 30.0%. The measurement of the apparent heat of wetting of dentin gave a mean value from 5 runs of 0.894 cal/m^2 with a completed standard error of 0.040 cal/m^2 for 6.86 ± 0.35 cal/g. From the magnitude of this value it appears that there may be some chemical interaction between water and the surface of the dentin. (1 cal = 4.1840 joules). The difference in the "apparent heat of immersion" by aqueous solutions containing ionic species or organic functional groups and the heat of wetting of dentin by pure water is indicative of any reaction of the added species with components of the tooth surface. Measurements of these heats of reaction should assist in developing methods for modifying tooth surface and in determining those groups that will bond effectively to tooth structure in an aqueous environment.

Key Words: Content of dentin, dentin, heats of wetting, organic, surface area.

The battle against corrosion, S. Lichtenstein, *Compressed Air Mag.* **71,** *No. 12, 12–13* (*Dec. 1966*).
Corrosion is discussed as a technological and economic "disease" eating away at metals and materials, depleting natural resources, and causing injury and death where accidents and explosions result from weakening of structures. Dollar estimates of costs to the Nation and the Federal Government are given. Anti-corrosion work of the National Bureau of Standards' Institute for Materials Research is described and highlights of a half-century of achievement are noted. Corrosion control is linked to progress in nuclear power, oceanography, water desalination, military operations, space and supersonic transport, health, safety and conservation.

Key Words: Economics of corrosion, industrial design, materials protection, structural failure, basic and applied research.

A new contribution–NBS and engineering standards, G. S. Gordon, *Safety Standards* **XVI,** *No. 1, 3, 4, 24, and 25* (*Jan.–Feb. 1967*).
The need for greater participation by NBS in helping to strengthen the nation's standards program was called for in the recent report of the LaQue Committee. The Office of Engineering Standards Liaison and Analysis (*OESLA*) has been established as the focal point at NBS for making available the technical resources of Bureau personnel *to assist* the Federal, State, and local governments, private engineering *standards-making bodies* and manufacturers in developing adequate representation of industrial, consumer and general public interests *in national and international standards activities.*

Key Words: OESLA, to assist, standard-making bodies, in national and international standards activities.

Additional thoughts on precision calibration of accelerometers, S. Edelman, *Test Engineering and Management* **XVI,** *No. 5, 17, 18, 38, and 39* (*Nov. 1966*).
This consists of a number of comments on an article by W. P. Kistler. It shows why reliable calibration of vibration measuring instruments requires careful measurements over the entire frequency range of interest.

Key Words: Accelerometer, vibration, calibration, frequency range, comparison calibration, shaker.

Air bath thermostat for use with absorption spectrophotometer, J. H. Gould, *Rev. Sci. Instr.* **37,** *No. 9, 1229–1231* (*Sept. 1966*).
An automatically controlled absorption cell thermostat with a useful range of from −150 °C to +60 °C for use with the Cary 14 spectrophotometer is described. This apparatus accepts ordinary cylindrical absorption cells to 5 cm in length.

Key Words: Spectrophotometry, thermostat, ultraviolet-visible, −150 °C to +60 °C.

Combination RF radiation and fluid pressure seal, M. B. Hall, N. T. Larsen, and W. E. Little, *Proc. IEEE* **54,** *No. 11, 1585–1586* (*Nov. 1966*).
A new type of microwave gasket for use, for example, between waveguide flanges has been developed at the NBS Boulder Laboratories. The gasket, consisting of perforated and metallized polytetrafluoroethylene film, reduces leakage from an X-band flange joint to below the level detectable with the test equipment used, i.e., below −90 db. The new gasket can be made thin and, hence, light. It provides simultaneously a microwave radiation and a fluid pressure seal, and the reflection it introduces can be made small. It is expected that variations of the materials of construction will provide for various other combinations of desirable properties.

Comparison of mass limiting two-phase flow in a straight tube and in a nozzle, D. K. Edmonds and R. V. Smith, *Proc. Symp. Two-phase Flow, University of Exeter, Devon, England, June 21–23, 1965, 1, 401–414* (*University of Exeter, Devon, England, 1966*).
This paper reports the experimental data obtained at mass-limiting and near-mass-limiting conditions for a straight tube and two nozzle test sections. The experimental system was a Refrigerant 11 flow loop. Fluid qualities entering the test sections were 0.042, 0.116, and 0.156.
It was noted that as the pressure differential between the exit-plane and the receiver was increased, the exit-plane pressure approached a constant value, for all test sections. The mass flow also approached a constant value for the straight tube but for the nozzles the mass flow continued to increase with increasing differential pressure but at a lower rate of increase. The deviations from the straight tube behavior were greater for the nozzle with the largest angle of convergence.
Predicted mass-limiting flow rates from the Fauske and a metastable model were compared with the experimental data. The models adequately predicted the flow rate for data where the exit-plane pressure was almost constant (within ± 30%).

Galvanic corrosion of metals in cementing materials, J. W. Pitts, *Military Engr.* **59,** *No. 387, 40–41* (*Jan.–Feb.* 1967).
A brief discussion is presented of some corrosion problems that have developed in recent years resulting from the use of dissimilar metals embedded in Portland cement concrete and gypsum plaster. It is shown how dissimilar metals embedded in such cementing materials

can form short-circuited galvanic cells and how corrosion of the anodes has led to failures of both steel-reinforced concrete containing aluminum conduit and of gypsum plaster-metal lath systems in which copper tubing was embedded. Examples of failures are cited. Some of the variables that affect the degree of corrosion are discussed and some general precautionary measures are recommended.

Key Words: Aluminum conduit, calcium chloride, concrete, corrosion in concrete, corrosion in plaster, dissimilar metals, galvanic corrosion, gypsum plaster.

Mass flowmeters in cryogenic service, W. J. Alspach, C. E. Miller, and T. M. Flynn, *Proc. ASME Flow Measurement Conf., Pittsburgh, Pa., September* 26–28, 1966, *pp.* 34–56 (1966).
This paper concerns cryogenic fluid mass flow measurement by a variety of techniques, including those that are available and those that are being developed. Attention is given to the principle of operation, performance results, and operational and design characteristics.
The problem of cryogenic fluid flowmeter calibration is examined and discussed with reference to available facilities, techniques, limitations, and accuracy. The problem of calibration for special cryogenic applications, such as slush hydrogen and cold gasses, where no calibration facilities are available are also examined. Inferred calibration from a substitute fluid calibration or design or design practices is also reviewed.
To improve the mass flow measurement of cryogenic fluids, discussions are directed towards measurement technique selection, density measurements for inferential mass systems, improvements in volumetric flow measurements, improvements in direct measuring mass flowmeters, and improvements in calibration.

Key Words: Accuracy, calibration, commodity transfer, cryogenic, cryogenic processes, density, flowmeters, mass flow, mass flowmeters, performance results, propellant management, substitute fluid, volume flow.

A modified Monte-Carlo quadrature, S. Haber, *Math. Compt.* **20,** *No. 95,* 361–368 (*July 1966*).
A modification of the simple Monte-Carlo method for evaluating multiple integrals is proposed. The method is a form of stratified sampling and may be used automatically, without adaptation to the integrand. It results in a moderate gain in accuracy.

Key Words: Quadrature, numerical analysis, errors, sampling, stratified sampling, and multiple quadrature.

Electronic data processing in urban transportation planning, B. M. Levin and R. E. Schoefer (*Proc. Second Annual Conference on Applications of E.D.P. Systems for State and Local Government, Apr. 1–2, 1966, New York, N.Y.), Book, The Large-Scale Public E.D.P. System: Its Problems and Prospects, pp.* 169–177 (*University of New York, N.Y., 1966*).
The goal of urban transportation planning is to develop a plan for an efficient, balanced transportation system for an urban area—one which will promote a desirable pattern of human activities. While the process has been standardized to some extent, each study must nevertheless acquire and manage a massive amount of information about the particular region with which it is concerned. From this information, models which can be used to predict future land-use patterns, travel demands, and the workings of the transportation system are developed and calibrated. Using computerized versions of these models, transportation planners have the capability to propose and test a large variety of future transportation systems, so that one which is well-suited to the future needs of the urban area can be found.

Key Words: Transportation planning, systems analysis, data processing, urban transportation.

Atomic standards of frequency and time, J. M. Richardson and J. F. Brockman, *Phys. Teacher* **4,** *No. 6, 247–256* (*Sept. 1966*).
The national standard of time is provided by an atomic device at the National Bureau of Standards. Thus, for the first time in our civilization, the basis of our measurement of time is atomic instead of astronomical. The major reasons for this change are that modern science can measure the resonance of an atom more accurately than it can measure the motions of stars and planets, all of the factors affecting atoms are better understood, and the atomic resonance appears to be more stable than planetary motions. This change has improved our accuracy of measurement by three orders of magnitude. Presently, the best atomic clocks are based on atomic cesium beams such as the three at NBS. Further research, however, may reveal a better choice of atom or method. NBS is presently using four radio stations to distribute time (and its reciprocal, frequency) to the Nation and over much of the globe but, again, research is being conducted on newer techniques which offer higher accuracies.
The change from astronomical to atomic time will have little effect on our daily living habits, but it will permit our technology to accomplish things we couldn't do before and to do the same things more economically.

Key Words: Atomic frequency standards, atomic time, cesium atomic beam, standard time scales, frequency and time standards, standards.

Electrical standards and measurements, F. K. Harris, I. L. Cooter, B. L. Dunfee, W. P. Harris, F. L. Hermach, and C. Peterson, *Electro-Technol.* **97,** *55–70* (*Jan. 1967*).
The basis of the electrical units and their derivation from the mechanical units is briefly reviewed. Methods used by the Electricity Division of the National Bureau of Standards for the establishment of measurement reference standards are discussed together with the techniques employed in extending the range of measurement from the reference standard to higher and lower values.

Key Words: Absolute measurements, electrical units, electrical reference standards, precise electrical measurements.

Time standards, J. M. Richardson, *Book, Encyclopaedic Dictionary of Physics Supplementary I, 351–355 (Pergamon Press Inc., New York, N.Y., 1966).*
A survey of time standards at the level of national and international standardization is given. General requirements for time standards are stated, and the degree to which astronomical and atomic standards meet these requirements is discussed. The construction of a scale of time from an oscillator rated in terms of an atomic standard is explained. The currently used atomic frequency standards, cesium, hydrogen, and thallium, are described as to transition involved, method of observation, and accuracy of results. The dissemination of time standards by HF, LF, and VLF radio, by communications satellite, and by portable clock is discussed.

A new radiometric equation and its application, H. J. Kostkowski, *Appl. Opt.* **5,** *No. 12, 1959* (*Dec. 1966*).
A simple equation has been found which gives, at any wavelength, the ratio of the spectral radiances of two arbitrary sources when their spectral radiances at some particular wavelength are equal. The main advantages of the equation are its simplicity and the fact that it does not involve temperature explicitly; a limitation is that Wien's radiation equation is required. The new equation is derived and various applications are given.

Key Words: Radiometry, optical radiation, spectral radiance, nonblackbody emission, sources, blackbodies.

An improved design for vacuum ultraviolet resonance lamps, A. M. Bass, *Appl. Opt.* **5,** *No. 12, 1967* (*Dec. 1966*).
A method is described for sealing lithium fluoride windows to resonance lamp discharge tubes so as to avoid damage to the seal by action of the discharge.

Key Words: Vacuum ultraviolet, electric discharge, resonance lamp, window seal.

Acoustical thermometer and the National Bureau of Standards provisional temperature scale 2–2θ (1965), H. Plumb and G. Cataland, *Metrologia* **2,** *No. 4,* 127–139 (*Oct.* 1966).
An acoustical thermometer has been developed at the National Bureau of Standards to determine values of temperature that approximate the Thermodynamic Temperature Scale. The instrument, called an ultrasonic interferometer in acoustical literature, has

been used to determine isotherms of the speed of sound in helium gas as a function of pressure. Each isotherm has been extrapolated to zero pressure to approximate the condition of an ideal gas; from the resulting intercepts, values of temperature were calculated.
The instrument and its operation are described and the data for isotherms, which have been determined at approximately every degree from 2–20 °K, are listed. The isotherm data have been treated both graphically and by electronic computer analysis (by the method of least squares) to yield values of temperature that are the basis for a new temperature scale—NBS Provisional Scale 2–20 (1965). When the scale is compared with other existing scales, T_{58} and NBS (1955), in regions of overlap, the agreement with NBS (1955) is excellent but noticeable departures from T_{58}—the helium-4 vapor pressure scale are indicated.

Key Words: Acoustical thermometry, isotherms below 20 °K, low temperature thermometry, primary thermometry, speed of sound, ultrasonic interferometer.

Anomaly in Young's modulus and internal friction of $5SrTiO_3 \cdot 3La_{2/3}TiO_3$ below 100 °C, R. W. Dickson, *J. Am. Ceramic Soc.* **49,** *No. 11, 628 (Nov. 1966).*
A rapid decrease in Young's Modulus with decreasing temperature suggests that some type of phase change may occur in $5\ SrTiO_3 \cdot 3\ La_{2/3}TiO_3$ near 80 °C despite the lack of evidence in x-ray patterns.

Key Words: Internal friction, phase change, resonance, strontium titanate-lanthanum titanate, vacancies, Young's Modulus.

Comparison Langmuir probe and spectrometric electron temperature measurements, R. S. Powers, Jr., *J. Appl. Phys.* **37,** *No. 10,* 3821–3826 *(Sept. 1966).*
Langmuir probes are often used for temperature measurements in plasmas, due to their convenience and to their ability to give time-resolved measurements. Since probe results are subject to several suspicions, we compare probe and spectrometric electron temperature measurements in a particular low-temperature plasma in which this is possible. We find probe temperatures to be high by amounts between 40% and 4% over an electron temperature range between 410 °K and 920 °K.

Key Words: Electron temperature, Langmuir probe, plasma, spectrometric.

Correcting for astigmatism in the Czerny-Turner spectrometer and spectrograph, A. B. Shafer, *Appl. Opt.* **6,** *159 (Jan 1967).*
It is shown that the Czerny-Turner spectrometer and spectrograph can be made approximately stigmatic by using torroidal mirrors.

Key Words: Czerny-Turner, Astigmatism, spectrometer, spectrograph.

Effects of a constant force on a Keplerian orbit, J. P. Vinti, *Proc. Intern. Astronomical Union Symp. No. 25, Aug. 15–Sept. 3, 1964, Athens, Greece, pp. 355–362 (1966).*
The paper applies the von Zeipel method to the perturbations by constant force of a satellite in an elliptic orbit. As expected, the methods fails in spherical coordinates but works in parabolic coordinates. The results account for the short-periodic and the first-order secular terms and go far enough to indicate that the long-periodic and the second-order secular terms can be calculated in physically achievable cases. The calculation of the latter effects depends on the resolution into constant and long-periodic terms of the Hamiltonian resulting after short-periodic terms have been eliminated. In contradistinction to the case where the perturbing potential is a zonal harmonic, this resolution requires an infinite Fourier series rather than a trigonometric polynomial. It is feasible whenever the applied force does not lie in the plane of the orbit. When the force is coplanar, however, the orbit eventually intersects the earth, so that there is less interest in following the orbit over a long interval of time.

Optical constants of germanium, R. E. LaVilla and H. Mendlowitz, *Appl. Opt.* **6,** *No. 1, 61–68 (Jan. 1967).*
We have attempted to assess the disagreement of various investigators on the optical properties of germanium in the far ultraviolet. The analysis subjected the reported data, out to about 25 eV to the following tests: 1. An internal consistency check when possible by applying the Kronig-Kramers dispersion relations to the optical constants. 2. An evaluation of the optical oscillator strength distribution for the spectrum under study. 3. Correlation of the values of $\mathrm{Im}\,\frac{1}{\epsilon^*}$ from the optical data with the characteristic electron energy loss spectrum for the material. 4. Evaluation of the oscillator strength sum for the electron energy loss distribution. A set of optical constants derived from the characteristic electron energy loss data are presented and discussed. Also, an estimate of source of the errors incurred in the application of the Kronig-Kramers dispersion relations are given and discussed in terms of optical data.

Key Words: Characteristic electron energy loss, far ultraviolet, germanium, Kronig-Kramers dispersion relations, optical properties, sum rules.

Pyroelectric effect in bone and tendon, S. B. Lang, *Nature* **212,** *704–705 (Nov. 12, 1966).*
The pyroelectric coefficients (at constant stress) of one of the phalanges, the femur, and the hoof tendon of a cow were measured. The coefficients, which ranged from 2.5 to 4.1×10^{-13} coul cm^{-2} $°C^{-1}$ over the temperature span, −35 to 60 °C, were the smallest yet measured in any material. The results indicate that the collagen of bone and tendon is responsible for both the piezoelectric and pyroelectric effects. The pyroelectric effect in bone and tendon is probably too small to be of physiological significance.

Key Words: Bone, collagen, hydroxyapatite, piezoelectricity, pyroelectricity, tendon.

Radiance temperature at 6500 Å of the graphite arc, R. D. Lee and E. Lewis, *Appl. Opt.* **5,** *No. 11, 1858 (Nov. 1966).*
The radiance temperatures of over twenty positive electrodes in a graphite arc were measured with the NBS photoelectric pyrometer and were found to range from 3786 °K to 3808 °K. The radiance temperatures were measured to an accuracy of 2 deg K (standard deviation uncertainty) with a pyrometer sensitivity of 0.2 deg K.

Key Words: Graphite arc, pyrometry, standard, temperature.

Reflection of soft x-rays by organic fibers, S. B. Newman, *J. Appl. Polymer Sci.* **10,** *1929–1935 (1966).*
An artifact observed in point projection microradiographs of polymeric fibers and filaments obtained with 8 A x-rays is recorded and described. The phenomenon has been related to fiber-beam geometry and the high reflection efficiency of soft x-rays for these materials.

Key Words: Fibers, microfocus tubes, microradiography, nylon, polyacrylonitrile, polyamides, reflection of x-rays, soft x-rays, x-rays.

Relation between refractive index and density of glasses resulting from annealing compared with corresponding relation resulting from compression, S. Spinner and R. M. Waxler, *Appl. Opt.* **5,** *No. 12, 1887–1889 (Dec. 1966).*
The change in refractive index and associated change in density of glasses on annealing has been determined by Tool, Tilton, and Saunders. The corresponding changes for the same glasses, produced by hydrostatic compression, are presented here and compared with those of Tool, Tilton, and Saunders. It is found that for a given increase in density on annealing the increase in index is greater than for the same measured increase in density on compression.
The results are interpreted in terms of equations developed by Lorentz-Lorenz, Pockels, and Mueller to show first, that in all cases, whether from annealing or compression, there is a decrease in polarizability on increase in density (these results are in agreement with those of previous investigators); and second, that the decrease

in polarizability for a given increase in density is greater on compression than on annealing.

Key Words: Annealing, glass, density, refractive index, hydrostatic compression polarizability.

Some approximations to the Planck function the intermediate region with applications in optical pyrometry, D. E. Erminy, *Appl. Opt.* **6,** *107–117 (Jan. 1967).*
For many applications a simple approximate equation for blackbody radiation can be more useful than is the Planck blackbody equation. An intermediate region exists where both the Rayleigh-Jeans equation and the Wien equation for blackbody radiation are inaccurate approximations to the Planck equation. Several approximate equations of simple mathematical form have been obtained which are more accurate in this intermediate region. These equations are applied to optical pyrometry to obtain formulae for brightness temperature and color temperature that can be used in the intermediate region.

Key Words: Spectral radiance, Planck equation, Wien equation, Rayleigh-Jeans equation, infrared and far infrared optical pyrometry, brightness temperature, color temperature, effective wavelength.

Spectral radiance of a low current graphite arc, A. T. Hattenburg, *Appl. Opt.* **6,** *95–99 (Jan. 1967).*
The spectral radiance of the anode of a low-current graphite arc has been determined throughout most of the 850 to 210 nm region, utilizing a recently developed high-accuracy spectroradiometer. The estimated standard deviation uncertainty varies from about 1.5% at the longer wavelengths to about 5% at the shorter. Results are given at twenty wavelength points in the region, and also as a continuous function of wavelength throughout most of the region, excluding some areas of high molecular band radiation originating in the arc stream.

Key Words: Spectral radiance, graphite, arc, spectroradiometer, temperature, blackbody.

The NBS photoelectric pyrometer and its use in realizing the international practical temperature scale above 1063 °C, R. D. Lee, *Metrologia* **2,** *No. 4, 150–162 (Oct. 1966).*
A photoelectric pyrometer has been developed with which the International Practical Temperature Scale (IPTS) above the gold point, 1063 °C, is realized about 5 times more accurately than the prevalently used disappearing filament visual pyrometer. Estimated uncertainties, at a 95% confidence level, of realizing the IPTS with the photoelectric instrument are 0.12 deg C at 1063 °C, 0.24 deg C at 1256 °C, and 3 deg C at 3525 °C. The design, evaluation, and calibration to realize the IPTS are discussed.

Key Words: Blackbody, International Practical Temperature Scale, optical, photoelectric pyrometer, radiance sources, standards, temperature.

Bonding adhesives and paints to treated concrete, W. C. Wolfe, *CSI Monograph 9M1, Construction Specifier, pp. 1–8 (Aug. 1966).*
The object of this investigation was to determine the effect of surface treatment of concrete on the adhesion of paints or asphaltic adhesives for asphalt or vinyl asbestos tile. Qualitative and quantitative tests were performed on treated and untreated concrete specimens. The results of the tests indicated that concrete curing and parting agents, oils, and waxes are more compatible with asphalt cutback than with asphalt emulsion adhesive. The tests did not show any oozing of adhesive between tiles or curling of tiles at the corners.
Cement-water paints adhered poorly to concrete treated with curing agents. Organic coatings adhered well to concrete treated with curing agents based on butadiene-styrene copolymer or chlorinated rubber. Likewise, paints formulated with butadiene-styrene copolymer or chlorinated rubber in hydrocarbon solvents adhered to most curing agents. Paints made up in hydrocarbon solvents were more compatible with curing agents, oils, and waxes than were water-based paints.

Characteristics of the laser probe for spectrochemical analysis, S. D. Rasberry, B. F. Scribner, and M. Margoshes, *Proc. XII Intern. Spectroscopy Colloquium, Exter, England, 1965, pp. 336–339 (Hilger and Watts, London, England 1966).*
An extended summary is given of a paper to be presented at the XII International Spectroscopy Colloquium. Exter, England, July 12–16, 1965. The paper discusses some practical aspects of the use of the laser probe for spectrochemical analysis of minute samples.

Ellipsometric-potentiostatic studies of iron passivity. I. Anodic film growth in slightly basic solutions, J. Kruger and J. P. Calvert, *J. Electrochem. Soc.* **114,** *No. 1, 43–39 (1967).*
Cathodically reduced iron was anodically oxidized at potentials in the passive region of the anodic polarization curve in slightly basic sodium borate-boric acid solutions by means of a potentiostat. The kinetics of film growth were studied using an ellipsometer coupled with a fast recording technique, which enabled a determination of the rate of film formation for times less than 1 sec. This study of the kinetics of film growth using a nonelectrochemical technique agreed with kinetic results based on total charge measurements. Three stages of growth were detected: (i) First stage—growth limited by a diffusion process in the solution; (ii) Second state—start of limitation of growth by the film involving the combination of several processes difficult to characterize by any rate law; (iii) Third stage—growth obeying either a logarithmic or inverse logarithmic rate law. The latter was found to imply that the passive film consisted of an outer layer poorly conductive for electrons.

Growth of calcium molybdate crystals by a temperature-gradient zone-melting technique, H. S. Parker and W. S. Brower, *(Proc. Intern. Conf. Crystal Growth, Boston, Mass., June 20–24, 1966), Crystal Growth, A Suppl. to J. Phys. Chem. Solids* **E–12,** *pp. 489–491 (Pergamon Press Inc., New York, N.Y. 1967).*
Renewed interest in the growth of synthetic calcite crystals has been stimulated by the possible use of calcite as a host crystal for maser materials. A crystal growth method is described in which $(NH_4)_2CO_3$, by vapor phase diffusion, is slowly brought into contact with a solution containing 2 wt per cent $CaCl_2$ and 20 wt per cent NH_4Cl. Transparent rhombs are obtained with edge dimensions of 3–4 mm, which are verified to be calcite by x-ray diffraction measurements.

Key Words: Calcite, crystals, crystal growth, vapor phase diffusion.

Approximate normal emissivity spectra in the infrared at elevated temperatures of single-crystal and polycrystalline calcium fluoride, W. B. Fussell and J. C. Geist, *Appl. Opt.* **6,** *No. 1, 119–124 (Jan. 1967).*
A single-beam ir spectroradiometric system has been used to measure the normal spectral emissivity of specimens of single-crystal and polycrystalline calcium fluoride in the ir at elevated temperatures. The wavelength range was 2–12 μ, and data were taken at sample temperatures of 500 °C and 600 °C. Room temperature data on the index of refraction of single-crystal calcium fluoride and its rate of change with temperature were extrapolated to 500 °C and 600 °C; the normal spectral reflectivities were computed from the extrapolated indices at these temperatures. Then the computed reflectivities were used to extract normal spectral absorption coefficients from the emissivity data. It was possible to compute absorption coefficients with reasonable accuracy at wavelengths of 6 μ, 8 μ, and 10 μ; the smallest estimated error was about 2% at 8 μ. The absorption coefficients increased markedly with temperature at these three wavelengths. The absorption coefficients of the polycrystalline material were consistently higher than the corresponding values for the single-crystal calcium fluoride. It was found that the spectral absorption coefficients at 8 μ and 10μ microns varied approximately as the 2.1 and 1.6 power of the absolute temperature, respectively, between room temperature and 600 °C. These exponents lie within the range predicted by theory.

The national standard reference data system, E. L. Brady, *J. Chem. Doc.* **7,** *No. 1, 6–9 (Feb. 1967).*
The National Standard Reference Data System is a government-wide effort to give to the technical community of the United States optimum access to quantitative data on the physical and chemical

properties of substances and their interactions, critically evaluated and compiled for convenience. The general functions of the System are to coordinate and integrate existing data evaluation and compilation activities into a systematic, comprehensive program, supplementing and expanding technical coverage when necessary, establishing and maintaining standards for the output of the participating groups, and providing mechanisms for the dissemination of the output as required. This program was established as a Federal policy in 1963 upon the recommendation of the Federal Council for Science and Technology. The National Bureau of Standards of the Department of Commerce has accepted responsibility for administering the effort. The plan of operation and the general status of activities initiated by the National Bureau of Standards will be described.

Key Words: National Standard Reference Data System, NSRDS, information centers, physical properties, data, properties.

Electrodynamic vibration standard with a ceramic moving element, T. Dimoff, *J. Acoust. Soc. Am.* **40,** *No. 3, 671–676 (Sept. 1966).*
This paper describes a new rectilinear vibration exciter specifically developed for accurate calibration of piezoelectric accelerometers. It is an electrodynamic shaker, using a permanent magnet with a ceramic moving element guided by an air-bearing system. The moving element has a simple circular cross section and the driving coil is wound directly onto it. Its first axial resonance is near 25 000 Hz. The working range of the shaker extends from 5000 to less than 5 Hz. The moving element includes a means of mounting an internal accelerometer that can be used as a secondary standard. Alternatively, the moving element/accelerometer assembly can be calibrated by a reciprocity method and used as an absolute standard. The results of measurements of transverse motion and harmonic distortion are presented, as well as an example of pickup calibration.

Interface kinetics and the stability of the shape of a solid sphere growing from the melt, S. R. Coriell and R. L. Parker, *(Proc. Intern. Conf. Crystal Growth, Boston, Mass., June 20–24, 1966), Crystal Growth, A Suppl. to J. Phys. Chem. Solids J–3, pp. 703–708 (Pergamon Press Inc., New York, N.Y., 1967).*
The effects of linear interface kinetics and of square law interface kinetics on the stability of the shape of a sphere growing in a diffusion field are investigated theoretically. Slow interface kinetics can greatly enhance the stability, by several orders of magnitude in certain cases. The sphere can be stable even if its surface energy is zero. Numerical estimates are made for salol and for tin.

Mechanical properties of chemically strengthened glasses at high temperatures, M. J. Kerper and T. G. Scuderi, *J. Am. Ceramic Soc.* **40,** *No. 11, 613–618 (Nov. 1966).*
Young's modulus, shear modulus, and modulus of rupture for two chemically strengthened glasses were determined at high temperatures. The Young's modulus and shear modulus decreased with increasing temperature, with a sharp inflection slightly above room temperature. The region of inflection indicated an internal friction peak. For comparison Young's modulus and shear modulus were determined as a function of temperature on a thermally tempered soda-lime-silica glass and on a semitempered borosilicate glass. Curves of these moduli, in contrast to those for the chemically strengthened glasses, did not reveal regions of inflection. The modulus of rupture is not affected by short exposure to heat up to 260 °C, but decreases appreciably when exposed to temperatures above 204 °C for 200 hr or more. Deflection measurements at room temperature showed that the two chemically strengthened glasses had about five times as much delayed elasticity as did thermally tempered soda-lime-silica glass.

On the solution of the Stefan problem for whisker growth, J. A. Simmons, H. Oser, and S. R. Coriell *(Proc. Intern. Conf. Crystal Growth, Boston, Mass., June 20–24, 1966), Crystal Growth, A Suppl. to J. Phys. Chem. Solids C–8, pp. 255–264 (Pergamon Press Inc., New York, N.Y., 1967).*
An integral equation which describes whisker length as a function of time is derived from the implicit exact solution of Simmons, Parker and Howard using a conservation principle. A convergent iterative method is employed to obtain numerically the exact growth curves and concentration profiles. Utilizing a dimensionless formulation, growth curves are shown to comprise (except for a short transient period) a one-parameter family dependent only on a dimensionless evaporation parameter. The Dittmar-Neumann and Curtis approximations are discussed and compared with the exact growth curves. Methods are given for calculating both the coefficient of surface self-diffusion and mean adatom stay time when deviations from the Dittmar-Neumann approximation occur. The Dittmar-Neumann approximation deviates significantly from the exact solution in some parts of the growth range; however, in those parts of the growth range where physical limits on the surface concentration are satisfied, it is not clear that this deviation is experimentally measurable.

Relation of fracture stress to the fracture pattern for glass rods of various diameters, M. J. Kerper and T. G. Scuderi, *Am. Ceramic Soc. Bull.* **45,** *No. 12, 1065–1066 (Dec. 7, 1966).*
Five different size glass rods, ranging in diameter from 0.16 to 1.5 in, were broken in flexure and the relationship between fracture stress and fracture pattern determined. Results showed that fracture stress decreased with increasing rod diameter. However, rod size did not affect the relationship between the size of the smooth, or "mirror," part of the fracture face and the fracture stress.

Procedures for precise determination of thermal radiation properties, J. C. Richmond, G. J. Kneissl, D. L. Kelley, and F. J. Kelly, *Tech. Report AFML–TR–66–302 (Air Force Materials Laboratory, Air Force Systems Command, Wright-Patterson Air Force Base, Ohio, Aug. 1966).*
The broad overall objective of this continuing program is to develop equipment and procedures for measuring the important thermal radiation properties of materials, particularly those used in aircraft, missiles and space vehicles, at temperatures up to the melting point of the most refractory material, and to develop physical standards for checking such equipment and procedures. During the period covered by this report the specific objectives were (1) continued development of the laser-source integrating sphere reflectometer, (2) an error analysis of the shallow cavity technique for measuring normal spectral emittance, and (3) a study of the feasibility of preparing emittance standards for use at temperatures above 1400 °K (about 2000 °F).
An error analysis of the shallow cavity technique for measuring total emittance of ceramic materials at very high temperatures showed that there was an error due to the translucency of the specimens that was as much as +60% for alumina, and a second error due to thermal gradients in the specimen that was on the order of −10%. Two new techniques were devised in the hope of greatly reducing the translucency error. Progress was made in developing codes to compute and correct for the thermal gradients present in the specimen. The laser-source integrating sphere reflectometer for measuring reflectance of specimens at very high temperatures was extensively redesigned to eliminate errors due to flux reaching the detector on the first reflection, and to convert the reflectometer from the substitution to the comparison mode. A literature search was made of techniques for measuring thermal radiation properties of solids at temperatures above 2500 °K (4000 °F).

The nucleation of Hg on W as observed by field-emission microscopy, S. C. Hardy *(Proc. Intern. Conf. Crystal Growth,* Boston, Mass., June 20–24, *1966), Crystal Growth, A Suppl. to J. Phys. Chem. Solids C–13, pp. 287–293 (Pergamon Press Inc., New York, N.Y. 1967).*
The nucleation of Hg on W has been studied under ultra high vacuum conditions in an electron field emission microscope. The temperature dependence of the critical supersaturation for formation of nuclei is found to fit the model of disc shaped critical nuclei with no entropy of mixing contribution to their free energy of formation.
At high temperatures, the critical supersaturation data indicate that nucleation occurs by the impingement of subcritical clusters.

Key Words: Nucleation, electron field emission, Hg W.

Thermal correction and crystal growth in horizontal boats, flow pattern, velocity measurement, and solute distribution,

H. P. Utech, W. S. Brower, and J. G. Early (*Proc. Intern. Conf. Crystal Growth, Boston, Mass., June 20–24, 1966*), *Crystal Growth, A Suppl. to J. Phys. Chem. Solids B–29, pp. 201–205* (*Pergamon Press Inc., New York, N.Y., 1967*).
The characteristics of thermal convection in open horizontal boats containing molten metals or fused salts subject to a horizontal temperature gradient are shown in a motion picture. A technique for determining flow direction and mean flow velocity in systems whose convective flow is characterized by erratic temperature fluctuations (e.g., metals and salts) was developed and checked by comparing velocities measured by this technique with those observed directly in the molten salt.
The effectiveness of a magnetic field in suppression convective flow illustrated by comparing the distribution of solute in a specimen solidified unidirectionally in the presence of a field with the distribution in a sample grown normally, i.e., without any field.

Key Words: Thermal convection, crystal growth, magnetic fields, solute distribution, molten metals, fused salts.

Wind effect on preexisting waves, G. Kulin, *Proc. 1965 ASCE Conf. Coastal Engineering, Santa Barbara, California, October 1965, ch. 16, pp. 369–389* (*American Society of Civil Engineers, 1966*).
Wind action on preexisting waves is examined experimentally in a wind-wave channel, in which the preexisting waves are generated mechanically by a paddle at the windward end of the channel. Air is blown over these waves, in the direction of wave travel, at velocities up to about 30 feet per second, with the formation of wind-generated waves essentially suppressed by addition of a wetting agent to the water. Wind shear forces on these regular wavy surfaces are deduced for a variety of wave geometries.

Key Words: Water waves, waves, wind stress on, wind waves, wave damping, wind setup, wind-wave interaction.

Physiological optics at the National Bureau of Standards, D. B. Judd, *Appl. Opt.* **6,** *No. 1, 13–26 (Jan. 1967).*
Published work in physiological optics at the National Bureau of Standards is summarized under the headings: evaluation of light-dark patterns, light measurements, color measurements, color differences, and color perception. The bearing of this work on standard methods of the American Society of Testing and Materials, of the Illuminating Engineering Society, and of the American Standards Association, and on recommendations of the International Commission on Illumination is indicated. The purposes and methods of current work are briefly described.

The new tungsten-filament lamp standards of total irradiance, R. Stair, W. E. Schneider, and W. B. Fussell, *Appl. Opt.* **6,** *No. 1. 101–105 (Jan. 1967).*
The National Bureau of Standards standard of total irradiance as presently issued in the form of a 50-W carbon filament lamp was originally calibrated more than fifty years ago. Recently, needs for higher accuracy and wider ranges of total irradiance have necessitated the setting up of three sizes (100 W, 500 W, and 1000 W) of tungsten-filament lamp standards of total irradiance. These standards operate at a higher temperature than was possible with the carbon-filament lamps, and are shielded, except for a narrow area of the bulb in front of the filament, so the reception of long wavelength flux from the lamps is reduced to a minimum. The new lamps were calibrated by the use of a blackbody at a known temperature together with a quartz plate whose spectral transmittance was accurately determined. The quartz plate limits the flux received from the blackbody to the spectral region below about 4.5 μ and thus reduces errors resulting from water vapor absorption at 6 μ and longer wavelengths. Comparisons show the new standards to be in close agreement with the carbon-filament lamp standard.

The role of the National Bureau of Standards in the establishment of measurement capability at the State level, T. M. Stabler, *Instr. Soc. Am. Preprint 16.1–3–66, pp. 1–3 (Oct. 24–27, 1966).*
The program of the Federal Government to supply new standards and instruments to each State is now underway. Ten States have been chosen to receive them beginning this winter. These States have had to provide suitable laboratories and qualified personnel to perform the calibrations and to promote measurement. The National Bureau of Standards will assist the States in the establishment of the laboratories and in the training of the technologists. The end result is to have established the State Measurement Center in all 50 States.

Key Words: Weights, measure standards, laboratory, training, States.

A vacuum ultraviolet flash photolysis apparatus, W. Braun A. M. Bass, and A. E. Ledford, Jr., *Appl. Opt.* **6,** *No. 1, 47–49 (Feb. 2, 1967).*
An improved apparatus for performing vacuum ultraviolet flash photolysis-kinetic spectroscopy has been constructed. The device consists of a compact coaxial arrangement of six capacitors and six electrode pairs, symmetrically placed about a hexagonal reaction vessel of large aperture. The reaction vessel contains LiF windows to transmit far ultraviolet radiation. The six pairs of electrodes and six capacitors are connected separately and are synchronously fired, uniformly illuminating the reaction cell. The photolytic light pulse duration is about 5 μsec. More than 10^{18} quanta enter the reaction vessel in the spectral region between 1050 Å and 1600 Å. The essential operating features of the apparatus are described.

Key Words: Vacuum UV, flash photolysis, apparatus description.

Analysis of the α, β, and γ relaxations in polychlorotrifluoroethylene and polyethylene: dielectric and mechanical properties, J. D. Hoffman, G. Williams, and E. Passaglia, J. *Polymer Sci. Pt. C, No. 14, 173–235 (1966).*
Theoretical models for the α_c and γ_c relaxation effects found in chain-folded polymer crystals (single crystal mats and bulk) are presented and compared with the available dielectric and mechanical loss data for polyethylene and polychlorotrifluoroethylene. Details of morphology and crystal structure that can be varied by crystallization and annealing procedures, e.g., roughness of chain-folded surfaces, number of intercrystalline links and cilia, number of chain-end defects and dislocations, and the existence of the extended-chain phase, are brought into the discussion. The α_c process, which consists of two overlapping mechanisms, is a result motions of chain folds and reorientation (with translation) of chains in the interior. (Chain twisting also occurs for long chains.) The theory connects the data on the *n*-paraffins and their polar derivatives (*n*- ketones, esters, ethers) with the results on polymers: the common feature is the chain reorientation and twisting process. A new theory of chain twisting is introduced. The γ_c relaxation is a result of reorientation of chains in a "loose" chain-end induced defect (a vacancy row) in the polymer crystal. When the effect of chain twisting is included, the theory successfully predicts the unusually broad and asymmetric loss curve found in the polymer, and is consistent with the experimental activation energies. The β relaxation arising in the amorphous component of PCTFE is analyzed, and its upward shift in temperature with increasing crystallinity discussed in terms of the Adam-Gibbs theory of relaxation in the glassy state. The γ_a amorphous relaxation, and the δ relaxation which is found at cryogenic temperatures, are also discussed.

Concepts, terminology, and notation for optical modulation, C. S. McCamy, *Photo. Sci. Eng.* **10,** *No. 6, 314–325 (Nov.–Dec. 1966).*
Reflectance, transmittance, and optical density are regarded as kinds of flux modulation factors. Transmittance is defined as the ratio of transmitted flux to the incident flux, while transmittance factor is here defined for an optical system as the ratio of the emergent flux with the sample in the system to the emergent flux with the sample removed. Transmission density is defined as the negative logarithm of transmittance factor. This is essentially a new definition to accord with an old practice. Reflection, transmission, and fluorescence are considered generically as propagation and generalized modulation terms are proposed. A coordinate system and functional notation are adopted to systematize the description of optical systems which use or measure modulation. Simplified notation of the form $D(g: S: g'; S')$ describes most cases. Terms, symbols, and notation are proposed for standardization.

Key Words: Modulation reflectance, transmittance, reflectance factor, transmittance factor, propagance, absorptance, optical density, contrast, symbols, and notation.

Condensation of dry air on a liquid hydrogen cooled surface in the pressure range 10^{-3} to 10 torr (Knudsen number of 10^{-4} to 1), J. Hord, *Cryogenics* **6,** *No. 5, 285–293 (Oct. 1966).*
The rate of condensation of dry air on a liquid hydrogen cooled surface has been determined experimentally and compared with analytical predictions. Free molecule flow theory appears adequate for high conductance systems at bulk air pressures up to 10^{-1} torr. At higher pressures this formulation predicts condensation rates which are too large. Continuum bulk flow flow theory and free molecule flow theory agree fairly well throughout the pressure range investigated; however, bulk flow theory is more compatible with experiment. Theoretical and experimental condensation rates are presented as a function of air bulk pressure and cryodeposit (solid air frost) surface temperature. Surging (slug flow) of static liquid hydrogen refrigerant inside small bore tubes was experimentally observed and is presented as a function of heat flux. The liquid hydrogen was vented to the atmosphere from a tube designed to provide 0.33 g acceleration along the tube axis.

Key Words: Air collector, air condensation, air sampling, air solidification at 20 °K, cryodeposit, cryodeposit surface temperature, cryopumping, cryopumping air at 20 °K in the transition pressure regime, geysering, heat transfer to air condensing at 20 °K, heat transfer to liquid hydrogen inside tubes, surging, whole air samples.

Elastic properties of NiTi as a function of temperature, S. Spinner and A. G. Rozner, *J. Acoust. Soc. Am.* **40,** *No. 5, 1009–1015 (Nov. 1966).*
Young's modulus, shear modulus, and internal friction of the intermetallic compound NiTi have been measured as a function of temperature from about −180° to 600 °C, in the kilocycle-per-second range. Annealed and cold-worked specimens were used. All the specimens showed the same general pattern, with a minimum in elastic moduli occurring about 70°–140 °C, depending upon the particular specimen, and a maximum in internal friction occurring some 50 °C below the minimum in elastic modulus. Young's modulus was the same for all the specimens (694 kbar) within experimental error, but the shear modulus of the cold-worked specimens was more than 10% higher than that for the annealed specimens.

Glass research at the National Bureau of Standards, G. W. Cleek, *Glass Ind.* **47,** *No. 12, 663–669 (Dec. 1966).*
A general account of the research and development in glass technology at the National Bureau of Standards is presented. A brief history of the Bureau's interest in glass is given, followed by a description of the present effort on specific projects in the Inorganic Glass Section.

Key Words: Glass research, glass technology, properties of glass.

Instrumental aspects of synchrotron XUV spectroscopy, R. P. Madden, D. L. Ederer, and K. Codling, *Appl. Opt.* **6,** *No. 1, 31–38 (Jan. 1967).*
Electron synchrotrons are becoming increasingly important as sources of extreme uv radiation for physical experiments. The NBS 180-MeV machine has been utilized for gas absorption studies over a four-year period, during which a 3-m grazing incidence spectrograph and monochromator have been designed, constructed and put into operation. The instruments are extremely stable to vibration and temperature variation, and are operating with a slit limited resolution of the order of 0.06 Å. The design principles and features of these instruments are described, and a highly successful prealignment procedure for grazing incidence spectrometers is outlined. The effect of the unusual characteristics of this light source on the illumination and performance of the spectroscopic instruments is discussed.

Inversion temperatures and pressures for cryogenic gases and their mixtures, R. D. Gunn, P. L. Chueh, and J. M. Prausnitz, *Cryogenics* **6,** *No. 6, 324–329 (Dec. 1966).*
A generalized Joule-Thomson inversion curve has been obtained from volumetric data for gases with acentric factors less than 0.10. The curve is plotted in coordinates of reduced pressure and reduced temperature and a deviation function is provided for gases which, because of quantum effects, do not conform to classical corresponding states behavior. Semiempirical mixing rules are recommended for calculating the inversion curve of gas mixtures. For two binary systems (hydrogen-methane and helium-nitrogen) it was found that at constant temperature, a plot of inversion pressure versus mole fraction goes through a strong maximum. Calculated results for mixtures compare favorably with the very limited experimental data now available.

Key Words: Corresponding states, cryogenic gases, generalized inversion curve, Joule-Thomson coefficient mixtures.

Moisture permeation of leather and plastics used in shoes, J. R. Kanagy, *J. Am. Leather Chemists' Assoc. Tech. Note* **LXII,** *No. 2, 115–122 (Feb. 1967).*
Data are given on moisture permeation of leather and plastics exposed both to water and water vapor. The rate of moisture permeation of some plastics is equivalent to that of some leather now used. The permeation of moisture through leather depends upon the tannage, and by adopting the proper tannage could be greatly increased. However, leathers that are highly permeable to water are not practical for use in shoes, and in this respect man-made materials will undoubtedly be able to compete with leather. Other properties, such as insulation and ability to mold to the foot, are characteristics which will continue to make leather a preferred material for shoes.

Note on the variation of the results of the Mullen burst test over the area of a hide, J. R. Kanagy, *J. Am. Leather Chemists' Assoc. Tech. Note* **LXII,** *No. 1, 63–67 (Jan. 1967).*
Variation of the Mullen test results was determined over hide by cutting the entire area into 3 by 3 inch pieces and testing each of the specimens. Percentage stretch with increase in load was determined, and the point at which grain crack occurred was noted. Grain-crack is prevalent in specimens from locations on the butt of the hide. In this position stretch increases rapidly with load because of the physical structure of the fibers. Ninety percent of the specimens which cracked were from the small area of the butt which constituted three to four square feet. The other areas of a full-grown cattle hide were almost entirely free of grain-crack when subjected to 600 pounds in the Mullen tester.

Key Words: Burst of leather, grain-crack, extension, Mullen test.

The dispersion of distributions derived from folding simple distributions, R. A. Schrack, *Nucl. Instr. Methods* **45,** *No. 2, 319–321 (1966).*
A graph is presented for obtaining the dispersion (full width at half maximum) of distributions, obtained by folding pairs of simple symmetric distributions. The gaussian, triangular, trapezoidal, and square distributions are considered.

Key Words: Folding, faltung, dispersion, distributions, gaussian, triangular, trapezoidal, square, convolution, variance.

The National Bureau of Standards and its contributions to geophysics, D. Baker, *Trans. Am. Geophys. Union* **17,** *No. 4, 563–568 (Dec. 1966).*
Almost from its inception the National Bureau of Standards has made contributions to the field of geophysics. Major contributions are reviewed, including gravity measurements, IGY participation, seismology, and atmospheric and ionospheric investigations.

Key Words: Geophysics, gravity, seismology, ionosphere.

Nitrogen sorption measurements and surface areas of hardened cement pastes, C. M. Hunt, *Highway Research Board Symposium on Structure of Portland Cement Paste, Washington, D.C., January 1965, Highway Research Board Special Report* **90,** *112–122 (1966).*
Surface area by nitrogen adsorption and also nonevaporable water were determined on hardened cement pastes of four water cement ratios, ranging from 0.251 to 0.501, and four ages, ranging from 1 day to 180 days.
Water-cement ratio made very little difference in the surface area of hardened pastes at 1-day but with pastes at later ages, evidence

suggests that surface area may reach a limiting value which is a function of the original water-cement ratio. The ratio of surface area by nitrogen adsorption to nonevaporable water was not constant but increased with increasing hydration in paste of water-cement ratio 0.501 and changed very little or even decreased slightly in paste of water-cement ratio 0.251.

Pressures exerted on complete dentures during swallowing, M. Ohashi, J. B. Woelfel, and G. C. Paffenbarger, *J. Am. Dental Assoc.* **73,** *No. 3, 625–630 (Sept. 1966).*
The projected areas of the tissue-bearing surfaces of dentures were determined by making tracings on tared pieces of cellulose acetate sheets. The upper dentures of 21 patients had projected areas ranging from 22.8 to 36.6 cm.² (3.5 to 5.7 in.²), the lower dentures from 14.5 to 24.4 cm.² (2.2 to 3.8 in.²). The areas of the upper dentures were from 1.2 to 1.9 times the area of the lower dentures. The forces exerted on complete dentures during swallowing were measured by a Brinell indentation method employed in a modified "Coble Intra-Oral Balancer." Forces ranged on the average from 1.5 to 15.8 kg. (3.3 to 34.8 lb.). The pressure on the upper dentures ranged on the average from 0.06 to 0.56 kg./cm.² (0.85 to 8.0 lb./in.²; for the lower dentures, 0.09 to 0.80 kg./cm.² (1.3 to 11.4 lb./in.²).

Proposal for the practical measurement of *p*H in amphiprotic and mixed solvents, R. G. Bates, *Intern. Union Pure Appl. Chem. Info. Bull. No.* **26,** *50–54 (Aug. 1966).*
Procedures analogous to those on which a practical *p*H scale has been based can be used profitably to establish operational acidity scales in certain other amphiprotic and mixed solvent media. A universal *p*H scale relating proton activity uniformly to the aqueous standard reference state is not yet a practical possibility, but separate scales for each medium can be achieved and will fulfill most of the requirements. The best choice of unit appears to be pa_H^* or $-\log(m_H \cdot {}_s\gamma_H)$, where ${}_s\gamma_H$ is referred to the standard state in each particular medium *s*. Data for reference solutions in 50 wt. percent methanol and the deuterium oxide are given.

Recent advances in U.S.A. research on dental amalgams and possible applications, G. C. Paffenbarger, *Intern. Dental J.* **16,** *No. 4, 450–465 (Dec. 1966).*
Current research on dental amalgam in the United States is developing information regarding the extrusion of amalgam restorations from cavities; the desirability of low mercury-to-alloy ratios; the design of universal technics for mixing and compacting; the effect of residual mercury content; the relation among compressive, tensile and transverse strengths; the phases present in the hardened amalgam; corrosion; and the advantages of amalgam made from spherical alloy powder.

Key Words: Dental, amalgam, research.

Analysis and computer simulation of the production and distribution systems of a tufted carpet mill, J. A. Yurow, *J. End. Eng.* **XVIII,** *No. 1, 135–140 (Jan. 1967).*
The problem of simulating a multiline tufted carpet mill by means of a continous flow simulation language is translated into the problem of simulating a mill producing only four lines. Simulation of the planning and allocation of production time for each line under yarn availability constraints is studied in detail.

Key Words: Simulation, mill, carpet, tufted, and industrial dynamics.

Earth temperature and thermal diffusivity at selected stations in the United States, T. Kusuda and P. R. Achenbach, *ASHRAE Trans.* **71,** *Pt. 1, 61–75 (Jan.–Feb. 1967).*
To provide information related to the heat transfer in underground installations, 63 sets of data showing annual variations of monthly average earth temperatures at various depths throughout the 48 contiguous States of the United States of America have been compiled and analyzed for the Office of Civil Defense. These data have been used to compute the annual average amplitude and phase angle of the earth temperature by a least-squares method. Thermal diffusivities of earth computed from the observed temperature data by both the amplitude method and phase lag method were compared for selected earth temperatue stations. The earth temperature characteristics were also compared with those of air and ground water temperatures.

Micrometer U-tube manometers for medium-vacuum measurements, A. W. Thomas and J. L. Cross, *J. Vacuum Sci. Technol.* **4,** *No. 1, 1–5 (Jan.–Feb. 1967).*
A family of U-tube manometers, suitable for use as standard instruments, has been designed and constructed at the National Bureau of Standards to cover the range of pressures from 100 to 1×10^{-2} torr. In these instruments the levels of the two liquid surfaces are measured by adjusting micrometers with conical points ground on the ends of the spindles. One hundred mm and fifty mm range mercury manometers, with spindles approaching the liquid surface from above, are used for differential or absolute pressure measurements up to 100 torr. Pressures less than 3.5 torr are measured with oil manometers, in which the micrometer spindles approach the surfaces from below. Measurements made with the mercury manometer have an uncertainty of about 4×10^{-3} torr plus eight parts in one hundred thousand of the reading. Measurements made with the oil manometer have an uncertainty of about 4×10^{-4} torr plus two parts in ten thousand of the reading.

Key Words: Vacuum measurement, manometers, U-tube, micrometer, oil, mercury, water.

Outdoor air psychrometric criteria for summer ventilation of protective shelters, T. Kusuda and P. R. Achenbach, *ASHRAE Trans.* **71,** *Pt. 1, 76–87 (Jan. 25–28, 1965).*
A forced ventilation system using outdoor air, powered either manually or by emergency power sources, often provides the best combination of reliability and economy for protective shelters where outdoor conditions and occupancy characteristics are not extreme. In above-ground shelters, an assumption that the ventilating air must remove all of the sensible and latent heat released inside the shelter is a reasonably good design criterion in most cases. This report analyzes the relation between ventilation rate, heat release inside the shelter, and outdoor and shelter psychrometric conditions based on this assumption.
The ventilation rates required to help the effective temperature in the shelter from exceeding certain selected values for various selected outdoor design criteria are calculated for the cities of Houston, Phoenix, and Minneapolis.
It is shown that none of the published noncoincident dry-bulb and wet-bulb temperature criteria expressed on a percentile basis are adequate for calculating ventilation rates on an equal-risk basis for various climates. A method for calculating ventilation adequacy factors that is applicable to any city for which suitable outdoor coincident dry-bulb and wet-bulb temperature data are available is described and illustrated.

The design of a federal statistical data center, E. Glaser, D. Rosenblatt, and M. K. Wood, *Am. Stat.* **21,** *No. 1, 12–20 (Feb. 1967).*
This paper treats the principles underlying the design of a Federal Statistical Data Center intended to provide a better integrated information network for use by Government, industry, and the research community in an age of large-scale computers.

Key Words: Statistical standards, Federal statistical system, automatic data processing equipment, disaggregation, probability master samples, matching, inherent computability, propagation of error computations, disclosure criteria, confidentiality audits.

Time-dependent behavior of an incompressible elastic fluid. Some homogeneous deformation histories, B. Bernstein, *Acta Mechanica* **II,** *No. 4, 329–354 (1966).*
The theory of the incompressible elastic fluid is designed to describe visco-elastic behavior under finite strain. In terms of this theory it is shown how to calculate the stress response to any strain history. The calculations are carried out and the results displayed for a number of homogeneous strain histories. A knowledge of the response to single step stress relaxation in a given geometry allows one to calculate easily response to any other history in the same geometry. Furthermore from biaxial stress relaxation data one may calculate the time dependent stress response in any geometry in a manner which resembles the method for predicting the equilib-

rium response in an isotropic elastic material. An important class of histories comprises the motions following the rest history. To calculate the stress response for such a motion over a given time interval it suffices to have stress relaxation data over the same time interval. Stress response is also calculated for some uniaxial strain histories as well as steady simple shear.

Key Words: BKZ theory, biaxial strain, constant rate of strain, creep, elastic fluid, elastic strain energy function, finite strain, nonlinear behavior, nonnewtonian fluids, normal stresses, pure shear, simple extension, simple shear, stress relaxation, time effects, uniaxial strain, visco-elasticity.

Avalanche radiation from the bulk of long, thin, forward-biased p^+-p-n^+ silicon diodes, G. G. Harman, *Appl. Phys. Letters*, **9**, *No. 5, 207–209 (Sept. 1, 1966).*
Avalanche radiation and other evidence has been found for extremely high electric fields (100 kV/cm) in long thin forward biased silicon diodes. The average applied fields were only 1000 V/cm. Explanations are given for the several effects that appear to be contributing to the observed phenomena.

Key Words: Silicon diodes, hot electrons, visible radiation.

Baffled piston radiator: expansion of potential in far, paraxial field, M. Greenspan, *J. Acoust. Soc. Am.* **40**, *No. 1, 251–252 (July 1966).*
The potential of a circular source, having radially symmetrical but otherwise arbitrary distribution, $v(r_0)$, of velocity over its face, is expanded as

$$\varphi = z^{-1}e^{ikz}\,(a_0 + a_1 z^{-1} + \ldots)$$

[cylindrical coordinates (r, θ, z): center of source at $r = z = 0$]. We find a_0 to depend only on the total volume velocity at the source. If $v(r_0)$ is known, all a_n can be calculated; if it is unknown, limits on a_n can be set.

Key Words: Piston radiator, radiator, piston, sound, diffraction, potential, acoustics.

Cerous magnesium nitrate: a magnetic temperature scale 0.2002-2 °K, R. P. Hudson and R. S. Kaeser, *Physics* **3**, *No. 2, 95–113 (1967).*
Isentropic demagnetizations from known starting conditions yielded a determination of the entropy-magnetic susceptibility, of $S-\chi$, relation for single-crystal spheroids of the paramagnetic salt cerous magnesium nitrate, CMN. Enthalpy differences, ΔQ, between the low temperature end-points thus reached and an (arbitrary) reference temperature near 1 °K (determined by gamma ray heating) yielded a corresponding $Q-S$ curve, whence one obtained $S-T$ and $\chi-T$ relations, T being the thermodynamic temperature. The salt exhibits a broad maximum in χ centered on $S/R = 0.32$, for which region the absolute temperature is determined to be 0.001_5 °K. Our results disagree significantly with those of other workers (even $S-\chi$, which is not subject to large experimental error) save for the observation that CMN obeys the Curie law at least down to 0.006 °K. At high temperatures ($T > 0.006$ °K), all specimens show a heat capacity $C/R = bT^{-2}$ with $b = 5.76 \times 10^{-6}$ deg^2. Superimposed upon this is a small "anomaly" first appearing at approximately 0.015 °K and reaching a maximum near 0.025 °K. The attribution of such an effect to small concentrations of magnetic impurities cannot be reconciled with the results of chemical analysis. Other evidence, moreover, supports the idea of a nonmagnetic origin for this anomaly.

Definition of temperature in the kinetic theory of dense gases, L. S. Garcia-Colin and M. S. Green, *Phys. Rev.* **150**, *No. 1, 153–158 (Oct. 7, 1966).*
The question of the appropriate definition of temperature in the kinetic theory of dense gases is discussed. An apparent contradiction in the value of the bulk viscosity between two methods of making the transition from the kinetic to the hydrodynamic stage is resolved. It is shown that the definitions of temperature through the kinetic energy and through the total energy are equivalent. The general question of the appropriate choice of macroscopic variables in nonequilibrium statistical mechanics is discussed. It is pointed out that the form of the equations of hydrodynamics is covariant with the definition of the macroscopic variables, but the molecular-distribution functions are invariant to this choice. In spite of the equivalence of temperature definition between a quantity which is a local integral of motion and one which is not, the principle that macroscopic observables are properly chosen to be "approximate single-valued integrals of motion" can still be maintained. The question of which temperature or bulk viscosity is measured is discussed in the context of specific experimental situations.

Effective charge carrier lifetime in silicon p-i-n junction detectors, J. A. Coleman and L. J. Swartzendruber, *(Proc. 10th Scintillation and Semiconductor Counter Symp., Washington, D.C., Mar. 23–24, 1966), IEEE Trans. Nucl. Sci.* **NS-13**, *No. 3, 240–244 (June 1966).*
An estimate of the effective charge carrier lifetime can be obtained from a determination of the collection efficiency as a function of the transit time for charge carriers produced by incident short-range radiation in a p-i-n junction detector. The results of this method have the advantage of being independent of both the charge carrier mobility and the depletion depth of the detector. Effective lifetimes as low as a few microseconds (τ_e) for electrons produced by natural alpha particles have been observed in several 2 mm thick lithium-compensated silicon detectors operating at room temperature. No significant bias dependent windows which might cause misleading interpretation of the results were observed. Window effects were investigated by measuring the changes in pulse height of detector output signals initiated by natural alpha particles incident on the detectors at angles up to 45 degrees. The electron lifetimes were observed to decrease when the detector was operated at liquid nitrogen temperature. The short effective lifetimes that can occur in lithium-compensated silicon set a lower limit on the field strengths that must be maintained for efficient charge collection in thick p-i-n junction detectors. Effective hole lifetimes can also be obtained using this technique but with the present geometry of lithium-compensated silicon detectors this measurement is more difficult if short-range particles are used. The effects of charge carrier lifetime and amplifier pulse rise and fall times on the observed radiation-induced pulse shapes are discussed.

Fermi controlled recombination as a junction design factor in GaAs laser diodes, N. N. Winogradoff and H. K. Kessler, *Int. J. Electronics* **21**, *No. 4, 329–335 (1966).*
The observation that the deliberate introduction of shallow donors in the p-type side of GaAs lasers resulted in a greatly improved efficiency in radiative recombination has been fully confirmed and found to be quite general. Our earlier field effect experiments indicate that this enhancement is due to a critical separation of the intrinsic and actual Fermi levels in the space charge region rather than to donor-acceptor transitions. A qualitative model, consistent with experimental observations and supporting this conclusion, is presented and used in the design of improved lasers yielding total peak power outputs in excess of 23 w at room temperature.

Lack of uniqueness in the international practical temperature scale above the gold point, H. J. Kostkowski, *Metrologia* **3**, *No. 1, 28–29 (Jan. 1967).*
The International Practical Temperature Scale (IPTS) above the gold point is shown to vary with wavelength. Although the extent of this variation is barely significant relative to the present uncertainty of realizing the scale, the IPTS should be unique; and to achieve this a wavelength must be specified in the definition.

Key Words: International Practical Temperature Scale, temperature, standards, radiation thermometry, optical pyrometer, infrared pyrometer.

Magnetization of iron for magnetometer calibrations, W. E. Case and R. S. Harrington, *Proc. IEEE* **54**, *No. 12, 2004–2005 (Dec. 1966).*
It is shown that ultra pure iron spheres allow a simple and accurate calibration of vibrating sample magnetometers over a field range from 600 to 5000 oersteds using only one voltage and field reading. The same spheres may also be used to calibrate other types of

magnetometers in this field range by simply assuming the magnetization M is related to the field H_0 by

$$M = \frac{3}{4\pi} H_0.$$

Key Words: Magnetometer calibration, magnetization of pure iron, measurement of magnetization, ferromagnetism.

Mechanical relaxation in polychlorotrifluoroethylene, J. M. Crissman and E. Passaglia, *J. Polymer Sci. Pt. C, No. 12, 237–245 (1966).*

Measurements of the viscoelastic functions Δ, G', G'', J', and J'' as functions of temperature from $-180°$ to $+180$ °C have been obtained using a torsion pendulum apparatus, for several samples of polychlorotrifluoroethylene having widely different crystallinities as determined by density. The low crystallinity samples show two relaxations: a very broad one (γ) centered at about -35 °C which appears to be split into two processes, and one (β) at 84 °C. In the higher crystallinity samples, a third process (α) appears at about 137 °C, and the high temperature side of the γ relaxation peak is lower in magnitude as compared to the lower crystallinity specimens. For the β peak, which is assumed to be associated with the glass transition, the peak value for G'' is essentially independent of crystallinity, while both Δ and J'' show decreases in magnitude with increasing crystallinity. The relationship between the magnitude of the relaxation peak and crystallinity, and dependence of this relationship upon the viscoelastic function chosen to characterize the relaxation are discussed.

Optical power increase in GaAs laser diodes coated with reflecting aluminum silicone mixture, H. K. Kessler, *Proc. IEEE Letter* **55,** *No. 1, 99–100 (Jan. 1967).*

GaAs laser output power has been increased by using the reflectance of an aluminum-silicone mixture coated on a laser diode. After such application, the light output increased from one side by 50%, and better heat dissipation from the diode was observed.

Key Words: GaAs lasers, optical power, aluminum-silicone compound, heat sink.

Radiative recombination within a space-charge region in a semiconductor, N. N. Winogradoff, *J. Appl. Phys.* **37,** *No. 10, 3916–3917 (Sept. 1966).*

Since light emission from forward biased junctions is usually due to radiative recombination through a recombination center, the minima in the light output observed when cathode rays or a narrow beam of light traversed a *p-n* junction can be explained in terms of the recombination statistics of the centers in the space charge region rather than in terms of the separation of the free carriers by the junction field as is commonly believed. Furthermore, it is shown that under certain conditions of excitation, the luminescence in the space charge region can be a maximum.

Key Words: Radiative recombination, space charge regions, *p-n* junctions, germanium, silicon and gallium arsenide.

Surface aspects of the thermal degradation of GaAs *p-n* junction lasers and tunnel diodes, H. Kessler and N. N. Winogradoff, *IEEE Trans. Electron. Devices* **ED-13,** *No. 10, 688–691 (Oct. 1966).*

Owing to the similarity of the junction widths and doping levels in epitaxially formed GaAs lasers and conventional tunnel diodes, the gradual degradation of the latter under use might be expected to be intensified in the case of lasers operating under high duty cycle or c.w. conditions.

It was found that the current voltage characteristics of both the lasers and tunnel diodes underwent considerable thermal degradation even when no bias was applied, and that the degradation was limited to *surface* or "junction edge" effects.

The degradation of the current-voltage characteristics was correlated with degradation in the light output under forward bias. It was concluded that degradation under forward bias was also a surface effect induced by heating rather than by deterioration of the junction in the bulk as commonly believed. Methods of controlling the degradations are discussed.

Key Words: Gallium arsenide, lasers, tunnel diodes, degradation, light emission, surface effects.

Other NBS Publications

J. Res. NBS 71A (Phys. and Chem.), No. 3 (May–June 1967), $1.00.

Measured relative enthalpy of anhydrous crystalline aluminum triflouride, AlF_3, from 273 to 1173 °K and derived thermodynamic properties from 273 to 1600 °K. T. B. Douglas and D. A. Ditmars.

The heat of formation of boron trifluoride by direct combination of the elements. E. S. Domalski and G. T. Armstrong.

An equation of state for fluid parahydrogen from the triple-point to 100 °K at pressures to 350 atmospheres. R. D. Goodwin.

The dissociation constants of some disubstituted anilines and phenols in aqueous solution at 25 °C. R. A. Robinson.

Third virial coefficient for air-water vapor mixtures. R. W. Hyland and E. A. Mason.

Recrystallization and melting of partially melted stark rubber. D. E. Roberts. (See above abstracts.)

Effects of a distribution of volume relaxation times in the annealing of BSC glass. P. B. Macedo and A. Napolitano. (See above abstracts.)

The National Bureau of Standards 1966, Misc. Publ. 282 (Nov. 1966), 35 cents.

Cast-iron radiators, R174–65 (Dec. 31, 1965), 10 cents. Supersedes R174–47.

Wire bar supports for reinforced concrete construction, PS7–66 (Aug. 1, 1966), 10 cents.

A grammar for component combination in chinese characters, B. K. Rankin, III, S. Siegel, A. McClelland, and J. L. Tan, Tech. Note 296 (Dec. 1966), 60 cents.

Infrared reflectances of metals at cryogenic temperatures—a compilation from the literature, P. F. Dickson and M. C. Jones, Tech. Note 348 (Oct. 14, 1966), 40 cents.

Acidity functions for amphiprotic media, R. G. Bates, Book, Chemistry of Nonaqueous Solvents, **1,** Sect. III, 97–128 (Academic Press Inc., New York, N.Y., 1966).

Collagen aggregation phenomena, J. M. Cassel, Biopolymers **4,** 989–997 (1966).

Proton broad-line N.m.r. study of ($^2H_6$) dimethoxy (^{11}B) borane, T. C. Farrar, J. Cooper, and T. D. Coyle, Chem. Commun. **17,** 610–611 (1966).

The adsorption kinetics of nitrogen on rhenium, M. D. Scheer and J. D. McKinley, Surface Sci. **5,** No. 3, 332–344 (Nov. 1966).

The melting point of Al_2O_3 in vacuum, S. J. Schneider and C. L. McDaniel, Rev. Hautes Temper. et Refract. **3,** 351–361 (1966).

Government, industry and engineering. NBS in a new setting, S. Lichtenstein, Automotive Ind. **135,** No. 10, 119–124 (Nov. 15, 1966).

Hadamard matrices of order cube plus one, K. Goldberg, Proc. Am. Math. Soc. **17,** No. 3, 744–746 (June 1966).

State standards and laboratories, T. M. Stabler, Scale J. **53,** No. 1, 3–14 (Oct. 1966).

Angle and channel dependence of resonance in e-He scattering near 60 eV, J. A. Simpson, M. G. Menendez, and S. R. Mielczarek, Phys. Rev. **150,** No. 1, 76–78 (Oct. 7, 1966).

Anomalous work function of the tungsten (110) plane, R. D. Young and H. E. Clark, Appl. Phys. Letters **9,** No. 7, 265–268 (Oct. 1, 1966).

Effect of nuclear alignment on the 14-MeV total neutron cross section of ^{165}Ho, H. Marshak, A. C. B. Richardson, and T. Tamura, Phys. Rev. **150,** No. 3, 996–1010 (Oct. 21, 1966).

Electron microscopy and diffraction of synthetic corundum crystals. II. Dislocations and grain boundaries in impurity-doped aluminum oxide, D. J. Barber and N. J. Tighe, Phil. Mag. **14,** No. 129, 531–544 (Sept. 1966).

Exact vibrational matrix elements for molecular hydrogen and the intensity of the quadrupole rotation-vibration spectrum. T. C. James, Astrophys. J. **146,** No. 2, 572–580 (Nov. 1966).

Interference in the photo-ionization of molecules, H. D. Cohen and U. Fano, Phys. Rev. **150,** No. 1, 30–33 (Oct. 7, 1966).

Resonances in inelastic electron scattering from H_2, M. G. Menendez and H. K. Holt, J. Chem. Phys. **45,** No. 8, 2743–2744 (Oct. 15, 1966).

The $A^1\Sigma$ transition of ^{39}KH and ^{39}KD. Vibrational numbering and molecular constants, I. R. Bartky, J. Mol. Spectry. **20,** No. 4, 299–311 (1966).

The absorption spectrum of cesium deuteride. The $A^1\Sigma$ state of CsH, I. R. Bartky, J. Mol. Spectry. **21,** No. 1, 25–28 (1966).

The absorption spectrum of RbD. Vibrational numbering of the $A^1\Sigma$ state of RbH, I. R. Bartky, J. Mol. Spectry. **21,** No. 1, 1–3 (1966).

The momentum autocorrelation function in a Bernoulli chain, R. J. Rubin and P. Ullersma, J. Math. Phys. **7,** No. 10, 1877–1885 (Oct. 1966).

What environment—for whom? G. E. Auman, Civil Service J. **7,** No. 1, 6–11 (July–Sept. 1966).

A broad-line proton magnetic resonance study of cobalt tetracarbonyl hydride, T. C. Farrar, F. E. Brinckman, T. D. Coyle, A. Davision, and J. W. Faller, Inorg. Chem. **6,** 161–163 (1967).

Exactly solvable nonlinear relaxation processes. Systems of coupled harmonic oscillators, K. E. Shuler and G. H. Weiss, J. Chem. Phys. **45,** No. 4, 1105–1110 (Aug. 15, 1966).

Flash photolysis of methane in the vacuum ultraviolet. I. End-product analysis, W. Braun, K. H. Welge, and J. R. McNesby, J. Chem. Phys. **45,** No. 7, 2650–2656 (Oct. 1, 1966).

Ion-molecule reactions in the condensed phase radiolysis of hydrocarbon mixtures. I. 2-methylbutane and 3-methylpentane, J. Am. Chem. Soc. **88,** No. 24, 5701–5707 (Dec. 20, 1966).

Radiation-induced polymerization of hexafluoropropylene at high temperature and pressure, R. E. Lowry, D. W. Brown, and L. A. Wall, J. Polymer Sci. **4,** Pt. A-1, No. 9, 2229–2239 (Sept. 1966).

Relaxation of moments derived from a master equation, K. E. Shuler and G. H. Weiss, J. Chem. Phys. **45,** No. 4, 1110–1112 (Aug. 15, 1966).

Vibrational spectrum of $ClNF_2$, J. J. Comeford, J. Chem. Phys. **45,** No. 9, 3463–3465 (Nov. 1, 1966).

Forces shaping the role of the architect, J. P. Eberhard, Proc. Second Architectural Center Conf., May 13–14, 1966, Boston, Mass., pp. 12 (Boston Architectural Center, Boston, Mass., May 1966).

Technology for the city, J. P. Eberhard, Intern. Sci. Technol. **57,** 18–29 (Sept. 1966).

The stress corrosion of metals, H. L. Logan, Book (John Wiley & Sons, Inc., New York, N.Y., Nov. 1966).

Accommodation faulting in Fe-Ni martensitic transformation, R. P. Reed, Acta Met. **14,** 1392–1394 (1966).

Brownian motion models, R. J. Rubin, Summer Institute on Spectral Theory and Statistical Mechanics, Brookhaven National Laboratory, Upton, L.I., New York, July-Aug. 1965), Brookhaven Natl. Lab. Publ. PNL993 (T422), (Clearinghouse for Federal Scientific and Technical Information, Springfield, Va. 22151, 1966).

Chlorine Kβ x-ray emission spectra from several chlorinated hydrocarbon and fluorocarbon molecular gases, R. E. LaVilla and R. D. Deslattes, J. Chem. Phys. **45,** No. 9, 3446–3448 (Nov. 1, 1966).

Coriolis zeta constants and force field for osmium tetraoxide, I. W. Levin and S. Abramowitz, Inorg. Chem. **5,** 2024–2026 (1966).

Effect of sample thickness and operating voltage on the contrast of Kossel transmission photographs, H. Yakowitz, J. Appl. Phys. **37,** No. 12, 4455–4458 (Nov. 1966).

Erratum: Polycrystalline spin-wave theory of ferromagnetic resonance compared with the tilting experiment, A. S. Risley, E. G. Johnson, Jr., and H. E. Bussey, J. Appl. Phys. **37,** No. 9, 3646 (Aug. 1966).

Flash photolysis of matrix-isolated cyanogen azide in solid nitrogen, L. J. Schoen, J. Chem. Phys. **45,** No. 8, 2773–2776 (Oct. 15, 1966).

Molecular emission spectra in the soft x-ray region, R. D. Deslattes and R. E. LaVilla, Appl. Opt. **6,** 39–42 (Jan. 25, 1967).

Newly measured and calculated wavelengths in the vacuum ultraviolet spectrum of neutral nitrogen, V. Kaufman and J. F. Ward, Appl. Opt. **6,** No. 1, 43–46 (Jan. 1967).

Observation of the $D\,^1\Delta \rightarrow x^1\Sigma+$ transition of CO in the vacuum-ultraviolet region, J. D. Simmons and S. G. Tilford, J. Chem. Phys. **45,** No. 8, 2965–2968 (Oct. 15, 1966).

Observation of the superconducting energy gap in a semiconductor (GeTe), P. J. Stiles, L. Esaki, and J. F. Schooley, Physics Letters **23,** No. 3, 206–207 (Oct. 17, 1966).

Resolving power predictions from lens design data, O. N. Stavroudis, Appl. Opt. **6,** No. 1, 129–135 (Jan. 1967).

Sodium-electron spin-exchange collisions, L. C. Balling, Phys. Rev. **151,** No. 1, 1–6 (Nov. 4, 1966).

Static theory of the giant quadrupole resonance in deformed nuclei, M. Danos, W. Greiner, and B. C. Kohr, Phys. Rev. **151,** No. 3, 761–772 (Nov. 18, 1966).

Superconductivity in semiconducting $SrTiO_3$, J. F. Schooley and W. R. Thurber (Proc. Intern. Conf. Physics of Semiconductors, Kyoto, Japan, Sept. 8–11, 1966), J. Phys. Soc. Japan **21,** Paper XVI-2, 639–642 (Suppl. 1966).

The photodetachment cross section, electron affinity, and structure of the negative hydroxyl ion, L. M. Branscomb, Phys. Rev. **148,** 11 (1966).

Thermal energy ion-neutral reaction rates. I. Some reactions of helium ions, F. C. Fehsenfeld, A. L. Schmeltekopf, P. D. Goldan, H. I. Schiff, and E. E. Ferguson, J. Chem. Phys. **44,** No. 11, 4087–4094 (June 1, 1966).

Vibration spectra of yttrium and uranium hydrides by the inelastic scattering of cold neutrons, J. J. Rush, H. E. Flotow, D. W. Connor, and C. L. Thaper, J. Chem. Phys. **45,** No. 10, 3817–3825 (Nov. 15, 1966).

Chemiluminescence of CH in the $O+C_2H_2$ reaction: Rotational relaxation and quenching, W. Brennen and T. Carrington, J. Chem. Phys. **46,** No. 1, 7–18 (Jan. 1, 1967).

Corrosion's many faces, S. Lichtenstein, Southern Eng. **85,** No. 1, 44–47 (Jan. 1967).

Dielectric constants of imperfect gases. III. Atomic gases, hydrogen, and nitrogen, R. H. Orcutt and R. H. Cole, J. Chem. Phys. **46,** No. 2, 697–702 (Jan. 15, 1967).

Formation of $NH(c^1\Pi)$ and $NH(A^3\Pi_i)$ in the vacuum-uv photolysis of HN_3, K. H. Welge, J. Chem. Phys. **45,** No. 11, 4373–4374 (Dec. 1, 1966).

Growth of calcite crystals, P. M. Gruzensky (Proc. Intern. Conf. Crystal Growth, Boston, Mass., June 20–24, 1966), Crystal Growth, A Suppl. to J. Phys. Chem. Solids D-3, pp. 365–367 (Pergamon Press Inc., New York, N.Y., 1967).

Introduction of the Acheson medalist, R. G. Bates, J. Electrochem. Soc. **113,** No. 12, 1–7 (Dec. 1966).

The crystal structure of twinned low-temperature lithium phosphate, C. Keffer, A. Mighell, F. Mauer, H. Swanson, and S. Block, Inorg. Chem. **6,** No. 1, 119–125 (Jan. 1967).

The ionization constant of deuterium oxide from 5 to 50°, A. K. Covington, R. A. Robinson, and R. G. Bates, J. Phys. Chem. **70,** 3820–3824 (1966).

The optical and magnetic spectra of copper doped dichloro(1–10–phenanthroline) zinc, G. F. Kokoszka, C. W. Reimann, and H. C. Allen, Jr., J. Phys. Chem. **71,** No. 1, 121–126 (Jan. 1967).

Time-dependent behavior of activated molecules. High pressure unimolecular rate constant and mass spectra, F. H. Mies and M. Krauss, J. Chem. Phys. **45,** No. 12, 4455–4468 (Dec. 15, 1966).

A functional inequality, S. Haber, Am. Math. Mo. **73,** No. 10, 1103–1104 (Dec. 1966).

Calculated heats of dilute solid solution among the alkali halides other than cesium salts, T. B. Douglas, J. Chem. Phys. **45,** No. 12, 4571–4585 (Dec. 15, 1966).

Matrix elements of general potentials in the harmonic-oscillator representation, R. M. Wilcox, J. Chem. Phys. **45,** No. 9, 3312–3316 (Nov. 1, 1966).

Measurement and calculation of CU II, Ge II, Si II, and C I vacuum-ultraviolet lines, V. Kaufman and J. F. Ward, J. Opt. Soc. Am. **56,** No. 11, 1591–1597 (Nov. 1966).

Measurements of relative oscillator strengths of some C II multiplets, J. R. Roberts and K. L. Eckerle, Phys. Rev. **153,** No. 1, 87–90 (Jan. 1967).

Recent advances in excitation of atomic spectra, M. Margoshes, Proc. XII Intern. Spectroscopy Colloquium, Exeter, England, 1965, pp. 26–42 (Hilger and Watts, London, England, 1966).

The effect of a two-dimensional roughness element on boundary-layer transition, P. S. Klebanoff, (Proc. Eleventh Intern. Congress Applied Mechanics, Munich, Germany, 1964), Book, Applied Mechanics, ed. H. Gotler, pp. 803–805 (Springer-Verlag Berlin, Germany, 1966).

The forbidden $I^1\Sigma^- - X^1\Sigma^+$ absorption bands of carbon monoxide, G. Herzberg, J. D. Simmons, A. M. Bass, and S. G. Tilford, Can. J. Phys. **44,** 3039–3045 (1966).

Two-quantum photoionization of Cs and I^-, J. L. Hall, IEEE J. Quantum Electron. **QE-2,** No. 9, 361–363 (Sept. 1966).

Determination of the composition of complexes and their instability constant by calorimetry. II. The complex in fused potassium chloride and cadmium chloride, W. H. Metzger, Jr., A. Brenner, and H. I. Salmon, J. Electrochem. Soc. **114,** No. 2, 131–138 (Feb. 1967).

Influence of paramagnetic resonance on the static susceptibility. The lattice-bath relaxation time of neodymium ethyl sulfate, G. A. Candela and R. E. Mundy, J. Chem. Phys. **46,** No. 1, 47–54 (Jan. 1, 1967).

Measurement of optical constants: optical constants of liquid mercury at 5461 Å, L. E. Smith and R. R. Stromberg, J. Opt. Soc. Am. **56,** No. 11, 1539–1542 (Nov. 1966).

Nitrogen on rhenium observed with the field emission microscope, R. Klein and J. W. Little, Surface Sci. **6,** No. 2, 193–207 (Feb. 1967).

Nonstoichiometric A15-type phases in the systems Cr-Pt and Cr-Os, R. M. Waterstrat and E. C. van Reuth, Trans. Met. Soc. AIME **236,** No. 8, 1232–1233 (Aug. 1966).

Production and reaction of atomic fluorine in solids. Vibrational and electronic spectra of the free radical HNF, M. E. Jacox and D. E. Milligan, J. Chem. Phys. **46,** No. 1, 184–191 (Jan. 1, 1967).

Structural interpretation of immiscibility in oxide systems: IV. Occurrence, extent, and themperature of the monotectic, E. M. Levin, J. Am. Ceram. Soc. **50,** No. 1, 29–38 (Jan. 1967).

The system Sc_2O_3-B_2O_3, E. M. Levin, J. Am. Ceramic Soc. **50,** No. 1, 53–54 (Jan. 1967).

Building code viewpoints, A. A. Bates (Building Research Institute Fall Conf., Codes Session, Washington, D.C., Nov. 16, 1966), J. Bldg. Res. Inst. **4,** No. 1, 48–49 (Jan.–Feb. 1967).

The city as a system, J. P. Eberhard, Proc. Mid-American Conf. Design, Kansas City, Mo., March 30–31, 1966, pp. 25–30 (Midwest Research Institute, Kansas City, Mo., 1966).

The RF connector, R. C. Powell, Microwave J. **10,** No. 3, 8 (Feb. 1967).

Processing of numerical test data, J. Mandel and T. W. Lashof, Book, Testing of Polymers, ed. J. V. Schmitz, **2,** ch. 2, 33–82 (Interscience Publ. New York, N.Y., 1966).

Optimum allocation of calibration errors, E. L. Crow, Ind. Quality Control **23,** No. 5, 215–219 (Nov. 1966).

Adsorption of polymers, R. R. Stromberg, Book, Treatise of Adhesives and Adhesion, **1.** Theory, ch. 3, 69–118 (Marcel Dekkers Inc., New York, N.Y., 1967).

A study of the angular and energy distributions of radiation at small distances from a point source of gamma rays or neutrons, C. Eisenhauer, Nucl. Sci. Eng. **27,** 240–251 (1967).

A survey of second breakdown, H. A. Schafft and J. C. French, IEEE Trans. Electron. Devices **ED-13,** No. 8–9, 613–618 (Aug.-Sept. 1966).

Divergence in the density expansion of the transport coefficients of a two-dimensional gas, J. V. Sengers, Phys. Fluids **9,** No. 9, 1685–1696 (Sept. 1966).

Elastic constants of single crystal UO_2 at 25 °C, J. B. Wachtman, Jr., M. L. Wheat, H. J. Anderson, and J. L. Bates, J. Nuclear Mater. **16,** 39–41 (1965).

Ferrimagnetic resonance low-field effects in rod samples, L. B. Schmidt, R. D. Harrington, and W. E. Case, Proc. IEEE **55,** No. 1, 120–121 (Jan. 1967).

Kinetics of growth of multicomponent chains, J. I. Lauritzen, Jr., E. A. DiMarzio, and E. Passaglia, J. Chem. Phys. **45,** No. 12, 4444–4454 (Dec. 15, 1966).

Nuclear hexadecapole interactions, R. J. Mahler, Phys. Rev. **152,** No. 1, 325–330 (Dec. 2, 1966).

Solid-vapour equilibrium in the system neon-methane, M. J. Hiza and A. J. Kidnay, Cryogenics **6,** No. 6, 348–354 (Dec. 1966).

Spin-relaxation effects on the EPR spectrum of gaseous S-state atoms, R. L. Brown and W. Brennen, J. Chem. Phys. **46,** No. 1, 385–386 (Jan. 1, 1967).

Surface aspects of the thermal degradation of GaAs *p-n* junction lasers and tunnel diodes, H. Kessler and N. N. Winogradoff, IEEE Trans. Electron. Devices **ED-13,** No. 10, 688–691 (Oct. 1966).

**Publications for which a price is indicated are available by purchase from the Superintendent of Documents, U.S. Government Printing Office, Washington, D.C. 20402 (foreign postage, one-fourth additional). The NBS nonperiodical series are also available from the Clearinghouse for Federal Scientific and Technical Information, Springfield, Va. 22151. Reprints from outside journals and the NBS Journal of Research may often be obtained directly from the authors.*

U.S. GOVERNMENT PRINTING OFFICE : 1967 OL—265-343

UNITED STATES
GOVERNMENT PRINTING OFFICE
DIVISION OF PUBLIC DOCUMENTS
WASHINGTON, D.C. 20402

OFFICIAL BUSINESS

JUNE 48129
UNIVERSITY MICROFILMS INC
SERIALS SECTION
300 NORTH ZEEB ROAD
ANN ARBOR MICHIGAN 48106

POSTAGE AND FEES PAID
GOVERNMENT PRINTING OFFICE

JOURNAL OF RESEARCH of the National Bureau of Standards — Vol. 71C, No. 3 — July–September 1967
C. Engineering and Instrumentation

Contents

Page

Procedure for high precision density determinations by hydrostatic weighing. Horace A. Bowman and Randall M. Schoonover with Appendix by M. W. Jones. 179

Study of the storage stability of the barium fluoride film electric hygrometer element. Frank E. Jones. 199

Torsion creep of circular and noncircular tubes. Leonard Mordfin. 209

Digitized low-frequency phasemeter assembled from logic modules. John E. McKinney. 227

Publications of the National Bureau of Standards.

Library of Congress Catalog Card Number: 62–3900

For sale by the Superintendent of Documents, U.S. Government Printing Office, Washington, D.C. 20402. Price 75¢ (single copy). Subscription price: $2.75 a year; 75¢ additional for foreign mailing.
UNITED STATES GOVERNMENT PRINTING OFFICE, WASHINGTON : 1967